Dendrohydrological reconstruction and hydroclimatic variability in southwestern British Columbia, Canada

by

Bryan J. Mood

B.Sc., Mount Allison University, 2013
M.Sc., University of Victoria, 2015

A Dissertation Submitted in Partial Fulfillment of the
Requirements for the Degree of

DOCTOR OF PHILOSOPHY

in the Department of Geography

Supervisory Committee

Dendrohydrological reconstruction and hydroclimatic variability in southwestern British Columbia, Canada

by

Bryan J. Mood

B.Sc., Mount Allison University, 2013
M.Sc., University of Victoria, 2015

Supervisory Committee

Dr. Dan J. Smith (Department of Geography)
Supervisor

Dr. David Atkinson (Department of Geography)
Departmental Member

Dr. Tobi Gardner (Victoria Capital Regional District)
Outside Member

Abstract

Supervisory Committee

Dr. Dan J. Smith (Department of Geography)
Supervisor

Dr. David Atkinson (Department of Geography)
Departmental Member

Dr. Tobi Gardner (Victoria Capital Regional District)
Outside Member

The hydrology of southwestern British Columbia is influenced by the region's mountainous topography and climate oscillations generated from the Pacific Ocean. While much of the region is characterized as a temperate rainforest, recent summers are defined by record-breaking droughts that focus attention on the threat to regional water supply security likely to accompany future climate changes.

The limited length and distribution of hydrological records in southwestern British Columbia provide poor context for resource managers tasked with developing policy and water management strategies. The purpose of the dissertation was to describe long-term variability in several key hydroclimatic variables and hydroecological interactions that may be used in updated water resource policy and management strategies. Specifically, the research focused on developing long-term proxy records of April 1 snow water equivalent (SWE), summer streamflow, spring lake levels, and salmon abundance from tree ring records. A secondary goal of the dissertation was to identify the role and influence of several key climate oscillations on regional long-term hydroclimatic and ecological variability.

Freshet contributions from melting snow are critical for sustained summer streamflow in southwestern British Columbia. Even so, few manual snow survey stations exist within the region are of sufficient length to understand the full range of natural SWE variability. Long-term April 1 SWE records were constructed by establishing statistical relationships with the radial growth of high-elevation trees and April 1 SWE records. Explaining 51% and 73% of the total variance in the instrumental SWE records in coastal and continental settings, the reconstructions provide high-resolution descriptions of April 1 SWE over the past three centuries and help position the remainder of the dissertation. Negative phases of the Pacific Decadal Oscillation (PDO) and El Niño-Southern Oscillation (ENSO) were shown to strongly influence April 1 SWE totals. Both reconstructions illustrate repeated step-changes in April 1 SWE during the last 300 years and show that coastal areas may be more sensitive to annual variability than snowpack that accumulates in more continental locations.

Water shortages in the Metro Vancouver area in recent summers are linked to low total winter snowpack and early spring melt. Dendrohydrological analysis of dry-season

streamflow was conducted to determine if the instrumental range has been underestimated over the past several centuries. A regionalized record of July-August streamflow for the Capilano and Seymour watersheds, which supply the Metro Vancouver area, was modelled from present to 1711using tree-rings. Explaining 54% of total variance over the instrumental period, the models show that below-average streamflow events are becoming more frequent. When compared to those characterizing the past 300 years, streamflow totals from 1977 to present have consistently fallen well-below the average long-term discharge. Further analyses indicated that negative ENSO and PDO conditions strongly influenced July-August runoff trends since 1711, as have climate regimes related to the Pacific North American pattern (PNA).

The increased frequency in recent years of reduced summer runoff in southwestern British Columbia has led many communities to rely on natural and dammed reservoirs to supplement their water needs. Where communities rely on natural lakes, this dependence may have socioeconomic consequences if lake levels fall below those necessary to supply built infrastructure. Unfortunately, there are few lake level records in southwestern British Columbia and none of sufficient duration to understand the full range of variability in natural lake systems. Harrison Lake is the only natural lake with a lake level record exceeding 50 years. Using the average April water level dataset, a dendrohydrological model was constructed that explained 49.5% of total variance. The model was used to reconstruct a proxy record of April water levels spanning the interval from 1711 to 1980. Averaging 9.37 m in depth, lake levels in Harrison Lake ranged from 8.9 to 10.0 m over the past 300 years. These variations were shown to be statistically associated with negative and positive phases of ENSO and positive phases of PDO. April water levels in Harrison Lake have been, on average, 0.13 m lower since the mid-1930s compared to the previous 200 years. This reduction in storage capacity amounts to a loss of almost 300-million litres of stored water since the start of instrumental records.

Salmon play a vital economic, cultural, and social role in many southwestern British Columbia communities. There is concern that salmon populations in the region are under threat, as changing climates alter and impact their spawning habitat. While various lines of research have sought to determine the response of salmon to these changing conditions, population records that extend only to 1951 hinder a complete understanding of the impacts. Two dendroecological models were constructed to provide a longer-term perspective of regional salmon-climate relationships. Explaining 48.2% and 48.9% of variance in observed Chinook and Coho salmon abundance since 1951, the models were used to construct proxy escapement records extending to the 1700s. Spectral analysis revealed that the reconstructions account for generational life histories and that low-frequency climate variability was associated with fluctuations in abundance. Both the Chinook and the Coho reconstructions show phase dependent relationships to climate oscillations generated from the Pacific Ocean. The Coho record is strongly linked to negative winter and spring ENSO, while the Chinook record was shown to be associated with negative PDO conditions. The identified relationships to teleconnections generated in the Pacific Ocean to our record indicates that both species are sensitive to oceanic interactions prior to entering natal habitats. Taken together, the reconstructions illustrate that the observational record encompasses a period of lower-than-average

abundance and that neither accounts for the full range of variability in annual abundance when considered over the past three centuries.

The proxy tree-ring records presented in this dissertation provide new information about climate-water resource relationships in southwestern British Columbia. Significant phase-dependent associations, especially to negative phases of the PDO and ENSO, were shown to exert long-term influences on the state of several critical hydroclimatic variables over the last 300 years. Additionally, the research illustrates that over the instrumental period, both streamflow and lake volumes in the region have consistently remained below those characterizing the previous two to three centuries. These findings are of direct use to resource managers tasked with developing new policy and strategies under present and future climate change, in that they offer singular insights into the full range of natural hydroclimatic variability in southwestern British Columbia.

Table of Contents

List of Tables

List of Figures

Acknowledgements

This dissertation is the culmination of countless complaints and copious cups of coffee. I wish to thank those that have endured me since my arrival in Victoria. I have cherished my time at the University of Victoria and the people that made it great.

Dan, thanks for always being around to help or lend an ear to my insatiable ranting. You took a true Maritimer and turned him into a west coaster – for better or worse. You've spoiled me with trips to remote locations throughout the Coast Mountains and beyond. I will never forget spending 19 days in the backcountry eating 'spaghetti wraps' with 'nachos for texture' because most of our food was buried on day two...

Thank you, David and Tobi, for your help with getting this dissertation put together. Your thoughts and perspectives were appreciated as I ventured towards the completion of my research.

To the UVTRL, thanks for having me. I know that I was distracting, inappropriate, and – well – full of shit 90% of the time but it was a great few years. I've forged friendships with so many people in the lab and know they will continue. A special thanks to Bethany, Cedar, Jill, and Jodi. You may not know it but I look up to each of you as role models and mentors. Each of you is a badass. Lauren, Lee, Ale, and Tavy, thanks for the help in the field and company! You're all gems!

To my futsal, seven-a-side, and intramural soccer teams, thanks so much for having me! Even with my constantly sprained ankle! I made a great group of friends while playing with you all. A special thanks to Aiden, 'baps', Ben, Britt, Byron, Evan, Kyle, and Shannon for being a great bunch of people and making me part of your amazing crew.

Cody, Devin, and Henry – thanks for always listening or being generally happy to see me on my rare visits to Nova Scotia. You're my best friends and I couldn't ask for better. Although you really didn't understand what I was going through, you always supported me.

Mom, Dad, Julie, and Haley, thanks for being a great supportive family! Never once did you ask those classic PhD questions 'when are you done' or 'when are you getting a job.' You trusted the process and me. I am forever grateful. Bodie, you can't read this, but you're cool too. Another thanks to Aris, you made sure I kept up with exercise and my mental health in check. Thanks, my 'Ariba'. You're adorable… most of the time.

Finally, thanks to my wonderful wife, Kaitlin. I'm here because I decided the best way to get to know you was studying. I would have flunked out of university if it weren't for you. You challenge and bring the best out of me… Even when I hate it! You are the best. You are my rock. I love you.

Dedication

For Kaitlin

Chapter 1: Introduction

1.1 Hydrology of southwestern British Columbia

The hydrologic regime of southwestern British Columbia (BC) is influenced by its dynamic topography and climate oscillations originating in the Pacific Ocean (Rodenhuis et al., 2009; Church and Ryder, 2010; Mote et al., 2018). Positioned adjacent to the Pacific Ocean and characterized by the Pacific Ranges of the BC Coast Mountains, moisture is delivered to the region primarily through orographic processes during the winter months (Church and Ryder, 2010). While much of the region is a temperate rainforest, recent summers were characterized by record-breaking, severe, drought conditions (River Forecast Centre, 2017). Attempts to understand the dynamics of these events in southwestern BC and to forecast the likelihood of future events are hindered by a relatively sparse network of instrumental records that rarely extend beyond 50 years (Coulthard et al., 2016). Limited records provide poor context for resource managers tasked with developing sound policy and management strategies for the region's water supply.

Elsewhere in western North America, proxy reconstructions of critical hydrological variables and their association to climate oscillations is an area of focused research (e.g., Meko et al., 2001; Pederson et al., 2011; Ballinger et al., 2018; Pathak et al., 2018; Welsh et al., 2019). The collective findings of this research illustrate that instrumental records underestimate worst-case scenario drought conditions and that current conditions are increasingly outside the range of observed variability (Belmechari et al., 2015; Coulthard et al., 2016). Of particular consequence, these studies reinforce the

strong regional hydroclimatic teleconnection to sea surface temperature variability in the Pacific Ocean (Rodenhuis et al., 2009; Ballinger et al., 2018; Pathak et al., 2018). While research has shown that related climate oscillations influence the hydroclimatic character of southwestern BC (Rodenhuis et al., 2009; Spry et al., 2014), directed research focused on examining and expanding upon the nature of these relationships over the long-term is sparse (e.g., Coulthard et al., 2016).

1.2 Hydroclimate relationships

Over the last 50 years, climate oscillations originating in the Pacific Ocean have been repeatedly linked to hydrological variability in southwestern BC (Bonsal and Shabbar, 2008; Rodenhuis et al., 2009). While research shows large-scale teleconnections are responsible for upwards of 30% of the annual hydroclimate variability in snowpack accumulation, there is only limited appreciation for how these relationships influence regional hydrology. In western North America, recent research highlights the role of non-stationary relationships between hydrological variability and climate oscillations that have yet to be documented in southwestern BC (Marcinkowski et al., 2013; Coulthard et al., 2016; Mote et al., 2018; Litzow et al., 2018). What is appreciated is that three large-scale climate oscillations play a part in defining regional hydroclimate dynamics: (1) the El Niño-Southern Oscillation (ENSO); (2) the Pacific Decadal Oscillation (PDO), and; (3) the Pacific North American pattern (PNA) (McCabe et al., 2004; Rodenhuis et al., 2009; Abatzoglou, 2011; Starheim et al., 2013a; Coulthard et al., 2016; Mote et al., 2018).

ENSO is characterized by temperature and pressure fluctuations in the equatorial ocean surface off the western coast of South America that lead to 'seesaw' interactions with the southeastern tropical Pacific and Australian-Indonesian region (McCabe et al., 2004; Bridgman and Oliver, 2006;). During warm (positive; El Niño) ENSO events, the jet stream splits producing both high and low latitude storm tracks that rarely influence southwestern BC (Shabbar et al., 1997). The Pacific storm track migrates equatorward and downstream during El Niño events in response to local enhancement of the Hadley circulation off the coast of western North America (Chang et al., 2002). Winters that follow the onset of El Niño conditions during the previous spring, tend to be warmer and drier than normal (Stahl et al., 2006). In contrast, during La Niña (cool, negative ENSO) years winters tend to be cooler in response to a northward shift in the Pacific jet stream that brings wetter conditions to southwestern BC and the Pacific Northwest (Stahl et al., 2006).

The PDO is a long-lived ENSO-like pattern of Pacific climate variability defined by sea surface temperatures (SST) (Mantua et al., 1997; Bridgman and Oliver, 2006). The PDO describes a forced response from the North Pacific to atmospheric variability associated with the Aleutian Low (AL) (Newman et al., 2003). While its behaviour is similar to ENSO, PDO tends to persist for decades rather than months with dominant periodicities at 15-25 and 50-70 years (Minobe, 1997; Mantua and Hare, 2002). Warm (positive) phases of PDO are associated with negative SST anomalies in the southwest Pacific that lead to positive winter temperature anomalies and higher-than-average precipitation totals in southwestern British Columbia and the Pacific Northwest. Cool PDO phases are associated with lower-than-average rainfall totals during the winter

months (Mantua et al., 1997; Chang et al., 2002; Bonsal and Shabbar, 2008; Abatzoglou, 2011).

The PNA pattern is an internal mode of atmospheric variability with alternating pressure patterns in the central Pacific Ocean and centres of action over western Canada and the southeastern United States (Latif and Barnett, 1994). It is characterized by out-of-phase atmospheric flows between the west coast of North America and eastern Pacific/southeastern USA (Yu and Zwiers, 2007). Its development is associated with episodes of atmospheric blocking introduced by high-pressure ridges in the eastern Pacific Ocean (Wallace and Gutzler, 1981; Bridgeman and Oliver, 2006). Along with the North Atlantic Oscillation (NAO), the PNA plays a crucial role in setting up winter temperatures in Pacific North America by creating strong pressure gradients off the coast of British Columbia (Wallace and Gutzler, 1981). Positive phases of the PNA are characterized by a strong AL, with southerly airflow along the west coast of North America and a high-pressure ridge over the Rocky Mountain cordillera (Wise et al., 2015). Negative phases of the PNA are associated with a weak AL with westerly zonal flows. While the Pacific storm track shifts southward during positive PNA phases, it shifts northward shifts during weaker phases (Yu and Zwiers, 2007).

There are clear relationships between climate oscillations and moisture delivery to southwestern British Columbia but our current understanding does not extend beyond the mid-20th century (Rodenhuis et al., 2009). While research highlights general changes between positive (warm) and negative (cool) phases of climate oscillations, most records are too short to understand how hydrological variables change over time and across phases. Longer-term understanding of spatial and temporal relationships between

dominant variables and hydroclimate are essential for the development of realistic policy and management strategies.

1.3 Research motivation

Present and future climate change poses a significant challenge for water resource management in western North America (Doll et al., 2015). Recent events in California offer an illustration of the economic, social, and ecological impacts of sustained droughts (Cook, 2019). Following five years of drought, reservoir storage in California decreased by upwards of 60% and many regions were left without running water (Cook, 2019). Hydroelectric power generation capacity was significantly reduced, necessitating an increased reliance on fossil fuels to supplement energy needs (Cook, 2019). Over 100-million trees died following drought-induced stress (Howitt et al., 2015), leading to a state-wide mortality event that continues to impact regional carbon and water cycles. While many ecosystem-services were also adversely affected, the related social impacts were psychological in nature and continue to be expressed by lingering health issues (Cochrane et al., 2004; Ding et al., 2011; Padhy et al., 2015; Kjellstrom et al., 2016).

While ongoing research focuses on past, present, and future trends of snowpack and streamflow in the western United States, there is only a limited understanding of the long-term hydroclimate state of southwestern BC. In a region where the water supply of many communities is reliant upon snowpack meltwater released during the spring and summer months, water shortages are certain if the winter snowpack is low or melts earlier in the year (Cayan et al., 2001; McCabe et al., 2004; Moore et al., 2010; Belmechari et al., 2015; Mote et al., 2018).

The downstream consequences of record low snowpack totals in 2014 and 2015 heightened water supply concerns in southwestern BC (River Forecast Centre, 2017). Uncertainty surrounds our understanding of how future climate change will impact the region's water supply, especially with expected reductions in annual snowpack totals (Mote et al., 2018). Developing an informed understanding of how the regional hydroclimate has varied in the past will provide the insights water resource managers require to improve current strategies and policies.

The purpose of this dissertation was first to examine how southwestern BC's hydroclimate varied prior to the instrumental record. Secondly, the research was intended to assess the long-term influence of low-frequency climate oscillations on that variability. The research objectives were to:

1. Develop multi-century reconstructions of snowpack and other hydroclimate-related variables in southwestern BC and determine their natural variability over the past few centuries;
2. Determine spatial and temporal relationships, synchrony, and variability of snowpack across southwestern BC, and;
3. Determine relationships between hydroclimate-related variables and climate oscillations generated from the Pacific Ocean and place our present understanding in a longer-term context.

1.4 Organization of dissertation

Following this chapter, Chapters 2, 3, 4, and 5 present the primary results of the dissertation. They are presented as individual manuscripts written and formatted for

refereed journal submission. Chapter 2 presents reconstructions of April 1 SWE over the past 300 years for continental and coastal regions experiencing different hydroclimate regimes in southwestern BC. Chapter 3 presents a regional 300-year dry-season (July-August) streamflow reconstruction for the Capilano and Seymour watersheds that provide 66% of the water supply for the 2.6-million residents of Greater Vancouver Regional District. Chapter 4 presents a long-term model of pre-instrumental April water level fluctuations in Harrison Lake over the past 300 years. Chapter 5 presents a regional-scale 300-year paleorecord of Chinook and Coho salmon escapement history within the Lower Fraser River watershed, and associates their associations to low-frequency Pacific Ocean teleconnections. The dissertation concludes with Chapter 6, where the main contributions and linkages between the different elements of the dissertation research are summarized, and ends with suggestions for future research.

Chapter 2: Snow Water Equivalent Variability Over Last 300 Years in Southwestern British Columbia Driven by Teleconnections

2.1 Article Information

Chapter 2 consists of a manuscript prepared for submission. The text and figures from the manuscript have been renumbered and reformatted for consistency within the dissertation.

2.1.1 Author names and affiliations

Bryan J. Mood[1*] and Dan J. Smith[1],

University of Victoria Tree-Ring Laboratory, Department of Geography, University of Victoria, British Columbia V8W 3R4, Canada.

*Corresponding Author Email: bjmood@uvic.ca

2.1.2 Author contributions

Mood developed the study, hypothesis, conducted and led field and laboratory work, statistical testing, wrote the manuscript, and produced all tables and figures. Smith provided funding for the research, provided guidance in formatting the study design, reviewed and edited the manuscript.

2.2 Abstract

Freshet contributions from melting seasonal snowpack are critical during hot, dry summer months for streamflow supply in southwestern British Columbia (BC), Canada. Recent below-average winter snow totals have generated cascading socioeconomic and ecological impacts that draw attention to the impending consequences of ongoing climate change. Within this region, knowledge of the year-to-year winter snowfall variability is

largely derived from a sparse network of short-duration (≤50 year) snow survey stations. In this paper, two long-term April 1 snow water equivalent (SWE) records were developed from living tree-ring chronologies. The dendrohydrological models accurately reconstruct April 1 SWE for coastal and continental regions to AD 1710 and 1725. The models demonstrate annual April 1 SWE dynamics in this region are strongly associated with negative (cold) phases of the Pacific Decadal Oscillation and the El Niño-Southern Oscillation, and show that coastal SWE dynamics demonstrate more year-to-year variability than in more continental settings. Continental SWE is also shown to be strongly associated with positive phases of the Pacific North American Oscillation while coastal SWE is not. The coastal SWE reconstruction identifies eleven significant step changes and continental SWE record illustrates eight step chances since the early 1700s. Both reconstructions contain generally synchronous step changes in the scale of annual SWE magnitudes. Two periods, between 1804-1821 and 1887-1927, suggest that coastal regions are more sensitive to minor changes in SWE when compared to continental areas on the leeward side of the BC Coast Mountains. The two models provide the first high-resolution description of April 1 SWE over the past 300 years in southwestern BC and offer significant insights for water resource policy makers and planners.

2.2 Introduction

Seasonal snowpack is a critical input to regional hydrologic dynamics in many regions of western North America. Storing winter precipitation that is released as meltwater during the spring and early summer freshet, these contributions provide runoff supplements at a time when the ecological, social, and industrial demands are highest

(Mote al., 2005, 2018; Rodenhuis et al., 2009). Snow is, however, vulnerable to changes in climate that influence both cover and depth (Abatzoglou, 2011; Mote et al., 2018). There is growing concern that the recent declines in April 1 SWE in the British Columbia (BC) Coast Mountains, Canada, are an outcome of shifting climates that are likely to persist (Rodenhuis et al. 2007; Déry et al. 2009, 2012; Mote et al., 2018).

In southwestern BC the water supply for many communities is dependent upon direct snowmelt contributions to streamflow and reservoir storage, as well as indirectly through contributions to groundwater recharge and throughflow (Eaton and Moore, 2010; Beaulieu et al., 2012; Olmstead, 2014; Koop et al., 2017). Record low April 1 SWE values in 2014 and 2015 contributed to summer-long water shortages in the Metro Vancouver area and emphasize the substantial water management challenges that potentially lie ahead for many communities in southwestern BC. With further reductions in mountain snowpack certain to result in increasingly severe and frequent summer streamflow droughts, focused research is required to describe the full range of natural variability in April 1 SWE and to understand the underlying relationships to long-term climate oscillations generated from the Pacific Ocean.

The instrumental record of winter snowfall variability in southwestern BC is derived from a sparse network of short-duration (≤50 year) snow survey stations (Rodenhuis et al., 2009; Mote et al., 2018). As short instrumental records provide only limited insight into long-term April 1 SWE variability, attempting to forecast future trends from these data for water supply management purposes is problematic (Rodenhuis et al., 2009). Short records lead to challenges in understanding whether recent low April 1 SWE values are ‘extreme’ relative to what has occurred in the past and whether the

assumed climatic relationships are stable over time. Most watersheds in the region have limited storage capacity and variability in their annual runoff depends primarily on broad-scale climate oscillations (Yu and Zwiers, 2007; Bonsal and Shabbar, 2008; Abatzoglou, 2011). Together several distinct climate oscillations act to enhance or diminish snow delivery during the winter (Rodenhuis et al., 2009) and influence snow availability into the summer.

In this chapter, April 1 SWE records extending over several centuries are reconstructed for southwestern BC from snow-sensitive Pacific silver fir (*Abies amabilis* Douglas ex J. Forbes) tree-ring chronologies. I use April 1 SWE records from coastal and continental regions to assess the influence of large-scale climate oscillations originating in the Pacific Ocean. The reconstructions provide the first high resolution descriptions of April 1 SWE over the past 300 years in southwestern BC, and are of immediate use to water resource managers charged with developing the strategies and policies required for adaptation to changing mountain snowpack.

2.3 Study Area and Research Background

The study area includes the Metro Vancouver area and the southern Pacific Ranges extending from Joffre Lakes to the Lower Fraser River within the southwestern BC Coast Mountains (Figure 2.1). Coastal settings in this region are moderated by proximity to the Pacific Ocean and experience short, cool summers and long, wet winters. Average air temperatures above 1000 m above sea level (asl) remain below 0°C for 0 to 5 months of the year and above 10°C for 1 to 3 months of the year (Pojar et al., 1991; Kottek et al., 1996). The study area includes BC's wettest ecological zone, where

Figure 2.1: Study area map showing the location of the tree-ring chronologies (white triangles) and snow survey stations (continental = white square with centre black square; coastal = white circle with cross) incorporated into this research. Note that coastal snow survey stations are located in regions with high orographic precipitation (western areas), while continental snow survey stations are in the Coast Mountains rain shadow (east).

precipitation totals range between 1700 to 5000 mm/yr and 70% falls as snow and/or rain during the winter months (Pojar et al., 1991; Spry et al., 2014) (Figure 2.2A). Most precipitation falls as a result of orographic interactions on the windward slopes of the Pacific Ranges. Precipitation totals decrease substantially on the eastern slopes, where persistent rain shadow conditions prevail (Pojar et al., 1991; Kottek et al., 2006; Church and Ryder, 2010; Moore et al., 2010) (Figures 2.2A and 2.2B).

The impact of decreased winter snow delivery and storage in southwestern BC is demonstrated by below-average April 1 SWE totals in recent years. In 2015, the 2014-2015 winter snowpack in the region was 49% of normal in January and reached a record low of 0% by June 1st (River Forecast Centre, 2017). Low April 1 SWE resulted in a severe summer streamflow drought and led to depleted water supplies necessitating use restrictions for the 2.6-million people residing in Metro Vancouver. Highlighting the importance of mountain snowpack for sustaining summer streamflow, the depleted runoff had cascading socioeconomic and ecological consequences that drew attention to the impending consequences of ongoing climatic changes in this region (Cook et al., 2018, 2019; Lledo et al., 2018).

Previous research within the study area identified a causal relationship between inter-annual/-decadal climate variability generated by atmosphere-ocean interactions originating in the Pacific Ocean and April 1 SWE variability (Sellars et al., 2008; Spry et al., 2014). These interactions include those characterized by the Pacific Decadal Oscillation (PDO), the El Niño-Southern Oscillation (ENSO), and the Pacific North American (PNA) pattern (Rodenhuis et al., 2009; Abatzoglou, 2011; Mote et al., 2018). Warm/cool phase relationships between April 1 SWE and ENSO show that an average

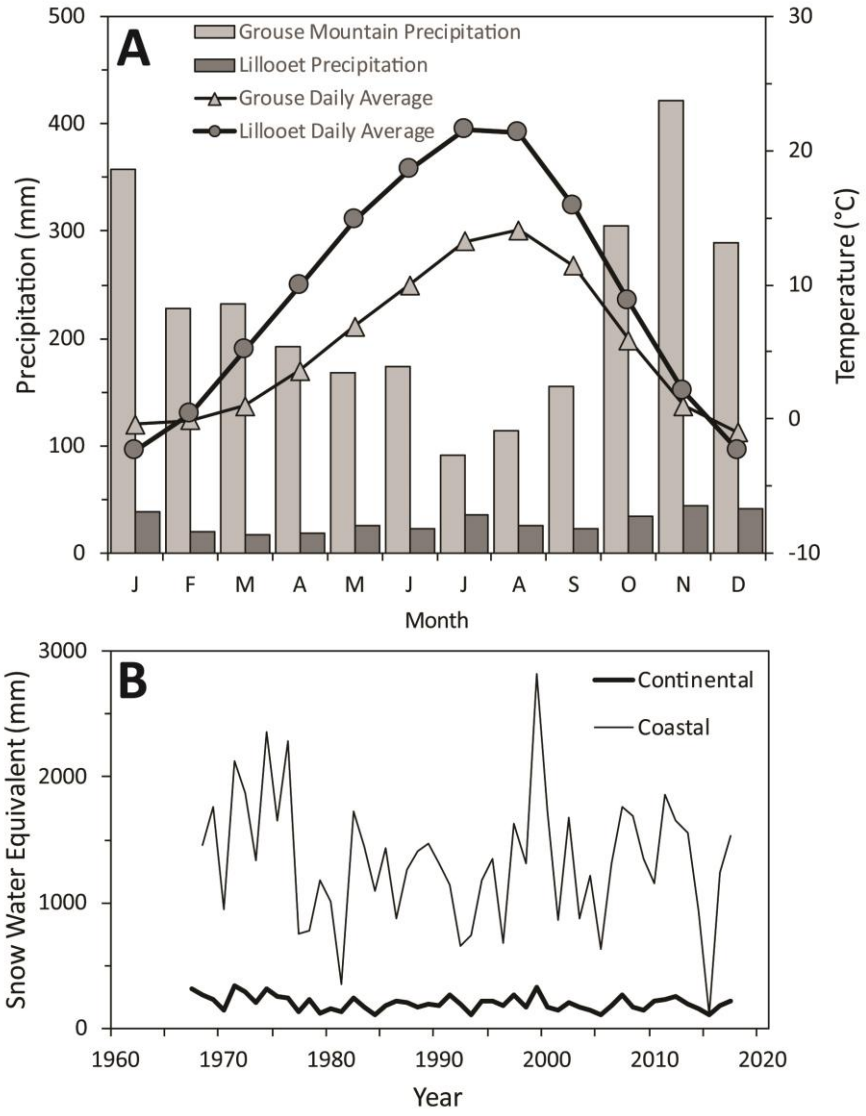

Figure 2.2: General climate information for the study region. (A) Climate normals (1981-2010) for coastal (Grouse Mountain, station ID: 1105658) and continental (Lillooet, station ID: 1114627) regions (ECCC, 2017) stations; (B) time series of average coastal and continental April 1 SWE records (River Forecast Centre, 2017).

variability of greater than 30% characterized the interval between 1951 and 2007 (Rodenhuis et al., 2009).

Relationships between April 1 SWE and PDO variability are less pronounced over the instrumental period, with only a 15% change in snowpack noted between warm/cool phases (Rodenhuis et al., 2009). The PDO is a large-scale climate system that influences the surface climate and hydrology of western North America (Whitfield et al., 2010). Phase changes in the PDO have a significant influence on the overall hydroclimate of southwestern BC (Moore and McKendry, 1996; Rodenhuis et al., 2009). The PDO is typically coupled with ENSO when describing changes in temperature and precipitation regimes associated with their variability (Whitfield et al., 2010). Temperature fluctuations are readily apparent between warm and cool phases of the PDO (Kiffney et al., 2002; Whitfield et al., 2010), and the PDO shift in 1976-1977 resulted in an abrupt change in average winter temperatures (Hartman and Wendler, 2005) throughout BC (Stahl et al., 2006; Fleming and Whitefield, 2010). In the BC South Coast region, precipitation is greater during cool phases of PDO and less during warm phases (Kiffney et al., 2002; Stahl et al., 2006). In southwestern BC, April 1 SWE is also greatly influenced by PDO (Moore and McKendry, 1996; McCabe and Dettinger, 2002). During cold phases of PDO the greatest seasonal SWE values are characteristically recorded on April 1st, while during warm phases lower than average SWE values are common (Moore and McKendry, 1996).

No statistical relationships between April 1 SWE and PNA are confirmed in the BC Coast Mountains, although it has been associated with the seasonal snow line elevation (Abatzoglou, 2011). The PNA does affect the overall hydroclimate of

southwestern BC through changes in winter storm intensity and frequency (Rodenhuis et al., 2009). Positive PNA results in anomalously high freezing levels and reduced snow coverage (Abatzoglou, 2011). April 1 SWE values are lower in continental regions when compared to coastal settings. I associate the different values with orographic precipitation patterns between coastal (windward; higher overall precipitation) and continental (leeward; rain shadow region) regions. This association suggests that continental locations experience more significant influences from the PNA, as snowfalls in these locations are more reliant on freezing level relationships than are coastal settings.

2.4 Methods

Pacific silver fir (PSF) is a conifer tree common to maritime climate regions in Pacific North America (Crawford and Oliver, 1990). Normally found at sites with deep, well-drained soils, stands of PSF are often found in association with other high-elevation tree species including western hemlock (*Tsuga heterophylla* (Raf.) Sarg.), mountain hemlock (*Tsuga mertensiana* (Bong.) Carr.), yellow-cedar (*Chamaecyparis nootkatensis* D. Don), and western red cedar (*Thuja plicata* Donn ex D. Don) (Pojar et al., 1991).

Snowpacks that persist into the summer months truncate the growing season of many tree species located close to the altitudinal treeline (Ettinger et al., 2011). At high elevation sites, PSF tends to be found where precipitation totals range from 750 to over 6500 mm/yr (Crawford and Oliver, 1990). Near the upper limit of its altitudinal range, the radial growth of PSF is dependent upon soil moisture derived from melting seasonal snow (Crawford and Oliver, 1990), and is also known to be limited by late-lying snowpack that persist into the growing season (Ettinger et al., 2011). Mountain hemlock

trees shares similar environmental requirements and, due to their strong, negative relationship to April 1 SWE, were previously used to reconstruct SWE dynamics in Pacific North America (e.g., Peterson and Peterson, 2001; Pederson et al., 2011; Coulthard et al., 2016; Welsh et al., 2019). By comparison, PSF has seen limited use as an environmental proxy, although it demonstrates strong statistical relationships to April 1 SWE at high elevation in the area (Ettinger et al., 2011).

2.4.1 Tree-ring data

PSF tree ring samples were collected with 5.2-mm increment borers at high-elevation sites in southwestern BC in the summer of 2016 using standard dendrochronological techniques (Fritts, 1976; Speer, 2010). After air drying and processing, the annual ring widths were measured at the University of Victoria Tree-Ring Laboratory (UVTRL) using a WinDendro™ digital measurement system (v. 2016a; Guay et al., 1992). Supplementary PSF tree-ring chronologies were downloaded from the International Tree-Ring Data Bank (ITRDB; NOAA, 2017). Site-specific tree-ring chronologies were constructed by converting the ring width measurements to standardised indices using the R package dplR to remove growth related trends (Bunn, 2008) with a 50-year cubic smoothing spline. The site-specific chronologies were subsequently combined with the supplementary chronologies using the bi-weight robust mean method to create a regional PSF chronology (Briffa and Melvin, 2011).

2.4.2 Snow water equivalent data

April 1 SWE data from manual snow survey stations were accessed using the online portal managed by the BC River Forecast Centre (River Forecast Centre, 2017). April 1 SWE data exceeding 45 years in length were downloaded and quality checked.

Where missing data was identified, the long-term mean was used to replace the null value. Data were separated into coastal and continental SWE based geographic location and linear associations between snow survey sites. Individual coastal and continental SWE sites were combined using a principal component analysis (PCA), with only principal components loadings >10% used for further analysis, to extract the underlying regional variance (Table 2.1). Coastal SWE_{PC} only used the first component for analysis, and successfully explained 89% of the variance in the time series. Continental SWE_{PC} was similar, using the first component of the analysis which explained 69% of the underlying variance (Table 2.1). The data could not be combined into a larger PCA because the two groups were not linearly associated.

2.4.3 Climate oscillation data

Proxy PDO and PNA records were downloaded from the NOAA Paleoclimate website (NOAA, 2017). The datasets were developed from tree-ring records that have repeatedly been linked to winter hydroclimate variability in western North America (D'Arrigo and Wilson, 2006; Trouet and Taylor, 2009; Asong et al., 2018). The PDO reconstruction provides an estimate of the Asian expression of the phenomenon, while the PNA reconstruction provides a winter period record (D'Arrigo and Wilson, 2006; Trouet and Taylor, 2009). While the Asian expression of the PDO is similar to observed trends in Pacific North America, it has different ENSO-related modulating characteristics.

2.4.4 Model estimation

Coastal and continental April 1 SWE records (coastal and continental SWE_{PC}) were correlated to the tree-ring data and climate indices using Pearson's correlations to

Table 2.1: Descriptive information of manual snow survey stations used in this study. Records were collected from the River Forecast Centre (2017) website. Two regions were targeted for reconstruction: (1) continental and (2) coastal. Continental locations are located east of the Pacific Ranges and characterized by lower average snowpack. Coastal stations are located in the Pacific Ranges and characterized by much greater snowpack averages (229 vs. 1367 SWE). Station ID is associated with River Forecast Centre designations; coordinates (latitude and longitude) are in decimal degrees; elevation is rounded to the nearest 10 m above sea level; mean April 1 SWE is calculated across the whole time series; span is the length of continuous April 1 SWE measurements from each station; length is the total number of years available for analysis; PCA loading represents the explanatory power of the first principal component from analysis.

Station ID	Latitude (DD)	Longitude (DD)	Elevation (m asl)	Mean April 1 SWE	Span (years AD)	Length (years)	PCA Loading
Continental							
1C05	50.70	-122.62	1720	609	1952-2014	62	
1C06	50.91	-121.82	1214	44	1955-2014	59	
1C09A	50.50	-120.98	1550	98	1958-2014	56	
1C14	50.78	-122.79	1400	167	1963-2014	51	
1C19	50.46	-121.05	1640	123	1967-2014	47	
2G06	49.50	-120.80	1490	334	1960-2014	54	
Continental SWE_{PC}							89%
Coastal							
1D08	49.58	-122.32	1195	1529	1968-2014	46	
1D10	49.83	-122.06	1555	1360	1968-2014	46	
3A01	49.38	-122.08	1130	1231	1936-2014	78	
3A09	49.46	-123.03	880	1479	1946-2014	68	
3A10	49.37	-122.96	1010	1235	1945-2014	69	
Coastal SWE_{PC}							68%

determine initial relationships between the variables. A pool of predictors was developed for the both coastal and continental April 1 SWE records and input through a multiple linear regression to provide a best-fit model. Model selection was based on adjusted R^2, multicollinearity (variance inflation factor or VIF), autocorrelation at lag 1 (Durbin-Watson or DW), and cross-validation statistics (Reduction of Error or RE).

2.4.5 Analysis of the reconstruction

The coastal and continental SWE_{PC} models selected for reconstruction were compared to measured winter ENSO, PDO, and PNA climate oscillations (October of the previous year to March) to reveal low-frequency influences on snowpack over the reconstructed and instrumental periods. A difference-of-correlations test was conducted on both the measured coastal and continental SWE_{PC} records, as well as on the reconstructed values, against positive and negative phases of the selected climate oscillations. Where only one phase illustrates a statistical relationship with the models, it indicates non-stationary (alterations in significance over time) responses to the specific oscillation.

A Morlet wavelet analysis using the R-package WaveletComp (Roesch and Schmidbauer, 2015) was used to illustrate fluctuations in power over the length of the full reconstruction period and to determine the average variability. An intervention analysis was conducted to determine significant long-term changes in reconstructed averages. The intervention analysis used a 30-year moving window to highlight where significant differences occurred between the preceding and proceeding 15 years of year *t* using a two-sample t-test. Periods of change in the long-term mean were calculated as departures from the average SWE_{PC} value over the full reconstruction.

2.5 Results

Five PSF chronologies were selected for use as coastal and continental SWE_{PC} proxies (Table 2.2). All the chronologies were significantly correlated to each other and were combined into a single index using regional curve standardisation (PSF_R). Consolidating the site-level tree-ring records enhanced the explanatory power and possible reconstruction period to the interval from 1710-2015. The indices had RBARs ranging from 0.350 to 0.491 and were significantly correlated to coastal and continental SWE_{PC} (Table 2.3). The selected climate oscillation reconstructions (PDO and PNA) span from 1565-1988 and 1725-1999, respectively (D'Arrigo and Wilson, 2006; Trouet and Taylor, 2009). The PDO reconstruction was significantly correlated with coastal SWE_{PC} while both PDO and PNA reconstructions were related to continental SWE_{PC} (Table 2.3).

Two models were developed from the coastal and continental SWE_{PC} records. The first principal component for coastal and continental SWE_{PC} were identified for reconstruction and used PSF_R, PDO, and PNA as predictors:

$$Coastal\ SWE_{PC} = -1.75*PSF_R + -0.34*PDO + 1.67$$

$$Continental\ SWE_{PC} = -2.41*PSF_R + -0.59*PDO + 0.22*PNA + 2.56$$

where coastal SWE_{PC} is the first component April 1 SWE from coastal manual snow survey stations; PSF_R is the regional Pacific silver fir tree-ring width chronology; PDO is a Pacific Decadal Oscillation reconstruction from D'Arrigo and Wilson (2006); continental SWE_{PC} is the first component April 1 SWE from continental manual snow

survey stations; and PNA is a Pacific-North American pattern tree-ring reconstruction from Trouet and Taylor (2009).

The Coastal SWE_{PC} reconstruction extends from 1710 to 1988 and explains 50.7% of variance, accounting for lost degrees of freedom, in the first principal component. The model has a DW statistic of 1.86, VIF of 1.62, and F-Ratio of 13.3 (Table 2.4). It was successfully cross-validated using the LOO method (RE = 0.41) indicating the model is robust. Regression and cross-validation statistics are shown in Table 2.4 and a time plot of the actual, modelled, and cross-validated coastal SWE_{PC} is shown in Figure 2.3A. The full reconstruction is illustrated in Figure 2.4A.

The continental SWE_{PC} reconstruction extends from 1725 to 1988 and explains 73.1% of variance, accounting for lost degrees of freedom, in the first principal component. The continental SWE_{PC} model has a DW statistic of 2.27, VIF of 1.095, and F-Ratio of 23.63 (Table 2.4). The model was successfully cross-validated using the LOO method (RE = 0.57) suggesting that the model is robust. Regression and cross-validation statistics are shown in Table 2.4 and a time plot of the actual, modelled, and cross-validated continental SWE_{PC} are shown in Figure 2.3B. The full reconstruction is shown in Figure 2.4B.

Both reconstruction models and calculated SWE_{PC} were tested against large-scale climate teleconnections originating in the Pacific Ocean. A difference-of-correlations test between ENSO, PDO, and PNA reveal significant relationships between Continental SWE_{PC} and negative ENSO, positive PDO, and positive PNA while Coastal SWE_{PC} was only associated with negative phases of PDO (Table 2.5).

Table 2.2: Times series information. Species/type are bold and italics represents time series used as predictors in the reconstruction. Tree-ring site numbers in brackets are ITRDB codes. The Pacific silver rir regional index (PSF_R) was developed by combining the five site-level chronologies used a bi-weight robust mean method (Briffa and Melvin, 2011). Climate oscillation indices were collected from NOAA (2017) for teleconnections that are known to influence the overall hydroclimate of western North America. RBAR is the average value across whole index; length is the span of years used for reconstruction. For tree-ring series, the length used for reconstruction is used only for where EPS > 0.85.

Study Site (Site No.)	Source	Lat (DD)	Lon (DD)	Elev. (m asl)	RBAR	Length
Pacific Silver Fir						
Deek's Lake	This study	49.52	-123.21	1050	0.350	1696-2015
Callaghan Lake	This study	50.18	-123.13	975	0.360	1696-2015
Seymour (CANA107)	Dobry et al. (1996)	49.52	-123.07	1000	0.491	1686-1992
Hurricane Ridge (WA081)	Schweingruber et al. (1991)	46.15	-122.15	1200	0.372	1698-1983
Mt. St. Helens (WA082)	Schweingruber et al. (1991)	47.98	-123.47	1200	0.437	1648-1980
Pacific Silver Fir Regional (PSF_R)					0.540	1648-2015
Teleconnections						
Pacific Decadal Oscillation (PDO_{DW})	D'Arrigo and Wilson (2006)					1565-1988
Pacific-North American (PNA_{TT})	Trouet and Taylor (2009)					1725-1999

Table 2.3: Pearson correlations between model parameters used in the reconstruction. All values shown are significant (*p<0.01*).

Time Series	Coastal SWE_{PC}	Continental SWE_{PC}
Pacific Silver Fir Regional (PSF_R)	-0.67	-0.68
Pacific Decadal Oscillation (PDO_{DW})	-0.67	-0.78
Pacific North American (PNA_{TT})		-0.66

Table 2.4: Reconstruction, cross-validation, and descriptive statistics. D-W = Durbin-Watson Statistic; VIF = variance inflation factor; SE = standard error; RE = reduction of error; RMSE = root mean squared error; CV = coefficient of variance.

Reconstruction	R^2	Adj. R^2	D-W	VIF	SE	F-Ratio
Coastal	0.55	0.51	1.87	1.57	0.70	13.30
Continental	0.76	0.73	2.27	1.10	0.59	23.60

Cross Validation	RE	RMSE
Coastal	0.41	0.66
Continental	0.57	0.54

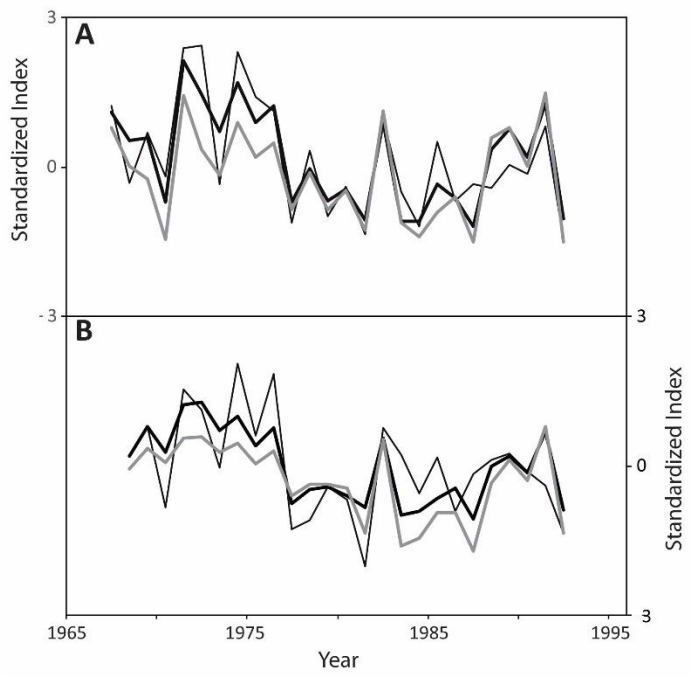

Figure 2.3: Time plot of calculated April 1 SWE principal components (thin black line), modelled (thick black line), and cross-validated (thick grey line) records of (A) coastal and (B) continental.

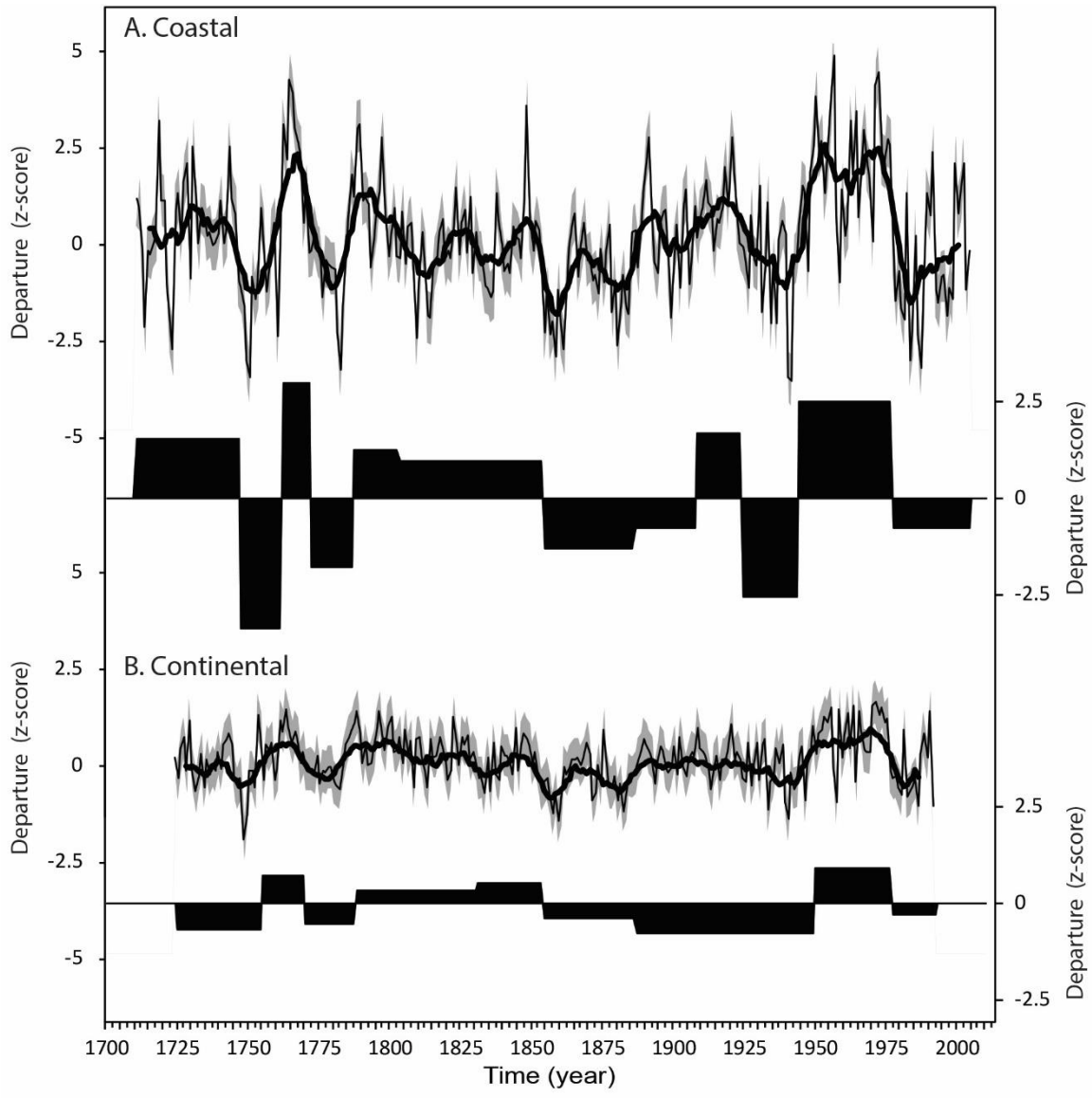

Figure 2.4: Time plot of reconstructed (A) coastal and (B) continental SWE plotted as departures from average (z-scores; thin black line) with a 5-year running mean (thick black line) and error (grey area) calculated from the cross-validation RMSE. Black-filled areas illustrate long-term changes in the mean value as identified by intervention analysis. Black-filled areas above 0 indicate long-term above average conditions while below indicate below average conditions. Step changes were detected using a two-sample t-test on the previous and future 15 years for year *t*. Long-term averages were calculated as the mean value between intervention years.

Table 2.5: Difference-of-correlations test results for Coastal and Continental SWE_{PC}. Climate oscillation indices were grouped into negative and positive values then correlated to both the calculated and modeled Coastal and Continental SWE_{PC}. Values shown are *p<0.05* while **bold** values indicate *p<0.01*. Where only one of two teleconnection phases have a significant relationship, it illustrates the possibility of a non-stationary response.

	Coastal SWE_{PC}	Modeled Coastal SWE_{PC}	Continental SWE_{PC}	Modeled Continental SWE_{PC}
Negative PDO (13)	-0.62	-0.63	-0.65	**-0.74**
Positive PDO (13)				
Negative ENSO (12)		**-0.80**	-0.65	-0.58
Positive ENSO (14)				
Negative PNA (12)				
Positive PNA (14)			-0.65*	-0.66

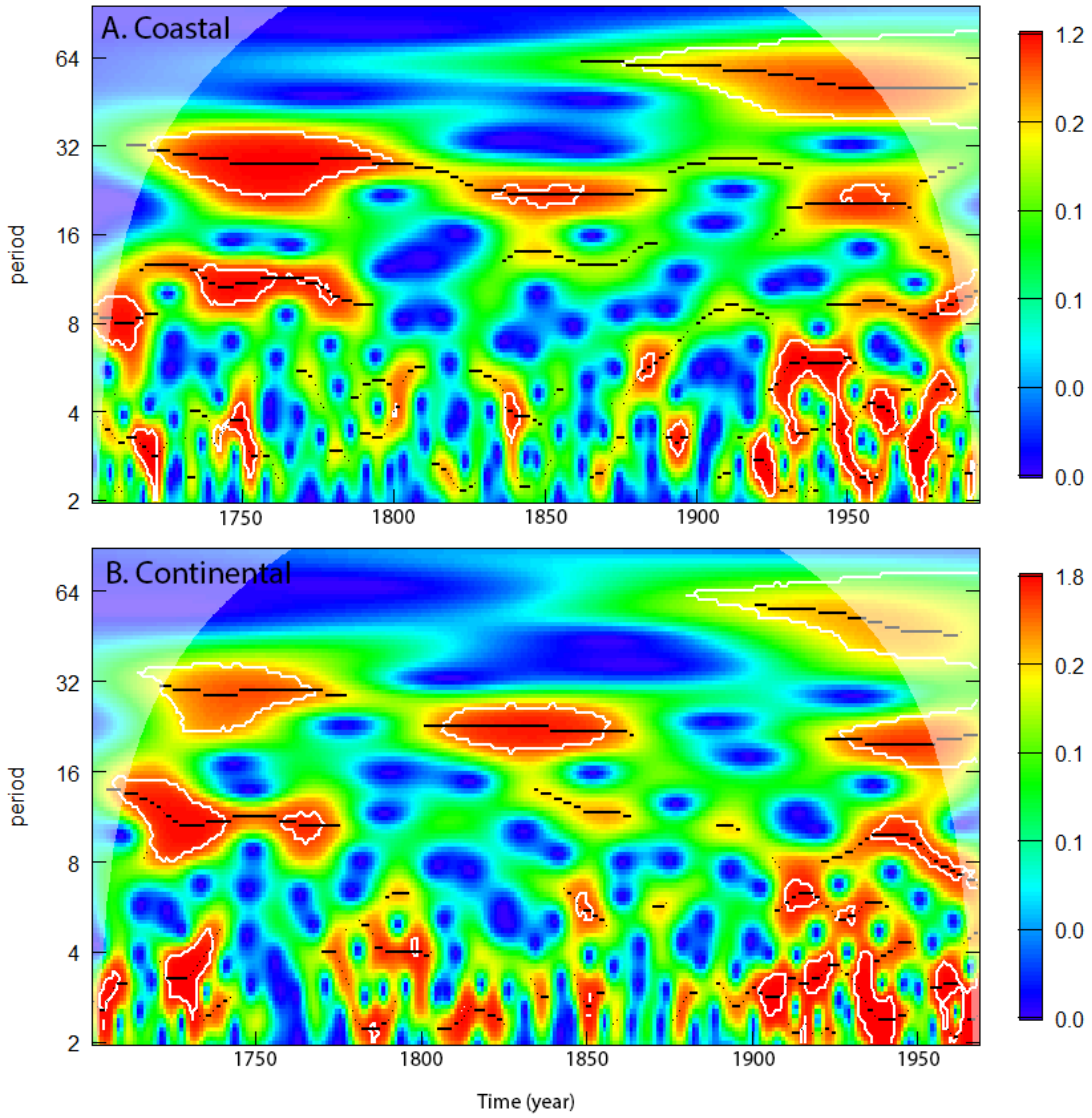

Figure 2.5: Morlet wavelet power spectrums of the coastal (A) and continental (B) SWE_{PC} reconstructions. The y-axis represents Fourier periods while the x-axis represents time. White enclosed areas represent a 95% confidence interval where significant wavelengths in the series are detected. Black lines represent power spectrum ridges and highlight nonstationary, significant frequencies across the time series. The lower contrast, or faded, areas on the left and right extremes of each figure represent areas outside of the analysis that is susceptible to zero padding effects. Note that A and B figures have different x-axes due to differing reconstruction lengths between the coastal and continental models.

Intervention analysis highlights periodic step-changes in the long-term average over time. Coastal PC_{SWE} was below average from 1746-1761, 1771-1786, 1853-1907, and 1923-1943 and above from 1710-1745, 1762-1770, 1787-1852, 1908-1942, and 1945-1992 (Figure 2.4). Continental PC_{SWE} was below average from 1725-1754, 1770-1787, and 1854-1949, and above average from 1755-1769, 1788-1853, and 1950-1992 (Figure 2.4). Morlet wavelet analyses highlight low-frequency decadal variability over the length of both records between 8 and 12 years (Figure 2.5).

2.6 Discussion

2.6.1 Model summary

The reconstruction models accurately estimate the first principal component of April 1 SWE for coastal and continental regions of southwestern BC. As is the case elsewhere in western North America (Mote et al., 2018), the findings highlight that April 1 SWE is associated with: (1) total winter precipitation; (2) winter temperature; (3) spring temperature, and; (4) climate oscillation phases. The model predictors indirectly account for these variables.

PSF_R variability constructed using regional curve estimation serves as a proxy for April 1 SWE. Deep or late-lying snowpacks typically result in a truncated growing season that leads to narrow growth rings (Ettinger et al., 2011). While many high-elevation reconstructions in western North America use mountain hemlock as a proxy for snowpack and/or summer streamflow (e.g., Pederson et al., 2011; Wood et al., 2011; Coulthard et al., 2016), PSF are more climatically-sensitive, retain a stronger climatic signal, and demonstrate coherent growth synchrony across populations at a broader range

of high-elevations (Ettinger et al., 2011). The robustness of PSF in this reconstruction serves to highlight its potential as an April 1 SWE proxy, thereby providing an independent record for validating reconstructions in the study region that currently rely solely upon mountain hemlock tree-ring records.

The analyses identify similar PDO influences on both SWE_{PC} reconstructions. Specifically, cool PDO phases have a strong effect on both coastal and continental SWE_{PC}. While this is likely influenced by the use of PDO as a predictor in our model, no significant relationships to positive/warm PDO phases were detected (Table 2.5). Cool PDO phases typically result in above average snowfall and lower than normal winter temperatures in this region (Rodenhuis et al., 2009). These impacts are consistent with equivalent streamflow regime-shifts associated with PDO phase changes in western Canada (Whitfield et al., 2010). Streamflow reconstructions derived from snow-sensitive trees on Vancouver Island, BC, serve to further emphasize importance of PDO-generated phase changes to regional hydroclimate regimes (Coulthard et al., 2016). These conditions allow the winter snowpack to persist into the growing season and reduce the annual radial growth increment of Pacific silver fir.

Positive PNA has a strong, negative relationship with regional SWE_{PC} records, but is a significant only in the continental SWE_{PC} reconstruction. PNA is known to influence freezing-levels in the study region and the association to the continental reconstruction is assumed related to the location and elevation of the stations included in our analyses. On average, the stations were 350 m higher than coastal stations (average of 1502 and 1154 m asl, respectively). This finding suggests that the overall effect of freezing level elevations on snowpack is an important indicator of overall supply and that

the importance of this relationship may have been underestimated in previous studies as many focus on PDO and ENSO (e.g., Rodenhuis et al., 2009; Fleming et al., 2016; Bevington et al., 2019).

2.6.2 Description of the reconstructed records and comparison

Both the coastal and continental SWE_{PC} reconstructions reflect similar intervals of high and low values. While there is general agreement between the two reconstructions, two intervals of below and above average values in coastal SWE_{PC} highlight important differences. During the interval from 1804-1821, continental SWE_{PC} had a negative trend but remained above the 300-year average. Following this, continental SWE_{PC} values remained close to the long-term average from 1887-1927, while coastal SWE_{PC} displayed an interval of above-average values from 1887-1896 and 1905-1927 (Figure 2.3).

While similar long-term trends of below and above average intervals are apparent in the reconstructions, the amplitude between the two series differs and is likely associated with the higher degree of variability associated with coastal manual snow survey stations. Average coastal April 1 SWE ranges from 1231 to 1529 SWE, while continental SWE values range from 44 to 609 SWE. The difference in the principal component SWE analyses are believed representative of natural variability in the two geographically distinct locations.

The intervention analysis shows that both SWE_{PC} reconstructions display comparable intervals of regional-scale variability over the duration of the reconstruction, with coastal SWE_{PC} exhibiting more statistically significant changes in the long-term average than continental SWE_{PC} (Figure 2.4). Notably, both reconstructions demonstrate synchronous above average values from 1788-1853. Following this interval, values

remained below the long-term average until 1908 and 1949 within the coastal and continental SWE_{PC} reconstructions, respectively.

Coastal SWE_{PC} displays a greater number of shifts away from the long-term average during early portions of the reconstruction. Reconstructed values were above the long-term mean until 1746, when below average values persisted from 1747-1761. Following this, above average SWE occurred from 1763-1771 until 1772-1787, when lower than average SWE conditions prevailed. Continental SWE_{PC} displays similar trends, with below average values until 1754 after which the SWE was above the mean from 1755-1769, after which SWE values remained below the long-term average until 1853.

2.6.4 Teleconnection influences

Both SWE_{PC} reconstructions illustrate significant relationships to Pacific Ocean teleconnections. While both use PDO as a predictor and continental SWE_{PC} uses PNA, there are notable differences between the observed and reconstructed records and phases of ENSO, PDO, and PNA. A significant relationship was identified between negative ENSO (La Niña) and both SWE_{PC} reconstructions that is likely caused by negative temperature and positive precipitation anomalies through the region (Stahl et al., 2006).

All the reconstructed and observed SWE records are significantly associated with negative phases of PDO (Table 2.5). Similar to ENSO variability, negative PDO typically results in negative temperature trends and to minor changes in precipitation totals in the study region (Stahl et al., 2006). Continental SWE_{PC} was significantly associated to positive phases of the PNA (Table 2.5). During the winter months, PNA influences overall precipitation delivery to the study region. Nonetheless, it's most important

attribute is the documented influence on freezing-level elevation (Abatzoglou, 2011). Changes to the freezing-level elevation have a substantial impact on snowpack totals and, thus, the potential end-of-winter snowpack storage. Small changes to the freezing-level elevation may have substantial impacts on the total snow available for melt during the hot, dry summer months where it is needed to sustain baseflow for regions downstream (Bealieu et al., 2002).

2.6.5 Usefulness in water policy and management

Winter snowpack contributes to streamflow runoff and water supply in southwestern BC during dry summer months (Moore et al., 2010). April 1 SWE contributes to the overall summer supply for many of the streams in the region (Bealieu et al., 2002). Developing an understanding of the underlying climate drivers is essential for water managers and my reconstructions provide a long-term perspective on April 1 SWE variability that highlights the underlying cyclical variability. Coastal SWE_{PC} displays more variability than continental SWE_{PC} and appears more sensitive to annual changes in winter precipitation and temperature. While continental regions may experience little change to SWE totals, small changes to either precipitation or temperature may have dramatic effects on end-of-season SWE in coastal regions.

These proxy records provide a better understanding of both the frequency and magnitude of low- and high-April 1 SWE over the last 300 years, changing the context of low SWE events in 2014 and 2015 by illustrating that average April 1 SWE levels in both regions have been lower than those we are experiencing today. I expect that predictive models incorporating these longer-term findings will enable water managers to anticipate the probability of future April 1 SWE and freshet dynamics. While additional variables

are needed in order to robustly forecast nival streamflow dynamics (e.g., spring and summer temperature), the long-term relationships revealed by this research should assist water managers charged with planning for future water shortages.

While rising temperatures are sure to impact April 1 SWE and overall water supply in southwestern BC, other impacts should be considered. I demonstrate that teleconnection influences are significantly associated with coastal and continental SWE_{PC} variability and should be taken into account for water management purposes. This association has been documented previously (Rodenhuis et al., 2009), with these findings emphasizing that this relationship is stable over time and is teleconnection phase dependent. This discovery provides information useful for proposing future water management and policy strategies.

2.7 Conclusions

I provide a 300-year perspective of April 1 SWE variability in southwestern BC, where my analyses show that SWE has varied more in coastal settings than in continental areas. Coastal SWE_{PC} was shown to alternate between above- and below-average values more frequently than continental SWE_{PC}. My reconstructions demonstrate that there are important differences associated with region-level climate paleorecords. Coastal SWE_{PC} was much more variable than continental SWE_{PC}, with the two additional intervals between 1804-1821 and 1887-1927 highlighting that the coastal regions may be more prone to changes in snowpack compared to continental areas on the leeward side of the BC Coast Mountains.

Climate oscillations generated from the Pacific Ocean region significantly influence long-term April 1 SWE variability throughout southwestern BC. La Niña, PDO, and PNA demonstrate significant relationships to continental SWE_{PC}, with only the PDO was found to be associated with coastal SWE_{PC}. ENSO and PDO play a vital role in the amount of snow delivered during the winter months, while PNA influences freezing-level elevation and, therefore, the amount of snow that can be stored at high altitudes.

Although I document periodic SWE_{PC} changes in both coastal and continental regions, climate change impacts on the seasonal snowpack are evident for southwestern BC. Highlighted by zero-percent-of-normal June 1 SWE and subsequent drought in 2015, even small changes to total snowpack in the BC Coast Mountains will have substantial impacts on the overall water supply for a region that supply is struggling to meet demand. The two 300-year records of the first principal component of April 1 SWE for southwestern BC provide a long-term perspective of natural snowpack variability and offer insights essential for water resource managers in this region.

Chapter 3: Post-1976 shortages in Greater Vancouver Regional District water supply unprecedented in past 300 years

3.1 Article Information

Chapter 3 consists of a manuscript prepared for submission to a referred journal. The text and figures have been renumbered and reformatted for consistency with the dissertation.

3.1.1 Author affiliations

Bryan J. Mood[1*] and Dan J. Smith[1]

[1] University of Victoria Tree-Ring Laboratory, Department of Geography, University of Victoria, British Columbia, Canada V8W 3R4

* Corresponding Author Email: bjmood@uvic.ca

3.1.2 Author contributions

Mood developed the study, hypothesis, conducted and led field and laboratory work, statistical testing, wrote the manuscript and produced all tables and figures. Smith provided funding for the research, provided guidance in formatting the study design, reviewed and edited the manuscript.

3.2 Abstract

Recent summer water shortages in Metro Vancouver necessitated use restrictions. Likely resulting from recent alterations in the regional snowmelt timing and rising summer temperatures, the persistence of these conditions over the next century poses a significant challenge for water supply management decisions. To understand the magnitude of recent drought events in the context of those that happened in the past, a

dendrohydrological reconstruction of regionalised July-August streamflow to 1711 for Metro Vancouver's Capilano and Seymour watersheds. July-August streamflow in these watersheds relies on snowmelt released by winter snowpack. I used the annual ring widths of mountain hemlock (*Tsuga mertensiana* (Bong.) Carr.) and Pacific silver fir (*Abies amabilis* Douglas ex J.Forbes) trees exhibiting a relationship to the seasonal snowpack as proxies for streamflow in a regression model. The model indicates that more multi-year, below-average, streamflow departures occurred during the instrumental record than over the 300 years modeled by the reconstruction. El Niño-Southern Oscillation (ENSO) was strongly associated with both reconstructed and measured streamflow for the study region. Similarly, the Pacific Decadal Oscillation (PDO) demonstrated strong statistical relationships with measured streamflow in the region. Over the duration of the reconstruction, significant decadal and multi-decadal periodicities were observed and may be linked to PDO. The research places the Metro Vancouver water supply in a longer-term context than was previously possible and provides a basis for advancing water supply planning decisions in the context of a rapidly changing climate.

3.3 Introduction

Summer streamflow droughts in 2014, 2015, and 2017 highlight the potential hydrological impacts of future climate changes on the Metro Vancouver area (Cohen et al., 2011). There is growing recognition of the need to understand the natural variability of basins contributing to the Metro Vancouver water supply (Milly et al., 2008; Olmstead, 2014; Koop et al., 2017). While hydrological modelling based on historic

instrumental records provides Metro Vancouver resource managers with some awareness of the possible range of streamflow variability (Rodenhuis et al., 2009), developing long-term strategies for the basins draining the Metro Vancouver watersheds is challenging (Poff et al., 2016). The relatively short instrumental records that exist may not capture the full range of natural streamflow variability (Metro Vancouver, 2011; 2017) and the high relief of the Metro Vancouver water supply basins render them susceptible to changes in timing and magnitude of the annual spring freshet (Murphy et al., 2015).

Dendrohydrology uses tree rings as a proxy for streamflow and can provide robust, annually-resolved records that extend hydrological information back centuries (Meko and Woodhouse, 2010). Most studies focus on large watersheds and typically target reconstruction of annual and seasonal streamflow records (Meko and Woodhouse, 2010; Margolis et al., 2011; Sauchyn et al., 2014; Sauchyn and Ilich, 2017; Stagge et al., 2018). The findings of these studies have been incorporated into water management strategies developed in the southwestern United States (Meko et al., 2001; Woodhouse and Lukas, 2006), western interior Canada (Sauchyn et al., 2014), and internationally (Pederson et al., 2011). Increasing attention is, however, being given to the reconstruction of monthly hydroclimatic data and its presentation in formats useful for water resource managers (Coulthard et al., 2016; Stagge et al., 2018).

Most dendrohydrological reconstructions focus on resolving streamflow records within arid and semi-arid regions where moisture sensitive tree species provide a ready proxy for annual changes in water availability (Meko and Woodhouse, 2010). In British Columbia (BC), recent tree-ring investigations expand upon climate-growth relationships to reconstruct streamflow records for watersheds susceptible to summer drought (Hart et

al., 2010; Starheim et al., 2013a; Coulthard and Smith, 2015; Coulthard et al., 2016). While these studies collectively provide a perspective on streamflow variability in BC that extends centuries into the past, they focus exclusively on watersheds where summer streamflow is sustained by snowmelt and/or glacier meltwater contributions. In contrast, the watersheds contributing to the Metro Vancouver water supply contain hybrid streams where only snowmelt and rainfall combine to make significant contributions to the annual streamflow regime (Eaton and Moore, 2010). Small changes in the seasonal snowpack, timing of the spring freshet, or alterations to the seasonal temperature regime may have significant impacts on summer streamflow within these watersheds (Mote et al., 2005; Stewart et al., 2005; Rodenhuis et al., 2009).

In this paper, I develop a reconstruction model of July-August streamflow for watersheds supplying Metro Vancouver using snowpack-sensitive mountain hemlock (*Tsuga mertensiana* (Bong.) Carr.) and Pacific silver fir (*Abies* amabilis Douglas ex J. Forbes) tree-ring chronologies. Based on statistical relationships established between the chronologies and instrumental records, I reconstruct 300-years of July-August streamflow history for the Capilano and Seymour rivers supplying 66% of the water to the Metro Vancouver area y. These dendrohydrological findings augment the instrumental records and provide information critical to developing an understanding of long-term streamflow variability within the Metro Vancouver water supply area.

3.4 Study Area

The Metro Vancouver water supply area is located on the windward side of the Pacific Ranges, BC Coast Mountains. The Capilano, Coquitlam, and Seymour watersheds

are the primary water supply source and are located in the North Shore Mountain range overlooking Metro Vancouver (Figure 3.1). The headwaters of all three watersheds are located in steep mountain basins, with runoff descending into U-shaped valleys and flowing into Georgia Strait. The Capilano River watershed originates at 1650 m asl on Capilano Mountain and covers a 196 km^2 area (Table 3.1). The river joins with 11 tributary streams before draining into the Capilano Reservoir at 160 m asl (Table 3.1). The Seymour River watershed originates at 1668 m asl on Obelisk Peak and flows through a long, narrow valley covering an area of 124 km^2, before draining into Seymour Reservoir (Table 3.1). The Coquitlam River watershed is located directly north of the City of Coquitlam and is the largest of the three Metro Vancouver watersheds. It covers an area 205 km^2 and contains Coquitlam Lake, a large naturally occurring lake that spans most of the north-south length of the Coquitlam watershed (Figure 3.1).

Metro Vancouver's water supply area is regulated by the Metro Vancouver Drinking Water Management Plan (DWMP) and serves as the source of municipal drinking water for the region, as well as for providing water used for fisheries habitat, recreation, culture and heritage, and power generation (Metro Vancouver, 2011). The DWMP is committed to using water more efficiently, "so that the supply stretches out into the future even as the region's population continues to grow" (Metro Vancouver, 2011:1). In 1905, the BC Government obtained a lease on the Capilano Watershed for water supply purposes (Metro Vancouver, 2017). Similar leases for the Seymour and Coquitlam watersheds were established in 1906 and 1942, respectively. The watersheds have experienced only minimal logging and road building activity associated with infrastructure access and development. While the water supplied by the watersheds is

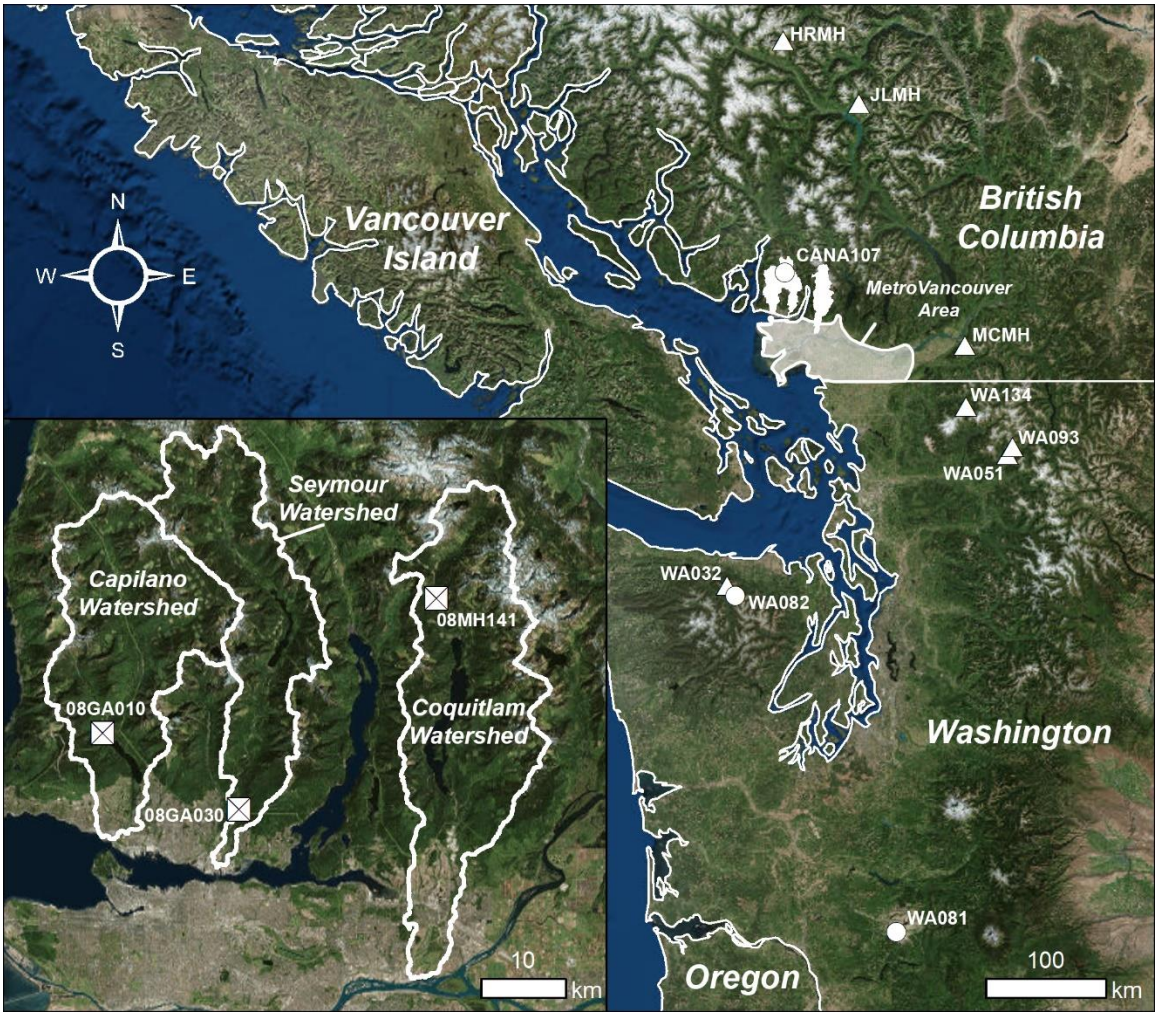

Figure 3.1: Study site map showing the location of the Capilano, Seymour and Coquitlam watersheds. Squares with X's indicate locations of hydrometric stations; circles represent Pacific silver fir tree-ring chronology locations; triangles represent mountain hemlock tree-ring chronology locations.

Table 3.1: Instrumental data information. Streamflow data was collected from the Water Survey of Canada (2017); climate information was collected from Environment and Climate Change Canada (2017), and; snow survey information was collected from River Forecast Centre (2017).

Type	Location	Station ID	Span	Coordinates (Decimal Degrees)	Drainage Area above gauge (km^2) / Elevation (m asl)
Streamflow Gauge	Capilano	08GA010	1914-2018	49.40, -123.14	173 km^2
	Seymour	08GA030	1928-2018	49.40, -122.98	179 km^2
Climate Station	Grouse Mountain	1105658	1971-2018	49.38, -123.08	1100 m asl
Snow Survey	Grouse Mountain	3A01	1936-2018	49.38, -123.08	1130 m asl

expected to meet the region's needs until approximately 2050 (Metro Vancouver, 2011), the consequences of anticipated climate changes pose significant long-term challenges to managing these water resources (Rodenhuis et al., 2009). A temperate, fully-humid, climate characterises the Metro Vancouver watershed area (mean annual temperature 5.2°C, 1981-2010 normal; ECCC, 2017) (Kottek et al., 2006) (Figure 3.2A), with the majority of annual precipitation resulting from orographic interactions and storms generated in the Pacific Ocean during the winter months (Berkelhammer and Stott, 2008; Spry et al., 2014). Typical of regional precipitation regimes, precipitation totals on the windward mountain slopes range from 1300 mm/year near the ocean to over 4000 mm/year at summit elevations (Jacob and Weatherly, 2003; Church and Ryder, 2010). Nearly 75% of this precipitation falls during the winter months (November to March) primarily as a result of low-pressure systems that bring snow to higher altitudes (>800 m asl) and rain to lower elevations (<300 m asl). Mid-elevation locations (300-800 m asl) are susceptible to rain-on-snow events throughout the winter (Abatzoglou, 2011; Spry et al., 2014). In contrast, most summers are dry and characterised by limited precipitation (Loukas et al., 1996).

The high relief and mixed (rain and snow) precipitation regime characterising the watersheds results in high monthly streamflow totals in November to January from rainfall and in April to June from snowmelt, with summer streamflow declining until October (Figures 3.2A and 3.2C). The instrumental records emphasise that the timing and magnitude of the annual freshet displays considerable year-to-year variability (Moore et al., 2010). Following the spring freshet, a significant proportion of the summer baseflow

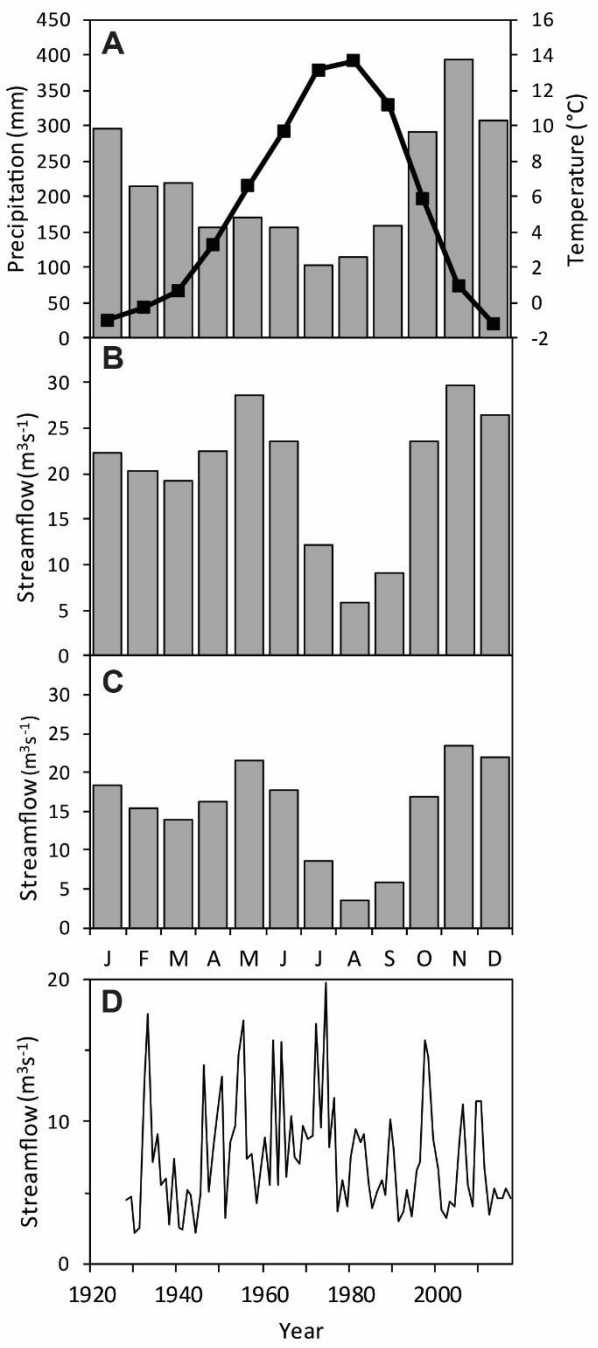

Figure 3.2: (A) Climate normal (1981-2010) for Grouse Mountain (Station ID: 1105658); monthly streamflow averages for the (B) Capilano (08GA010) and (C) Seymour (08GA013) watersheds; and, (D) combined July-August streamflow record of the Capilano and Seymour watersheds (Sources: ECCC, 2017; WSC, 2017).

is tied to the emergence of shallow groundwater sourced to melting snow. Snow-derived summer streamflow is typically lowest in July and August (Figure 3.2B and 3.2C) when it averages 7.5 m^3s^{-1} for the Capilano and Seymour watersheds with a relatively high variance (16.0 m^3s^{-1}) over the length of the common period (1958-2017) (Figure 3.2B). Over the instrumental period, minimum July-August streamflow occurred in 1944 (2.1 m^3s^{-1}) and the maximum recorded streamflow occurred in 1974 (19.7 m^3s^{-1}) (Figure 3.2D). These hydroclimatic conditions suggest that summer streamflow droughts in the Metro Vancouver area are directly associated with shallow spring snow and early spring freshets (Moore et al., 2010).

The hydroclimatic character of the Metro Vancouver watersheds is influenced by inter-annual and -decadal climate variability generated by atmospheric-ocean interactions in the Pacific Ocean (Sellars et al., 2008; Spry et al., 2014). The most significant of these interactions include those described by the El Niño-Southern Oscillation (ENSO), the Pacific Decadal Oscillation (PDO), and the Pacific North American (PNA) pattern. Their inherent variability is known to influence temperatures, as well as the timing and magnitude of precipitation events, throughout southwestern BC during the winter months (Bonsal and Shabbar, 2008; Abatzoglou, 2011).

ENSO is a naturally occurring phenomena of ocean temperature variability centered in the equatorial Pacific Ocean that displays phase changes every six to 18 months (Bridgman and Oliver, 2006). Alternating between two phases (positive/El Niño and negative/La Niña), it has an impact on winter precipitation patterns across the Pacific Ranges (Rodenhuis et al., 2009).

The PDO is a large-scale climate system that influences the surface climate and hydrology of western North America (Whitfield et al., 2010). It is often characterised as a long-lived ENSO-like pattern of Pacific climate variability derived from sea surface temperature interactions with the atmosphere (Mantua et al., 1997). Similar to ENSO, phase changes in the PDO have substantial impacts on moisture delivery and winter snowpacks in south coastal BC (Moore and McKendry, 1996; Rodenhuis et al., 2009). During positive (warm) or negative (cold) phases of the PDO, winter snowpack totals are impacted significantly, resulting respectively in increases or decreases in snowmelt contributions to summer baseflow (Rodenhuis et al., 2009). Negative (cold) phases of PDO are associated with below-average temperature and positive precipitation anomalies during the winter months, with positive phases correlated to above-average temperatures and negative precipitation regimes (Mantua et al., 1997; Moore et al., 2009). The relationship between the PDO and streamflow is complex, as it relies specifically on the hydrologic regime of a given watershed (Mote, 2003; Hamlet et al., 2005; Whitfield et al., 2010). In this study, I examine hybrid watersheds that typically have higher-than-average flows in May-August during cool phases of the PDO due to increased snowpack and below-average temperatures (Fleming et al., 2007).

The PNA is a quadripolar pattern associated with alternating pressure systems in the Pacific Ocean, as well as to centres of action over western Canada and the southwestern United States (Wallace and Gutzler, 1981; Latif and Barnett, 1994). While lacking a well-defined periodicity, the PNA is influenced by both the PDO and ENSO, and has impacts on freezing level elevations across the Pacific Northwest (Yu and Zwiers, 2007; Abatzoglou, 2011).

3.5 Methods

Dendrohydrological reconstructions have been successful in dry, continental environments where the annual radial growth of a tree can be directly associated with seasonal moisture deficits (Fritts, 1976; Belcmecheri et al., 2015). In BC, these moisture-deficit settings are primarily restricted to the interior of the province (Moore et al., 2010), where tree rings have been used to reconstruct summer (July-August) flow records extending back over 300 years for the Atnarko, Chilko, and Skeena rivers (Hart et al., 2010; Starheim et al., 2013a).

Small, temperate, conifer rainforest dominated watersheds, such as those characterising windward slopes in coastal BC, are problematic for dendrohydrological analysis due to the absence of moisture-limited tree species. Despite this difficulty, research on Vancouver Island and in the Pacific Northwest identified the snowpack sensitivity of high elevation stands of mountain hemlock and Pacific silver fir trees (Smith and Laroque, 1998; Gedalof and Smith, 2001; Ettinger et al., 2011). While the relationship between the radial growth of mountain hemlock trees and snowpack is well documented (Smith and Laroque 1998; Marcinkowski et al., 2015; Coulthard et al., 2016), the association of Pacific silver fir growth to April 1 SWE is limited to observations describing the initiation of cambial growth following snowmelt at high elevation locations (Hansen-Bristow, 1986; Ettinger et al., 2011). Coulthard and Smith (2015) and Coulthard et al. (2016) were able to develop proxy streamflow records for rivers on Vancouver Island using climate-growth relationships of mountain hemlock trees.

3.5.1 Tree-ring data

In Pacific North America, the radial growth of trees located close to treeline is most often restricted by cool air temperatures that inhibit photosynthetic production during the growing season (Fritts, 1976; Smith and Laroque, 1998; Ettinger et al., 2011), and/or by cold soil temperatures that impedes soil nutrient uptake during the early months of cambial expansion (Delucia, 1986; Peterson and Peterson, 2001; Marcinkowski et al., 2015). However, the radial growth of some subalpine tree species is also physically limited by late-lying snow, which delays the initiation of the growing season (Smith and Laroque, 1998; Coulthard et al., 2016). In addition, the rapid melting of late-lying mountain snow typically leads to greater overland flow and less soil moisture recharge resulting in overall poor conditions for primary and secondary tree growth (Fritts, 1976).

In this paper, I capitalise on the annual growth records of mountain hemlock and Pacific silver fir trees exhibiting April 1 SWE-related growth responses. I developed a regional network of tree-ring chronologies from high-elevation mountain hemlock and Pacific silver fir records archived in the International Tree-Ring Data Bank (ITRDB). Age-related growth trends were removed using the R package dplR to allow inferences to be made on climate-related radial growth variability (Bunn, 2008). The site chronologies were detrended using a cubic smoothing spline with a 50-year wavelength in order to remove age-related growth trends and low-frequency variability. For many trees, environmental conditions in the previous year predetermine radial growth in the following year (Fritts, 1976). This physiological response was removed by using ‘residual’ detrended series that had zero-autocorrelation and are statistically compatible to the streamflow records targeted for reconstruction.

Each residual series was first examined for a relationship to the seasonal snowpack using a Pearson's correlation to April 1 SWE recorded by a local manual snow survey station (Table 3.1). April 1 SWE records were used in the analyses, as data from the other winter months were sporadic or of considerably shorter duration. It is also considered an accurate estimate for winter-season total precipitation (Bohr and Aguado, 2001). Based on identified relationships between the selected series and April 1 SWE, several approaches were considered for reconstruction. First, individual series were examined to isolate specific climate-growth relationships. Second, regional series were developed by combining individual tree-ring series into a single series using the bi-weight robust mean method (Fritts, 1976). Finally, individual site series were used in a principal component analysis to extract the underlying variability between study sites where 5 or more site-level chronologies existed. Only components accounting for >10% of the underlying variability were used for this study.

3.5.2 PDO data

The PDO is the leading principal component of sea surface temperature in the North Pacific Ocean (20°N and northward) and used to infer decadal trends of temperature and precipitation (Mantua et al., 1997; Rodenhuis et al., 2009; Whitfield et al., 2010). Reconstructed winter PDO values were retrieved from the NOAA National Climatic Data Center website (D'Arrigo and Wilson, 2006). While developed for the eastern North Pacific Ocean, the record demonstrates significant correspondence with teleconnection indices in Pacific North America (D'Arrigo and Wilson, 2006).

3.5.3 Hydrological data

Mean monthly streamflow records for the Metro Vancouver watersheds were retrieved from the Water Survey of Canada website (WSC, 2017). Following Coulthard et al. (2016), the records were seasonalized by summing July and August data (m^3s^{-1}) to obtain total discharge at the presumed end of the nival-based flow season. Pre- and post-regulated records for both basins were tested for significant differences although prior engagement with Metro Vancouver Water Services indicated records representative of natural variability (Mayer, *personal communication*). Following this, streamflow records from the Capilano (1914-2018) and Seymour (1929-2018) were normalized for basin area, and were then combined to obtain an average July-August record extending from 1929 to present (Q_{JA}). The Coquitlam Watershed streamflow record was not used in further analysis because of insufficient length (1982-2018) and gauged data accounted for a small component of the drainage area. September was excluded from our analysis as variability is primarily derived from rain rather than snow.

3.5.4 Climate analysis

Climate variables influencing summer streamflow were determined through correlation of Q_{JA} to monthly and seasonal climate records. To assess the relationship between snowmelt and streamflow, I tested relationships of Q_{JA} to current year April 1 SWE records. Similarly, correlations between April 1 SWE and the tree-ring data were examined to reveal shared relationships.

3.5.5 Reconstruction model

A dendrohydrological reconstruction model was developed using a multiple linear regression of Q_{JA} data in year *t* on candidate predictors in year *t* and *t-1*. Lagged

predictors were entered to allow for tree-ring information of previous years to inform climate conditions in a given year. Several streamflow models were developed based on different predictors, with each evaluated based on its explanatory power (adjusted R^2), autocorrelation (Durbin-Watson; DW), multicollinearity (variance inflation factor; VIF), uncertainty (standard error of the estimate; SE), the significance of the regression equation (*F*-ratio), and cross-validation success (reduction of error; RE). I targeted Q_{JA} as it has the overall lowest flow values during dominantly nival contribution months of streamflow.

3.5.6 Analysis of model

The statistical properties of the overlap interval in the instrumental and reconstructed records were compared with one another, as well as to measured streamflow. This procedure allowed for an assessment of the model capacity to approximate the gauged streamflow record. Extreme high- and low-streamflow years were derived from the 95^{th}- and 5^{th}-percentile thresholds as calculated from the full reconstruction period.

Associations between the reconstruction and ENSO, PDO, and PNA were also investigated. A difference-of-correlations test was used to determine whether negative or positive phases of the teleconnections were statistically associated with the measured and reconstructed values. Second, the R-package WaveletComp was used to conduct a wavelet power spectrum analysis of the reconstructed streamflow record to illustrate fluctuations in power modes over time (Roesch and Schmidbauer, 2015). Finally, an intervention analysis over the full reconstruction period was completed to detect any long-term changes in mean Q_{JA}. Intervention years were selected by using a 30-year

moving window to identify periods where there was a significant difference between the first and last 15 years using a two-sample t-test. Periods of step change were calculated as a significant departure from the reconstructed mean.

3.6 Results

3.6.1 Data

Five mountain hemlock (MH) and three Pacific silver fir (PSF) tree-ring chronologies were selected for use (Table 3.2). While only one of these tree-ring chronology sites was located within the Metro Vancouver water supply area, both tree species are known to be sensitive to regional-scale climate (Gedalof and Smith, 2001; Speer, 2010). The mountain hemlock chronologies were all significantly correlated and were combined using a principal component analysis (PCA) representative of underlying radial growth variability. Only the first component was used from the PCA (PC_{MH}) in this study. Consolidating the five chronologies enhanced the explanatory power of the model but restricted the reconstruction period to 1711-1992 (Table 3.2). The three PSF chronologies were similarly significantly correlated to one another and were combined using a bi-weight robust mean into a single regional series extending from 1648 – 1992 (Table 3.2). The PSF chronologies were not used in a PCA due to the limited number of available chronologies (<5).

The five MH chronologies used for the PCA had RBARs ranging from 0.313 to 0.428, while the three PSF series RBARs range from 0.372 to 0.491 (Table 3.2). All the chronologies were significantly correlated to April 1 SWE ($p<0.01$) from the closest

Table 3.2: Times series information. Species/type are italicized and bold represents time series used as predictors in the reconstruction. Mountain hemlock PC (PC_{MH}) was developed by conducting a principal component analysis (PCA) on the five site-level chronologies listed. Pacific silver fir did not have a sufficient number of sites to conduct PCA (<5) and site-level chronologies were combined into regional chronologies using a bi-weight robust mean method (Briffa and Melvin, 2011). Climate oscillation indices were collected from NOAA (2017) for teleconnections that are known to influence the overall hydroclimate of western North America. [a] = correlations among tree-ring series collected from each site; [b] = only the length of the tree-ring index where the expressed population signal (EPS) was ≥0.85 is documented; [c] = RBAR is the average value across whole index where EPS was ≥0.85 and PC loading is the total explained variance from PCA analysis.

Time Series Name (Code)	Inter-series correlations [a]	Coordinates (Decimal Degrees)	Elevation (m asl)	Length [b]	RBAR/PC Loading [c]
Mountain hemlock					
Oakes Peak (WA051MH)[1]	0.520	48.63, -121.37	1140	1610 - 1992	0.313
Thornton Lakes (WA093MH)[2]	0.602	48.67, -121.33	1370	1706 - 1992	0.379
Heather Meadows (WA134MH)[3]	0.492	48.87, -121.68	1310	1685 – 2006	0.313
Joffre Lake (JLMH)[4]	0.607	50.34, -122.48	1550	1711 - 2012	0.428
Mount Cheam (MCMH)[5]	0.593	49.17, -121.69	1390	1637 - 2000	0.384
Mountain Hemlock PC (PC_{MH})				**1711 - 1992**	**69.3%**
Pacific silver fir					
Mt. St. Helens (WA081)[6]	0.645	46.16, -122.15	1200	1648 – 1980	0.437
Seymour Watershed (CANA107)[7]	0.662	49.52, -123.04	1000	1686 – 1992	0.491
Hurricane Ridge (WA082)[6]	0.618	47.93, -123.41	1560	1698 – 1983	0.372
Regional Pacific Silver Fir (PSF)	**0.651**			**1648 – 1992**	**0.402**
Climate Reconstruction					
Pacific Decadal Oscillation (PDO_{DW})[8]				**1700 – 1980**	

[1] Graumlich and Brubaker (1986); [2] Peterson and Peterson (2001); [3] Bunn (2012); [4] Wood et al. (2011); [5] Johnson and Smith (2010); [6] Schweingruber et al. (1991); [7] Dobryand Klinka (1996); [8] D'Arrigo and Wilson (2006)

Table 3.3: Correlations between series used in the reconstruction model and snow water equivalent (SWE) from the closest proximity station and regionalised streamflow. All values are significant (*$p<0.01$*)

Time Series	April 1 SWE	July-August Streamflow
Mountain hemlock Principal Component (PC_{MH})	-0.48	-0.45
Pacific Decadal Oscillation (PDO)	-0.19	-0.55
Pacific silver fir (PSF)	-0.51	-0.47
July-August Streamflow (Q_{JA})	0.35	

proximity manual snow survey station and composite Q_{JA} record (Table 3.3). The selected PDO reconstruction (PDO_{DW}) was also significantly correlated to both April 1 SWE and Q_{JA} (Table 3.3).

3.6.2 Reconstruction model

The following model was identified for reconstruction:

$$Q_{JA} = 1.73 + (-0.20 * PC_{MH}) + (-1.51 * PSF) + (0.33 * PDO_{DW})$$

where: Q_{JA} is the normalized average of July-August streamflow for the Capilano and Seymour watersheds; PC_{MH} is the first principal component of the combined mountain hemlock tree-ring index network for southwestern British Columbia and PSF is the regional record of Pacific silver fir growth in the region, and; PDO_{DW} is a reconstruction of PDO by D'Arrigo and Wilson (2006).

The reconstruction spans the period from 1711 to 1992 and explains 47% of Q_{JA} variance, accounting for lost degrees of freedom (Table 3.4). The reconstruction model has a DW statistic of 1.84, VIF of 1.091, and F-Ratio of 19.58 (Table 3.4). Regression, descriptive, and cross-validation statistics are shown in Table 3.4. The model was successfully cross-validated using the LOO method (RE = 0.09). A time plot of actual, modelled, and cross-validated Q_{JA} is shown in Figure 3.3. July-August streamflow was hindcast over the length of the tree-ring records following successful identification and cross-validation of the model (Figure 3.4).

Table 3.4: Reconstruction, cross-validation, and descriptive statistics. D-W = Durbin-Watson Statistic; VIF = variance inflation factor; SE = standard error; RE = reduction of error; RMSE = root mean squared error.

Reconstruction	R^2	Adj. R^2	D-W	VIF	SE	F-ratio
	0.49	0.47	1.84	1.091	0.67	19.58
Cross-Validation	RE	RMSE				
	0.09	0.65				

Table 3.5: Difference-of-correlations tests for measured ENSO, PDO, PNA values against measured and reconstructed regional streamflow. **Bold** values indicate *p<0.05*; **Bold, underlined** indicates *p<0.01*. Where only one teleconnection phase is significantly related to Q_{JA}, it illustrates the possibility of a non-stationary response.

		Reconstructed Q_{JA}			Measured Q_{JA}		
	Teleconnection Phase						
Season	*Sample Size*	ENSO	PDO	PNA	ENSO	PDO	PNA
DJF	Positive	**0.31**	**0.60**			**-0.35**	
	n	57	47			47	
	Negative		**0.54**		**-0.40**		
	n		45		37		
MAM	Positive	**0.45**		**0.44**			
	n	58		20			
	Negative	**0.26**			**-0.55**	**-0.33**	
	n	64			30	39	
JJA	Positive		**0.72**				
	n		45				
	Negative		**0.65**	**-0.53**	**-0.40**	**-0.43**	
	n		47	21	35	43	
SON	Positive		**0.53**				
	n		42				
	Negative	**0.30**	**0.50**		**-0.39**	**-0.48**	
	n	63	50		34	48	
Annual	Positive	**0.39**	**0.85**				
	n	58	46				
	Negative	**0.29**	**0.82**	**0.48**	**-0.56**	**-0.48**	
	n	64	46	22	36	45	

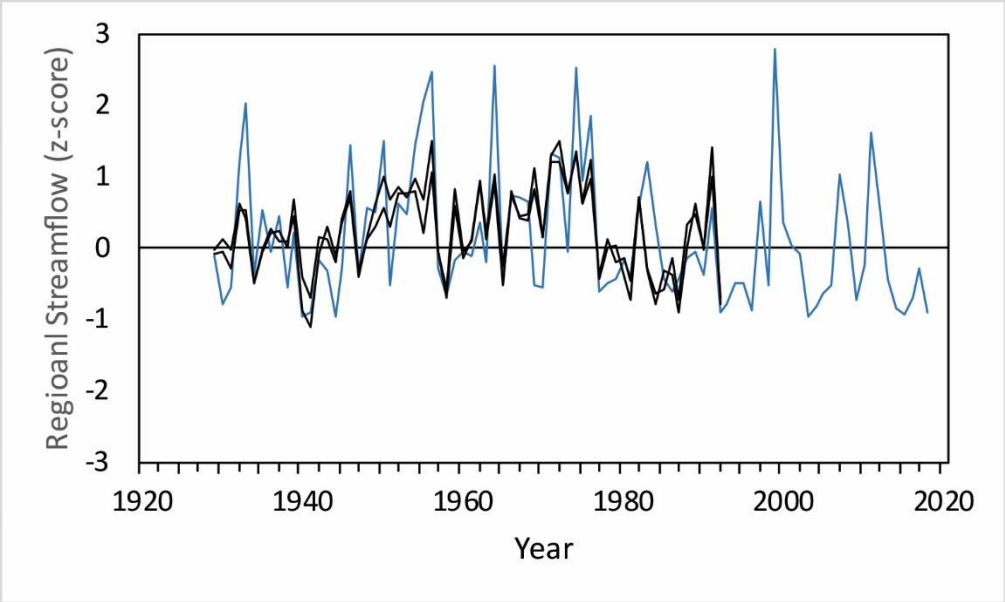

Figure 3.3: Time plot of the measured (blue), reconstructed (thick black), and validation (thin black) Q_{JA} records from the model calibration.

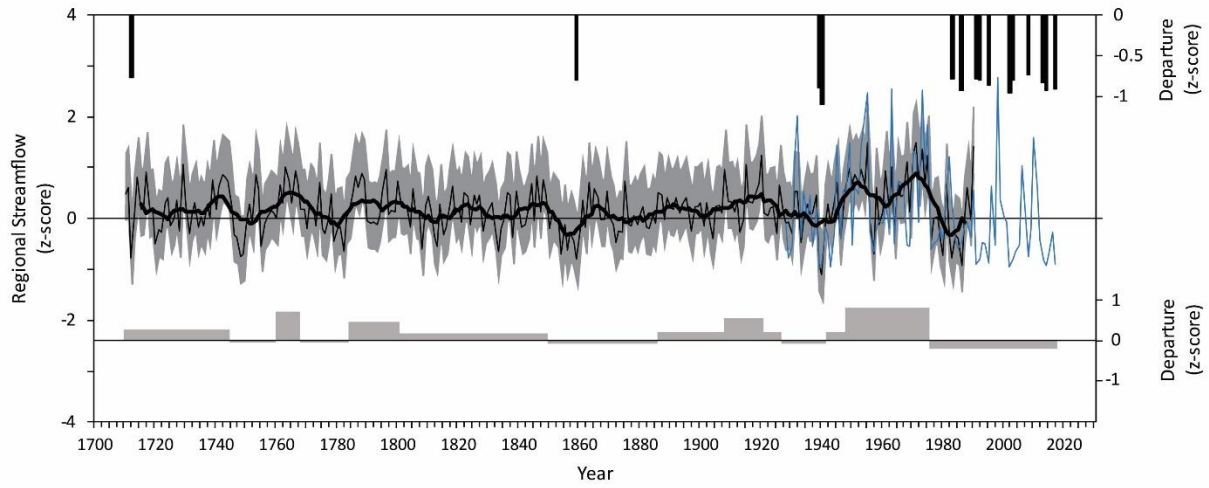

Figure 3.4: Time plot of reconstructed regional streamflow (z-scores; thin black line) with a 10-year running mean (thick black line) and gauged data (blue line). Error associated with the reconstruction is presented as the grey area surrounding the data and calculated using RMSE from the validation. The black histograms (top) represent 5th-percentile Q_{JA} for the reconstruction. The grey-filled area below the reconstruction represents changes in the long-term mean. Grey-filled (bottom) areas above 0 indicate long-term above average conditions while below indicate below average conditions. Step changes from one long-term mean to another are where significant intervention years were detected using a two-sample t-test between the previous and future 15-years at year *t*. Intervention averages were calculated as the mean value between intervention years.

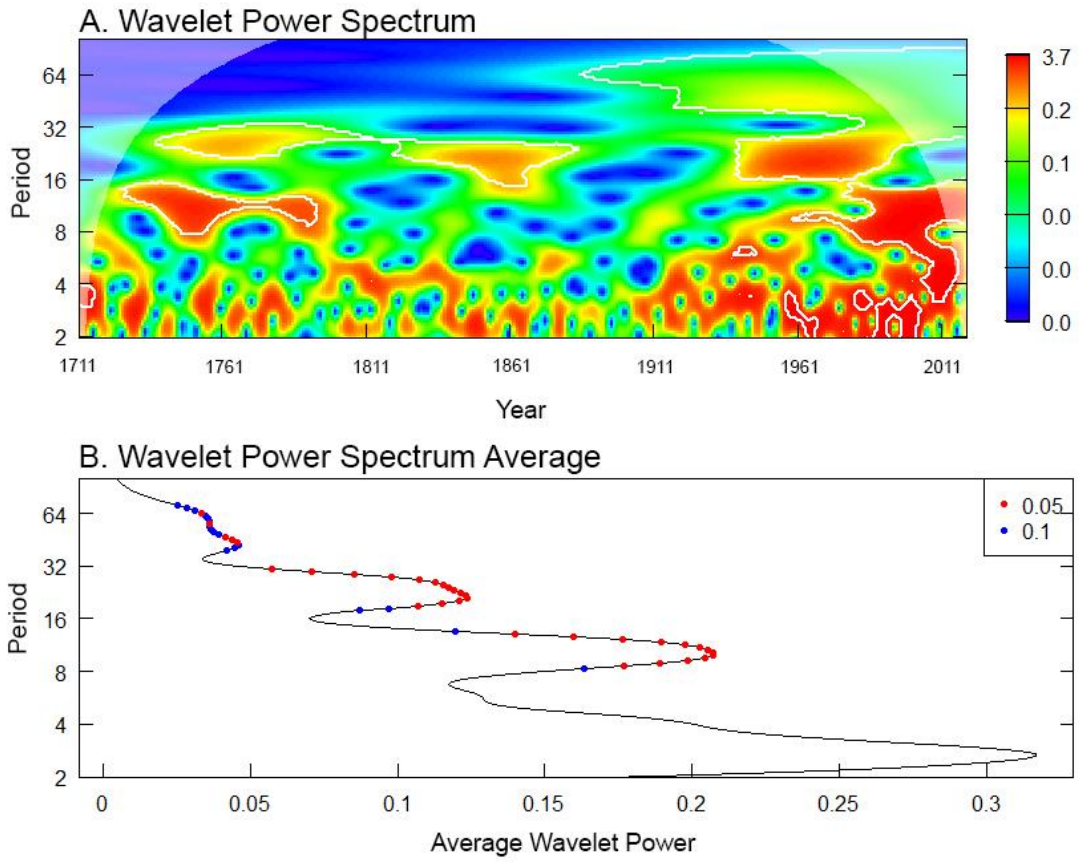

Figure 3.5: (A) Wavelet power spectrum of the proxy streamflow record. The vertical axis shows Fourier periods while the horizontal axis are years. White-enclosed regions along the time series where significant frequencies are detected. The faded regions on the left and right of the image represent areas where sample depth is too low to describe low-frequency variability and susceptible to zero-padding effects. (B) Average wavelet power as represented by the average power value of rows, or Fourier periods, in (A). Blue and red points represent statistically significant wavelet power averages ($p<0.10$).

3.6.3 Validation and analysis of reconstruction

Both measured and reconstructed normalized Q_{JA} were tested against the PNA, PDO and ENSO teleconnection indices. A difference-of-correlations test revealed associations with both positive and negative phases of the PNA (positive spring [MAM]; negative summer [JJA], and; positive annual values); an interaction with negative PDO (both phases during winter [DJF] and summer [JJA], positive autumn [SON]; and positive annual values), and; a link with ENSO (positive winter [DJF]; both phases of spring [MAM]; negative autumn [SON]; and positive annual values) (Table 3.5).

Wavelet power spectrum analysis showed multiple significant periodicities over the full reconstruction (Figure 3.5A). At the decadal scale, there was an 8-16- and 16-32-year periodicity (Figure 3.5B). Significant multi-decadal periodicities were also detected (Figure 3.5B). The intervention analysis identified 13 punctuated shifts in streamflow average over the combined instrumental and reconstruction periods, with several large departures from the long-term average (0) in 1711-1745 (+0.23), 1761-1768 (+0.58), 1785-1801 (+0.36), 1909-1921 (+0.45), 1949-1976 (+0.65), and 1977-present (-0.15) (Figure 3.4).

3.7 Discussion

3.7.1 Model Summary

The proxy model of Q_{JA} estimates variability in the Capilano and Seymour watersheds (Figure 3.4). Comparison of this record to previous research highlights that Q_{JA} variability in the Metro Vancouver water supply area is dependent upon: (1) winter

snowpack; (2) spring/summer air temperatures; and, (3) summer precipitation. The model predictors account for these climate variables. The regional mountain hemlock PCA and Pacific silver fir records were shown to serve as a robust proxy for April 1 SWE. It should be noted that the streamflow gauge located in the Seymour Watershed is down river from the Seymour Reservoir and dam, and is regulated. However, monthly flow rates are similar to that of the Capilano streamflow gauge which is located up river from the Capilano Reservoir and Cleveland Dam, and provides a record of natural discharge. Additionally, no significant difference was detected in flow values per- and post-regulation (or damming). This was also corroborated by Metro Vancouver Water Services (Mayer, *personal communication*). While I am confident in my reconstruction's ability to capture July-August discharge rates for both watersheds, artifacts of flow regulation may be present in the model.

3.7.2 The reconstructed record

The reconstructed Metro Vancouver streamflow record describes an increased frequency of low-flow events over the combined instrumental record (1929-2018) that is highlighted by consecutive years below the normalized mean (0) (Table 3.6). While from 1929-2018 eight multi-year, below-average Q_{JA} events were documented, prior to 1929 only 10 multi-year, below-average Q_{JA} were identified over more than double the length of time (89 vs. 218 years). Prior to the instrumental record, consecutive years of below-average flow were detected from 1720-1723 (3 years; -0.33 departure), 1746-1751 (5; -0.43), 1755-1761 (6; -0.06), 1779-1785 (6; -0.22), 1790-1795 (5; -0.05), 1832-1836 (4; -0.25), 1850-1861 (11; -0.30), 1870-1875 (5, -0.22), 1876-1881 (5; -0.05), 1882-1886 (4; -0.11). During the observed period, consecutive years of below-average flow occurred

from 1927-1931 (4 years; -0.08 departure), 1939-1942 (3;-0.69), 1976-1981 (5; -0.30), 1982-1987 (5; -0.55), 1991-1996 (5; -0.68), 2000-2006 (6; -0.49), 2008-2010 (2; -0.49), and 2012-2018 (6; -0.68) (Figure 3.7). While 1850-1861 represented the longest period of consecutive years below-average Q_{JA}, multi-year below average flows are characteristically higher magnitude than those documented in my reconstruction. Further, six of eight consecutive years of below-average flow occur after 1976. The greatest magnitude single-year below average Q_{JA} values also typically occur during the instrumental period. Thirteen of the fifteen worst single-year, low-flow events occur during the instrumental record with eleven occurring after 1976 and only two prior to the pre-instrumental record based on my proxy reconstruction (Table 3.6).

Wavelet analysis revealed significant decadal and multi-decadal periodicity over the duration of the reconstruction. This variability was most prevalent from the mid-17th to early-18th century, and after 1950 (Figure 3.6). Similar to other regional paleoclimate records, little or only sporadically significant decadal streamflow variability was revealed from the early 18th to the 19th century (e.g., Gedalof and Smith, 2001; Hart et al., 2010; Starheim et al., 2013a; Coulthard et al., 2016). This interval is often associated with a weakening of the PDO (Gedalof and Smith, 2001) and its influence may be amplified by the use of it as a predictor in the model.

Highlighted by the intervention analysis, the 1976/77 PDO shift marks an extreme step change in the reconstruction, where normalized July-August streamflow from 1945-1976 was +0.65 of the reconstructed average but from 1977-2018 the average fell to -0.15 (Figure 3.4). This change represents an overall step of 0.80 when compared to the average long-term normalized July-August streamflow. The reconstruction identifies

Table 3.6: Fifth- and ninety-fifth percentile flows from the reconstructed Q_{JA} record. **Bold** represent flows during the instrumental record. Z-scores are the calculated average for both reconstructed basins.

Fifth-Percentile		Ninety-fifth Percentile	
Year	Z-score	Year	Z-score
1941	**-1.10**	**1999**	**2.77**
2003	**-0.95**	**2011**	**1.60**
2015	**-0.93**	**1972**	**1.50**
1987	**-0.92**	**1956**	**1.48**
2018	**-0.91**	**1991**	**1.41**
1940	**-0.89**	**1974**	**1.35**
1996	**-0.86**	**1971**	**1.29**
2014	**-0.84**	1921	1.24
2004	**-0.80**	**1976**	**1.24**
1860	-0.80	**1969**	**1.11**
1993	**-0.79**	1730	1.07
1992	**-0.78**	1916	1.07
1984	**-0.78**	**2007**	**1.04**
1713	-0.77	**1964**	**1.06**
2009	**-0.74**	1764	1.01

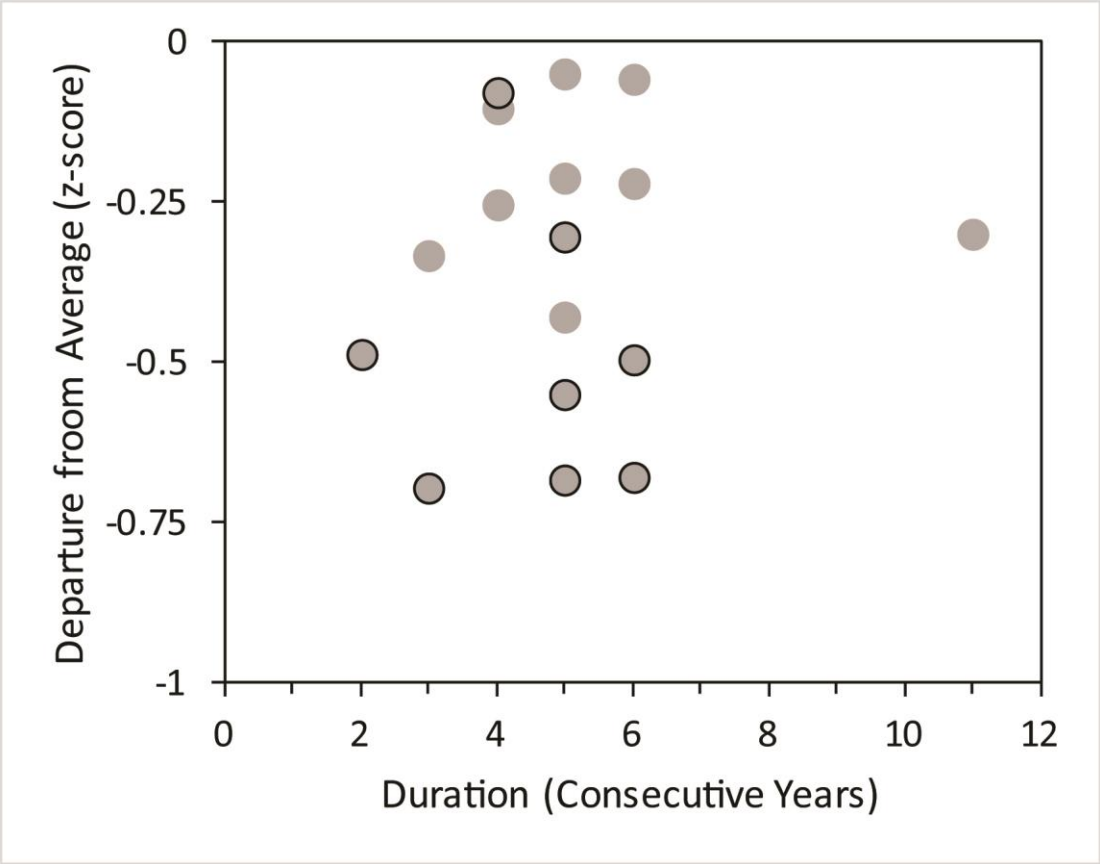

Figure 3.6: Scatterplot of consecutive year July-August below-average streamflow defined as recurring discharge values below the full-reconstructed mean (0) over greater than one year. Values lower in the y-axis indicate higher severity lower-than-average streamflow during July and August while longer duration values along the x-axis illustrate prolonged intervals of sustained below-average flows. Grey circles represent values based on the reconstructed proxy record prior to the instrumental record. Grey circles with black borders represent consecutive-year below-average July-August streamflow within the instrumental period (1929-2018).

similar punctuated step changes that led to period shifts in mean flow levels throughout the record (Figure 3.4) but none of these demonstrates as great a shift as the 1976/77 change.

While the long-term results corroborate previous instrumental analyses in southwestern BC (Rodenhuis et al., 2009), the reconstruction does suggest that streamflow within the Metro Vancouver watersheds was characteristically more variable over the instrumental period when compared to conditions over the past three centuries. Of particular note was the discovery that greatest step change in July-August streamflow variability in the last 300 years occurred within the instrumental period (Figure 3.4). If substantiated by further study, this finding offers the possibility that current water management strategies are founded on gauged records that incorporate the extreme range of streamflow variability likely to be experienced within the Metro Vancouver watersheds.

3.7.3 Influence of synoptic-scale climate variability

Significant relationships were detected with ENSO, and both modelled and measured normalized Q_{JA} over the reconstruction period. Rodenhuis et al. (2009) describe changes in the annual snowpack that exceed more than 30% between warm and cool phases of ENSO and noted that hybrid streams in this region may shift to pluvial regimes during El Niño years (Rodenhuis et al., 2009). I observe a significant relationship with the reconstruction model and positive ENSO at annual and seasonal (winter and spring) timescales.

The difference-of-correlations analysis showed that Q_{JA} is significantly related to PDO at annual and seasonal timesteps. Intital analysis corroborated this, as I used PDO as

a predictor in the reconstruction model. However, the difference-of-correlations test results associated with PDO are likely biased and not representative of actual phase-dependent relationships. PDO_{DW} artifacts likely exist in the proxy record and are acting to amplify the apparent relationships seen in Table 3.5.

The PNA appears to have a significant relationship to reconstructed, but not calculated, Q_{JA}. Changes in the PNA pattern typically result in changes to the amount of snow retained until the dry season at higher elevations in the Coast Mountains (Rodenhuis et al., 2009; Abatzoglou, 2011). Decreases in the persistence of late-lying snowpack until the late spring were expected to result in reductions to the groundwater recharge component, followed by decreased streamflow totals during the following summer months. This relationship is important, as it emphasises that the PNA is a critical variable influencing snowpack storage in southwestern BC. The relationship between Q_{JA} and PNA is likely the result of PDO's use in the reconstruction and it's modulating effect on PNA (Yu and Zwiers, 2007). While prior studies in this region have identified a relationship between streamflow variability and the PNA (Starheim et al., 2013a), its impact on streamflow within the Metro Vancouver watersheds remains poorly understood (Rodenhuis et al., 2009).

3.7.4 Other records

I compared these findings to previous streamflow reconstructions from mainland BC (Figure 3.7) and Vancouver Island (Coulthard et al., 2016). My record contains 10 intervals where July-August streamflow was below average for five or more consecutive years: from 1720-, 1746-1751, 1755-1761, 1779-1785, 1790-1795, 1832-1836, 1850-1861, 1870-1875, 1876-1881, 1882-1886, 1927-1931, 1939-1942, 1976-1981, 1982-

1987, 1991-1996, 2000-2006, 2008-2010, and 2012-2018 (Figure 3.4). While several of these low-flow intervals were synchronous with reduced flows in the Skeena (54,400 km^2), Atnarko (2,400 km^2), and Chilko (6,900 km^2) rivers (Hart et al., 2010; Starheim et al., 2013a), most of the low-flow events in this reconstruction are not regionally represented. For example, there are numerous periods when streamflow was either average or above in the Skeena, Atnarko, and Chilko rivers, while the Metro Vancouver watersheds were experiencing below-average July-August streamflow (Figure 3.7). The lack of correspondence between Metro Vancouver streamflow trends and these disparate watersheds is likely related to the larger size of the latter (Hart et al., 2010; Starheim et al., 2013a). Additionally, June-July streamflow records were reconstructed for Chilko River while all others modelled July-August. Corroborating these findings, streamflow records for watersheds of similar size (48 to 355 km^2) on Vancouver Island display similar intervals of below-average July-August streamflow over the length of the reconstructed record (Coulthard et al., 2016).

Streamflow sources and topography highlight further distinctions between the streamflow reconstructions. The Skeena, Atnarko, and Chilko rivers headwaters are all located on the leeward side of the Coast Mountains, where the hydroclimatic regime is markedly different than that experienced by the Metro Vancouver (Moore et al., 2010). The Chilko River reconstruction was derived from a hydrometric station located immediately downstream of Chilko Lake, while my model uses instrumental records from streamflow gauges located upstream of natural/manmade reservoirs (Hart et al., 2010). The Skeena, Chilko, and Atnarko rivers are also partly glacierized (Hart et al.,

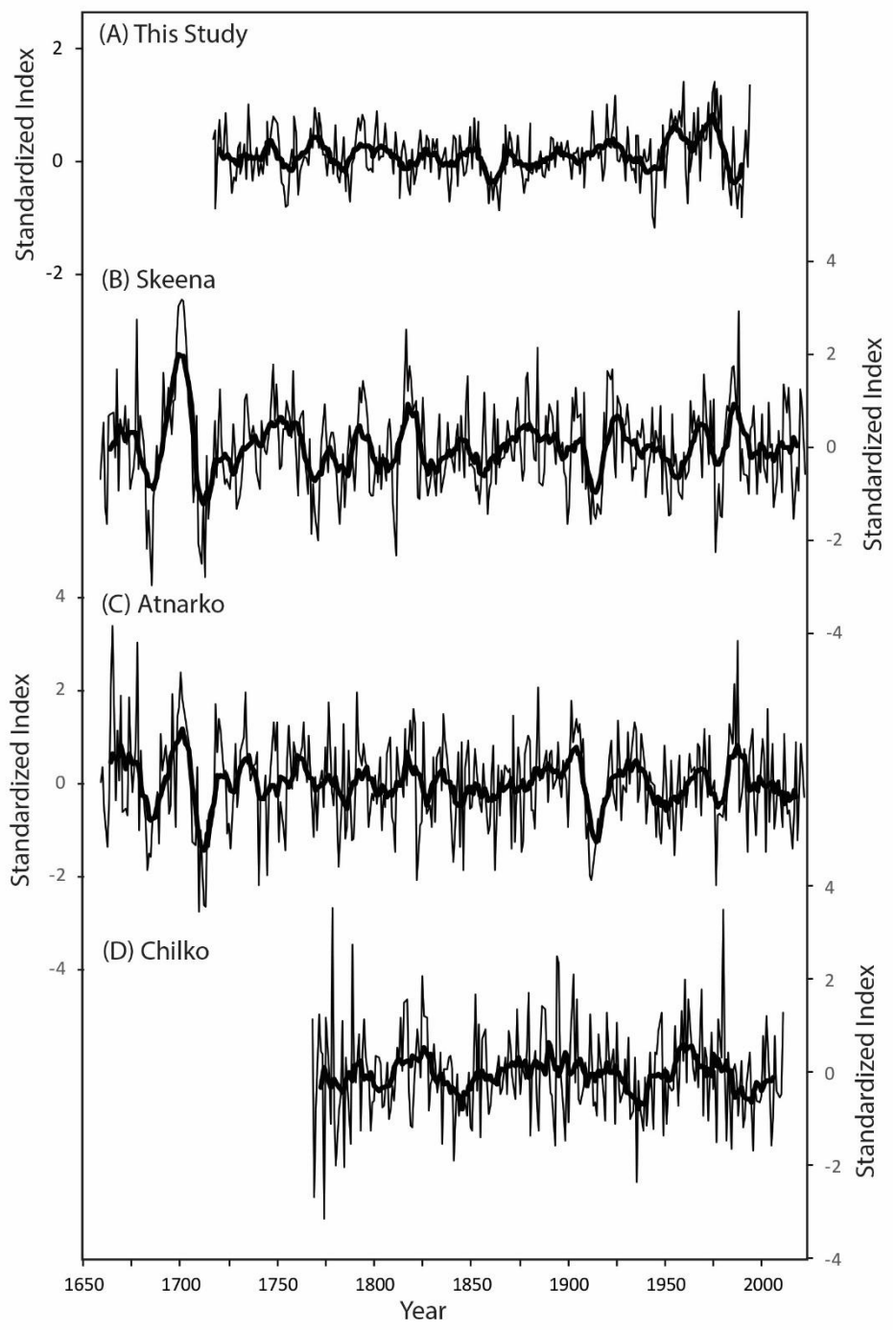

Figure 3.7: Comparison of the (A) this study to streamflow reconstructions of the (B) Skeena, (C) Atnarko, and (D) Chilko watersheds. Thick black lines indicate a moving 10-year average.

2010; Starheim et al., 2013a), whereas glaciers are absent in the Metro Vancouver of the rivers on Vancouver Island is attributed to their low relief and to prevalent rain-shadow effects along the eastern slopes of the Vancouver Island Insular Mountains (Coulthard et al., 2016).

3.8 Conclusions

In combination with the instrumental records of normalized regional July-August streamflow, the proxy runoff records presented in this chapter provide long-term insight into rivers contributing to the Metro Vancouver water supply. The proxy Q_{JA} record extends from 1711 to 1992 and shows that these rivers have experienced periodic changes in average discharge over the long-term. For example, from 1711-1745 (+0.23), 1761-1768 (+0.58), 1785-1801 (+0.35), 1909-1921 (+0.45), and 1945-1976 (+0.66) Q_{JA} was likely well-above average during summer months that were targeted for reconstruction.

An important outcome of the research was the discovery of significant step changes in Q_{JA}. While the findings have implications for future water management strategies, I also report that the duration of the July-August streamflow step change initiated in 1977 and still continuing, if I include measured records, (41 years) is likely unprecedented in duration when compared to the long-term Q_{JA} average. While changes to streamflow behavior between 1976 and 1977 in southwestern BC are often associated with the PDO (e.g., Sellars et al., 2008; Whitfield et al., 2010), this relationship is not stable over the length of either the instrumental or reconstructed record within the Metro Vancouver water supply area. Instability is highlighted by the calculated Q_{JA} record's

correlations with negative PDO across both seasonal and annual scales as well as wavelet analysis which reveals fluctuations is power frequency over time.

Consecutive years of below average Q_{JA} are increasingly frequent over the length of the instrumental record and especially following 1977. Of the lowest 5^{th}-percentile Q_{JA} years, 87% occur during the instrumental record and 73% after 1976. Further, low-flow events leading to streamflow droughts in the summers of 2013-2018 may be related to a punctuated regime shift initiated in 1976/77 which was the last identified period change in mean streamflow values. This shift appears to have resulted in persistent and unprecedented changes to the streamflow characteristics of both Capilano and Seymour watersheds. The research presented within this chapter places the Metro Vancouver water supply in a longer-term context than the instrumental record and provides a basis for advancing future water supply planning decisions related to climate induced-changes to the spring freshet.

Chapter 4: Tree-ring reconstruction of Harrison Lake dynamics to 1711, southwestern British Columbia, Canada

4.1 Article Information

Chapter 4 consists of a manuscript prepared for journal submission. The text and figures from the manuscript have been renumbered and reformatted for consistency within the dissertation.

4.1.1 Author names and affiliations

Bryan J. Mood* and Dan J. Smith

University of Victoria Tree-Ring Laboratory, Department of Geography, University of Victoria, British Columbia V8W 3R4, Canada

*Corresponding Author Email: bjmood@uvic.ca

4.1.2 Author contributions

Mood developed the study, hypothesis, conducted and led field and laboratory work, statistical testing, wrote the manuscript and produced all tables and figures. Smith provided funding for the research, provided guidance in formatting the study design, reviewed and edited the manuscript.

4.2 Abstract

Water resources in western North America are increasingly threatened as streamflow and ecological droughts associated with changing winter precipitation and temperature regimes become commonplace. In southwestern British Columbia (BC), natural lakes and manmade reservoirs in mountainous areas supplied by rainwater and melting snow provide the domestic water supply for millions of residents in the South

Coast region. Annual fluctuations in lake and reservoir levels can have widespread social, ecological, and economic consequence. Their full range of variability, however, is rarely fully represented by short or, in some cases, non-existent historical records. Using shared environmental relationships between the radial growth of high-elevation trees and spring lake levels, I extend the record of April lake levels at Harrison Lake, the largest lake in the southwestern BC, using regional tree-ring chronologies and supplementary climate oscillation reconstructions. The proxy model developed in this study successfully uses a regional mountain hemlock tree-ring series, a Pacific Decadal Oscillation reconstruction, and El Niño-Southern Oscillation reconstruction to extend the record of April lake levels for Harrison Lake back to 1711, explaining 49.5% of variability. The reconstruction highlights that lake levels during the modelled period averaged 9.37 m, a value that is 0.13 m high than the instrumental mean. This modest drop in water level represents a long-term volumetric change of -283,400 ± 4050 m^3 for Harrison Lake during the month of April. The full reconstruction highlights several intervals where the 10-year average water level was below the reconstruction mean from 1722-1743, 1760-1772, 1787-1802, 1887-1894, 1908-1924, and 1946-present. Tests revealed significant relationships between positive PDO and both phases of ENSO. No significant relationships between PNA and the reconstruction were identified. The reconstruction provides the first long-term, annually resolvable perspective of lake level variability from tree-rings in BC, and will be of immediate use for reservoir and water supply planning for communities in the region.

4.3 Introduction

Water resources in western North America are increasingly threatened by present and future climate changes (Dettinger et al., 2015; Musselman et al., 2017; Seager and Ting, 2017; Mote et al., 2018). Streamflow droughts resulting from changing winter precipitation patterns and temperature regimes are becoming commonplace, leaving many communities more reliant on natural lakes and reservoirs as their primary water supply source (Moore et al., 2010; Turner and Galelli, 2016; Bhave et al., 2018). In recent years, however, many of these water bodies have fallen to historic low water levels as freshet contributions from melting winter snowpacks are reduced (Christensen and Lettenmaier, 2006; Eaton and Moore, 2010; Castle et al., 2014),

In southwestern British Columbia (BC), Canada, lakes and reservoirs in mountain drainages support the domestic water supply needs of millions in Vancouver and the surrounding area. While planning forecasts suggest the region has a sufficient supply to sustain current and anticipated population and economic activities (Metro Vancouver, 2011), recent water use restrictions and shortages emphasize that historic trends may not describe the full range of natural variability in supply and storage capacity (c.f., Rodenhuis et al., 2009; WSC, 2017). Providing longer-term insights into the storage capacity of natural lakes, and documenting any relationships to natural climate variability, would provide water resource managers with information essential for planning for and mitigating the effects of droughts.

Annual fluctuations in the volume of water retained by natural lakes reflect seasonal moisture variability and year-to-year water balance changes (van der Maaten et al., 2015). Historic lake level records provide a robust representation of the

accompanying volumetric changes and can be employed to describe the underlying hydroclimate relationships (Medellin-Azuara et al., 2008). Extending lake level records beyond the instrumental period is, however, problematic (van der Maaten et al., 2015), and to my knowledge there are no annually-resolved paleolake level records in southwestern BC.

Long-term records of lake level fluctuation have been reconstructed in other settings using tree-rings (e.g., Holzhauser et al., 2005; Gillies et al., 2015; van der Maaten, 2015), where the focus was on closed-basins or large lakes located in lowland areas (Meko, 2006; DeRose et al., 2014). In this paper, I investigate dendrohydrological associations between the radial growth of mountain hemlock trees (*Tsuga mertensiana* (Bong.) Carr.) and fluctuations in the lake level of Harrison Lake in southwestern BC.

Dendrohydrological methodologies are typically employed to develop annually-resolved proxy reconstructions of hydroclimatological conditions that extend decades to centuries before the instrumental period (Meko and Woodhouse, 2010). Most applications focus on developing streamflow records in regions where moisture sensitive tree species record a relationship to year-to-year moisture variability (Meko and Woodhouse, 2010). Recent applications in BC demonstrate that high-elevation tree species located at sites characterized by late-lying snowpacks also provide a proxy of summer runoff from nival- (snow) and hybrid-regime (snow and rain) watersheds (Hart et al., 2010; Coulthard et al., 2016). While these studies provide robust records of annual dry-season streamflow, they do not account for storage variability in downstream lakes that buffer runoff during periods of extended below-average streamflow (Gillies et al., 2015; van der Maaten et al., 2015).

The instrumental record of Harrison Lake water levels extends from 1933 to 2018 and provides an opportunity to explore lake level-tree growth relationships in a snow-dominated mountain watershed. In this chapter, I describe associations between mountain hemlock trees found growing at high elevation to late-lying snowpack and Harrison Lake, an alpine lake supplied by freshet runoff from seasonal snowpacks. The objectives of the study were to: (1) develop a record of Harrison Lake's average April lake level (HLL_A) variability; (2) use the reconstruction to characterize lake-level changes over the length of the tree-ring record; (3) determine the hydroclimatic influences on overall variability; and, (4) highlight the importance of developing long-term lake level variability records for water resource managers. April lake levels were targeted because they represent water stored in Harrison Lake prior to contributions from the spring freshet.

4.4 Study Area

Harrison Lake is situated in a deglaciated U-shaped valley positioned close to the southern extent of the Pacific Ranges in the BC Coast Mountains (Monger, 1989; Desloges and Gilbert, 1991) (Figure 4.1). Located close to the outlet of the Lillooet River into the Fraser River, the lake is 62 km in length and covers an area of 218 km^2. Its maximum depth is 279 m and it contains approximately 3.3-trillion litres of water. The Harrison Lake watershed is 7870 km^2, with most of the water flowing into the lake originating from upstream sections of the Lillooet River (8% glacier cover) (Slaymaker et al., 2017). Lillooet Lake located 50 km upstream buffers the glacier-related input to Harrison Lake and most of the annual variability in the watershed is associated with local snowpack, groundwater, and other components of the hydrological cycle (Desloges and

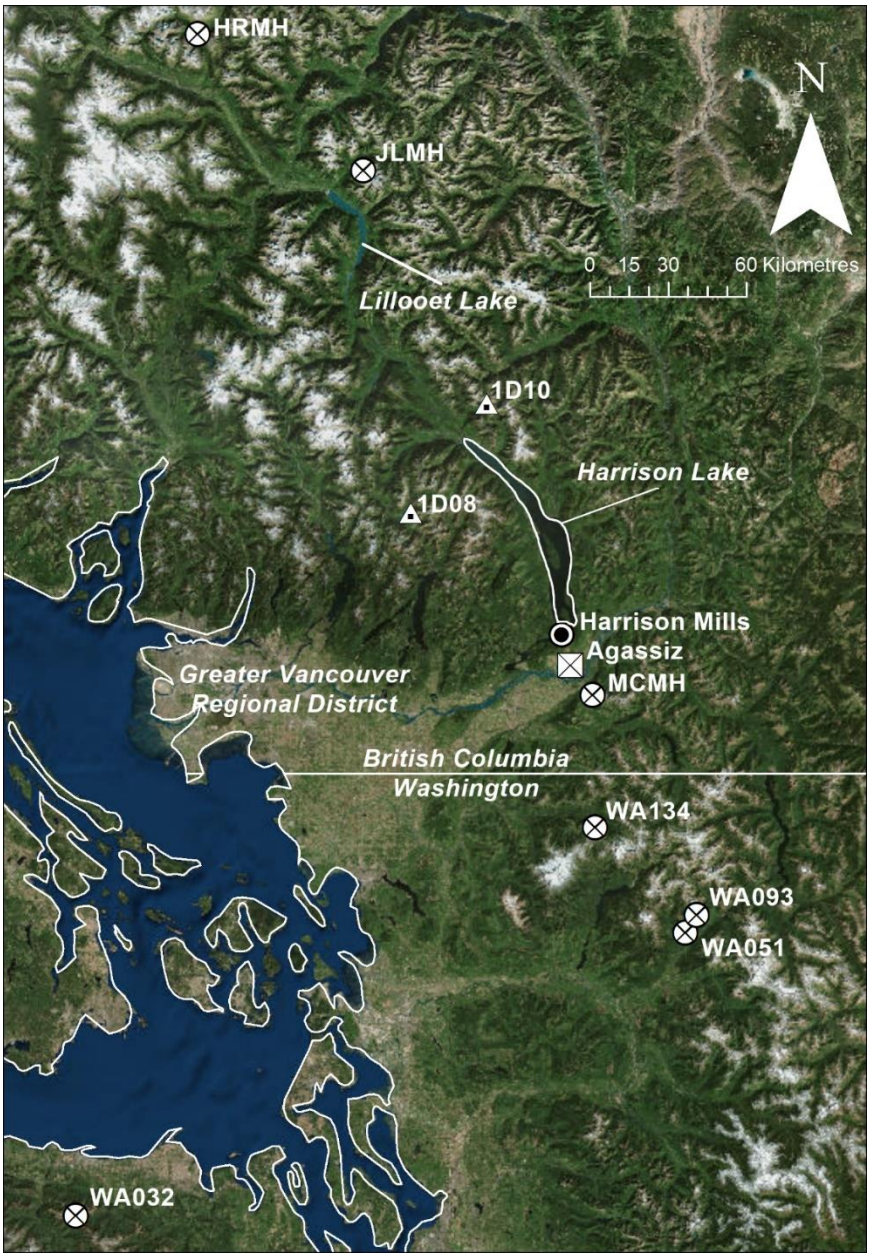

Figure 4.1: Study site map showing the location of Harrison Lake. Circles with X's indicate tree-ring chronology locations; the square with X at Agassiz indicates the location of the climate station used in this study, the black circle with white outline at Harrison Mills indicates the location of the water level station on Harrison Lake; the triangles with a black circle indicates the location of the manual snow survey stations used in the study (Source: WSC, 2017).

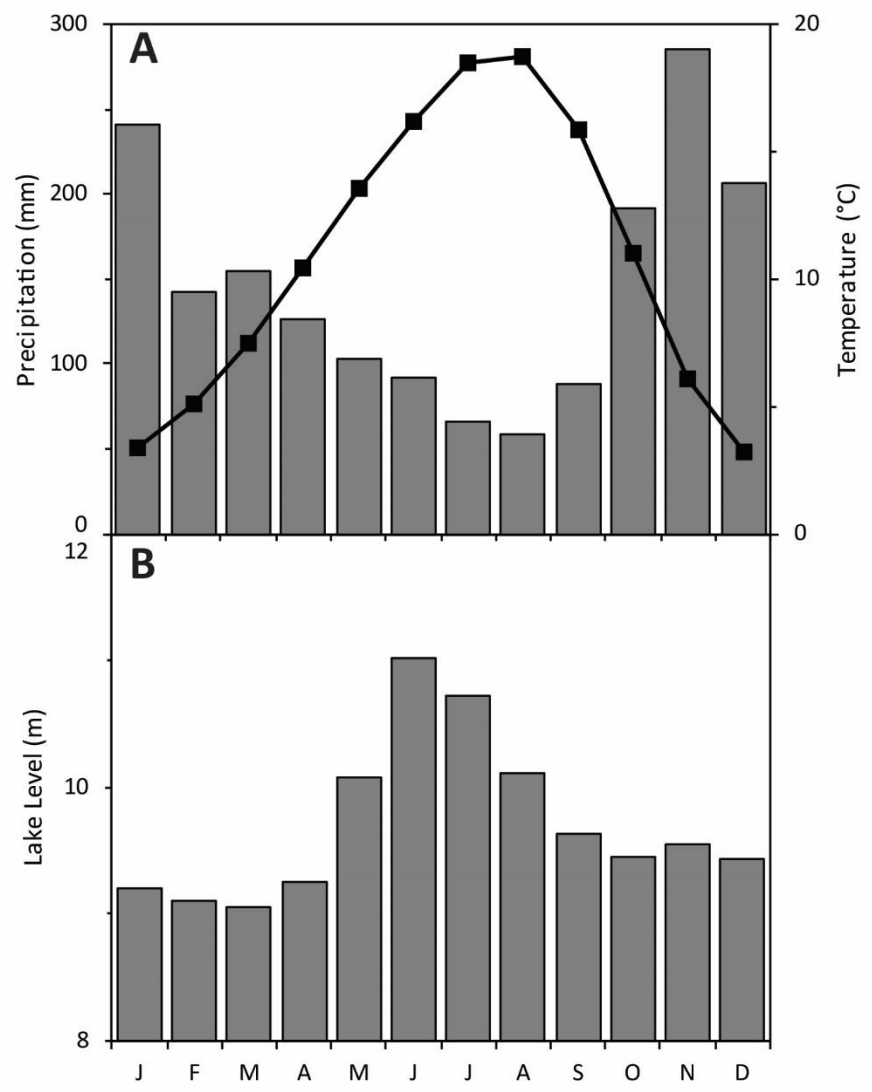

Figure 4.2: (A) Climate normals (1981-2010) for Agassiz climate station (Station ID: 1100120) where the grey bars represent monthly precipitation totals and the black line with squares indicate average monthly temperatures. (B) Harrison Lake average water levels (08MG012; 1933-2016) for each month of the year.

Gilbert, 1991).

Average monthly air temperatures in the vicinity of Harrison Lake range from 3.2 to 18.7°C (Figure 4.2A). Annual precipitation totals at Harrison Lake average 1750 mm (1981-2010 Climate Normal; Station ID: 1100120) (ECCC, 2017). The lake is supplied by water originating from rainfall at lower elevations during the winter and snowmelt/rainfall contributions during the spring and summer months.

Water levels in Harrison Lake vary over the course of a year. Based on the instrumental record (station ID: 08MG012; 1933-2018), they are typically lowest from January to February when the water supplying the lake is stored as winter snowpack at higher elevations (Figure 4.2B). From May to August, lake levels are at their highest – peaking in June (Figure 4.2B). The highest recorded lake level on record (13.3 m) occurred in June 1948, while the lowest level was recorded in February 1979 (8.21 m). This paper focuses on reconstructing average monthly April water levels in Harrison Lake (average 9.25 ± 0.23 m), at a time of year when the lowest lake level (8.72 m) occurred in 2008 (Figure 4.2B).

Harrison Lake is located at the southernmost extent of the Pacific Ranges of the BC Coast Mountains (Figure 4.1). Its hydroclimatic character is affected by inter-annual and -decadal climate variability generated from the Pacific Ocean (Moore et al., 2010). The dominant atmosphere-ocean interactions influencing the basin include those characterised by the El Niño-Southern Oscillation (ENSO), Pacific Decadal Oscillation (PDO), and Pacific North American (PNA) pattern. The inherent variability ascribed to these teleconnections are known to influence the timing and magnitude of precipitation falling during the winter months (Bonsal and Shabbar, 2008; Abatzoglou, 2011).

ENSO is a naturally occurring phenomenon of ocean temperature variability in the equatorial Pacific that experiences phase changes every six to 18 months (Bridgman and Oliver, 2006). Alternating between two phases (positive/El Niño and negative/La Niña), it has an impact on winter precipitation patterns across the Pacific Ranges (Rodenhuis et al., 2009). The PDO is often characterised as a long-lived ENSO-like pattern of Pacific climate variability derived from sea surface temperature variability (Mantua et al., 1997). Similar to ENSO, phase changes in the PDO can have substantial impacts on moisture delivery to the southern BC Coast Mountains (Rodenhuis et al., 2009). The PNA is a low-frequency, quadripolar, teleconnection associated with alternating pressure patterns between the Pacific Ocean and centres of action over western Canada and the southwestern United States (Wallace and Gutzler, 1981; Latif and Barnett, 1994). While lacking a well-defined periodicity, it is influenced by both the PDO and ENSO and has impacts on freezing level elevations across the Pacific Northwest (Yu and Zwiers, 2007; Abatzoglou, 2011).

4.5 Methods

Dendrohydrological reconstructions have been completed within several regions of coastal BC and Washington State (Gedalof and Smith, 2001; Peterson and Peterson, 2001; Marcinkowski et al., 2015). Prior research identified ecophysiological relationships between April 1 snow water equivalent (SWE) and the radial growth increment of high elevation trees (Graumlich and Brubaker, 1986; Smith and Laroque, 1998), and utilized those associations to reconstruct a variety of preinstrumental snowpack and teleconnection characteristics (e.g., Gedalof and Smith, 2001; Pederson et al., 2011).

More recently, identification of similar hydroclimate relationships allowed for the construction of dry-season streamflow records for nival regime watersheds on Vancouver Island (Coulthard et al., 2016).

Pre-instrumental lake level records constructed from tree-ring indices depend upon the identification of similar radial growth-hydroclimatic relationships (e.g., Stockton and Fritts, 1973). In western North America, documentation of these associations enabled the reconstruction of long-term lake-level records for Lake Athabasca, Alberta and Saskatchewan (1801-1999; Meko, 2006) and Great Salt Lake, Utah (1429-2005; DeRose et al., 2014). In this application, tree ring records from snow-sensitive high-elevation mountain hemlock trees are used to model the April lake level at Harrison Lake.

4.5.1 Hydrometric and climate data

Harrison Lake was selected for study as its instrumental lake level exceeds 50 years, more than twice that of Lillooet Lake (80 vs 36 years). While Harrison Lake is positioned downstream of Lillooet Lake, the water level of the latter is more directly impacted by glacial meltwater released from the Lillooet Icefield (Desloges and Gilbert, 1991; Heideman et al., 2017; Slaymaker et al., 2017). Lake level data were retrieved from the Harrison Hot Springs station (ID: 08MG012; WSC, 2018) (Table 4.1) located at the southern extent of the lake.

Climate data from the closest proximity station to Harrison Lake at Agassiz, BC, (Station ID: 1100120) (Table 4.1) was retrieved from Environment and Climate Change Canada (ECCC, 2017). Monthly temperature and precipitation records were also downloaded using ClimateBC v.5.50 (Wang et al., 2012). The program downscales

PRISM monthly 2.5*2.5 arc min data based on the 1961-2000 reference period. Snowpack data was obtained from the River Forecast Centre website for the Stave Lake (ID: 1D08) and Nahatlatch Lake (ID: 1D10) stations (River Forecast Centre, 2017). April 1 SWE values were used in the analysis, as they typically exhibit a robust relationship to maximum annual snowpack depths in the region (Bohr and Aguado, 2001; Winkler et al., 2010; Pederson et al., 2011) (Table 4.1).

Both ENSO and PDO have a substantial influence on the winter hydroclimatic dynamics in southwestern BC (McCabe and Dettinger, 1999; Flemming and Quilty, 2006; Stahl et al., 2006; Fleming and Whitfield, 2010; Moore et al., 2010). ENSO and PDO teleconnection paleorecords were downloaded from the National Oceanic and Atmospheric Administration (NOAA) website (D'Arrigo and Wilson, 2006; Li et al., 2011; NOAA, 2017).

4.5.2 Tree-ring data

The annual radial growth increment of coniferous trees located at high elevation in Pacific North America is generally impacted by energy limitations (Ettinger et al., 2011). In some instances, the radial growth is restricted by growing season temperatures that inhibit photosynthetic production (Fritts, 1976). In other situations, late-lying snowpacks reduce the length of the growing season and the opportunity for cambial development (Smith and Laroque, 1998; Ettinger et al., 2011; Coulthard et al., 2016). Late-lying snowpacks are believed to restrict cambial expansion (e.g., Smith and Laroque, 1998) and/or to prolong cold soil temperature regimes that reduce the ability of tree roots to uptake nutrients during the early months of radial growth (Marcinkowski et al., 2013; Peterson and Peterson, 2001). In this chapter, I hypothesized that the same

snowpack characteristics that influence the radial growth of mountain hemlock trees were reflected, inversely, by the lake levels of Harrison Lake during April. I capitalised on this association to reconstruct April lake level variability beyond the instrumental record.

For this study, I developed a network of high-elevation mountain hemlock tree-ring chronologies from tree-ring series previously collected by researchers associated with the University of Victoria Tree-Ring Laboratory (UVTRL) and/or those archived in the International Tree-Ring Data Bank (ITRDB). Age-related growth trends were removed using the R package dplR to allow for inferences to be made on climate-related radial growth variability (Bunn, 2008). The tree-ring chronologies were detrended using a cubic smoothing spline with a 50-year wavelength. Growth from the previous year often influences growth of the current year and this effect was removed by using 'residual' detrended series that have zero-autocorrelation to correspond with the lake level records targeted for reconstruction.

4.5.3 Climate analysis

Initially, relationships between the tree-ring, climate, and teleconnection indices, snowpack, and lake-level records were examined using Pearson's correlation. A pool of predictors was established based on the significant relationships documented in the outputs. Several approaches were considered for modelling robust reconstruction variables. First, individual series were combined into a regional-level chronology using regional curve standardisation methods (Briffa and Melvin, 2011). Second, species with ≥5 site-level series were combined into a principal component analysis (PCA) to discern the underlying variability between study sites. Only components accounting for ≥10% of the total variability were considered for use in this study.

Table 4.1: Instrumental data information retrieved from Environmental and Climate Change Canada (2017), Water Survey of Canada (2017), and River Forecast Centre (2017).

ID	Name	Lat (DD)	Lon (DD)	Elevation (m asl)	Variable	Duration
Climate Station						
1100120	Agassiz	49.24	-121.76	15	Temperature and Precipitation	1889-2007
Water Level Station						
08MG012	Harrison Lake Near Harrison Hot Springs	49.31	-121.77	15	Lake Level	1933-2016
Snow Survey Stations						
1D08	Stave Lake	49.58	-122.32	1195	April 1 SWE	1968-2014
1D10	Natalatch Lake	49.83	-122.06	1555	April 1 SWE	1968-2014

4.5.4 Model development and analysis

A reconstruction model was developed that used statistically significant relationships between the pool of predictors (mountain hemlock tree-ring series and climate index reconstructions) in a multiple linear regression for Harrison Lake April lake level (HLL_A). The output model was validated using multiple diagnostic statistics: (1) adjusted R^2, a descriptor of the overall explanatory power of the model; (2) a Durbin-Watson statistic (DW) which describes the influence of *t-1* on *t* or autocorrelation, (3) multicollinearity, using variance inflation factor (VIF), which measures artificial inflation of predictors on the predictand; and, (4) cross-validation, using reduction of error (RE), which is a measure of overall model performance and evaluation. The HLL_A reconstruction was compared to regional climate records to reveal the underlying drivers of April lake level variability. Specifically, measurements of climate oscillations generated from the Pacific Ocean (PDO, ENSO, and PNA) were examined against the reconstructed and measured HLL_A using a difference-of-correlations test.

4.6 Results

4.6.1 Data

Five mountain hemlock chronologies were selected for use as predictors (Table 4.2). The chronologies were significantly correlated to one another and were combined using a principal component analysis (PCA). The resulting chronology was representative of underlying regional radial growth trends and explained 69% of annual variability. Only the first component was used from the PCA (PC_{MH}). Consolidating the five

Table 4.2: Time series information. Species/type area italicized and bold represents time series used as predictors in the reconstruction. Mountain hemlock PC1 was developed by conducting a principal component analysis (PCA) on the five site-level chronologies listed. Climate oscillation indices were collected from NOAA (2017) for teleconnections that are known to influence the overall hydroclimate of western North America. [a] = correlations among tree-ring series collected from each site; [b] = only the length of the tree-ring index where the expressed population signal (EPS) was ≥0.85 is documented; [c] = RBAR is the average value across whole index where EPS was ≥0.85 and PC loading indicates the variance explained by the first component of the PCA.

Time Series Name (Code)	Inter-series correlations[a]	Coordinates (Decimal Degrees)	Elevation (m asl)	Length[b]	RBAR/PC Loading[c]
Mountain hemlock					
Oakes Peak (WA051MH)[1]	0.520	48.63, -121.37	1140	1610 - 1992	0.313
Thornton Lakes (WA093MH)[2]	0.602	48.67, -121.33	1370	1706 - 1992	0.379
Heather Meadows (WA134MH)[3]	0.492	48.87, -121.68	1310	1685 – 2006	0.313
Joffre Lake (JLMH)[4]	0.607	50.34, -122.48	1550	1711 - 2012	0.428
Mount Cheam (MCMH)[5]	0.593	49.17, -121.69	1390	1637 - 2000	0.384
Mountain Hemlock PC (PC_{MH})				1711 - 1992	69.30%
Paleorecords					
Pacific Decadal Oscillation (PDO_{DW})[6]				1565 – 2004	
El Nino-Southern Oscillation ($ENSO_L$)[7]				900 – 2002	

[1] Graumlich and Brubaker (1986); [2] Peterson and Peterson (2001); [3] Bunn (2012); [4] Wood et al. (2011); [5] Johnson and Smith (2010); [6] D'Arrigo and Wilson (2006); [7] Li et al. (2011).

chronologies into a regional network enhanced the explanatory power, but restricted the reconstruction period to 1711-1980. The regional chronology was significantly correlated to both April 1 SWE and HLL_A.

Previously generated ENSO and PDO reconstructions were incorporated into the HLL_A reconstruction model, as April water levels will vary depending upon springtime freshet contributions. Both teleconnections significantly influence on moisture delivery and air temperatures during the winter months (Moore et al., 2010). During warm and cool phases of ENSO, the regional snowpack changes by an average of -11% to +21%, respectively (Rodenhuis et al., 2009). Similar, but lower magnitude snowpack trends are associated with the PDO, ranging from changes of -1% and +14% during positive and negative phases, respectively (Rodenhuis et al., 2009). In this study, the ENSO and PDO indices were significantly associated with April 1 SWE over the instrumental period (Table 4.3).

4.6.2 Model development and diagnostics

April water levels at Harrison lake were modelled as follows:

$$HLL_A = 9.37 + (-0.07PC_{MH}) + (0.17PDO) + (-0.11ENSO)$$

where: HLL_A is the April lake level of Harrison Lake; PC_{MH} is the first principal component of the regional mountain hemlock tree-ring index network; PDO is a Pacific Decadal Oscillation tree-ring reconstruction presented by D'Arrigo and Wilson (2006); and, ENSO is a El Niño-Southern Oscillation reconstruction compiled by Li et al. (2011).

Analysis of HLL_A highlighted the strong association between April 1st SWE and April lake levels, and the selected model predictors account for this. The reconstruction spans the 1711-1980 interval and explains 49.5% of HLL_A (Table 4.4). The model has a DW of 1.8, VIF of 1.12, F-ratio of 14.7, and RE value of 0.14 (Table 4.4). A time plot comparing measured, reconstructed, and cross-validation HLL_A is shown in Figure 4.3.

The full reconstruction of lake level changes from 1711-1980 is shown in Figure 4.4. The long-term HLL_A average over this interval was 9.37 ± 0.20 m, a value that is 0.12 m higher than that recorded during the instrumental period, and represents a volumetric change of -2.834 ± 0.004 million litres during instrumental period for April lake levels.

4.7 Discussion

4.7.1 Model evaluation

The reconstruction accurately models HLL_A and extends the lake level record to 1711. The reconstruction shows that over the period of record there were several intervals where the 10-year average was below the long-term mean (9.37 m) from 1722-1743 (-0.03m), 1760-1772 (-0.11m), 1787-1802 (-0.07m), 1887-1894 (-0.04m), 1908-1924 (-0.05m), and 1946-present (-0.15m) (Figure 4.4).

The HLL_A record was compared to those large-scale climate oscillations known to significantly influence the regional hydroclimate (Moore et al., 2010). A difference-of-correlations test demonstrated a significant relationship ($p<0.05$) to PDO and ENSO (Table 4.5). Positive PDO phases were positively correlated with HLL_A, while both

Table 4.3: Correlations between model parameters, April Harrison Lake water levels, and local snow survey stations (April 1 SWE values). **Bold-underlined** indicates *p<0.01*.

	April Harrison Lake Levels	Nahalatch Lake (1D10)	Stave Lake (1D08)
Mountain Hemlock PC1	-0.01	**-0.75**	**-0.72**
Pacific Decadal Oscillation (PDO_{DW})	**0.42**	**-0.82**	**-0.85**
El Nino-Southern Oscillation ($ENSO_L$)	**-0.42**	-0.15	-0.11

Table 4.4: Reconstruction, cross-validation, and descriptive statistics for modelled April levels of Harrison Lake. D-W = Durbin-Watson Statistic; VIF = variance inflation factor; SE = standard error; RE = reduction of error; RMSE = root mean squared error.

Reconstruction	R^2	Adj. R^2	D-W	VIF	SE	F-ratio
	0.53	0.49	1.80	1.12	0.20	14.70
Cross-Validation	RE	RMSE				
	0.13	0.19				

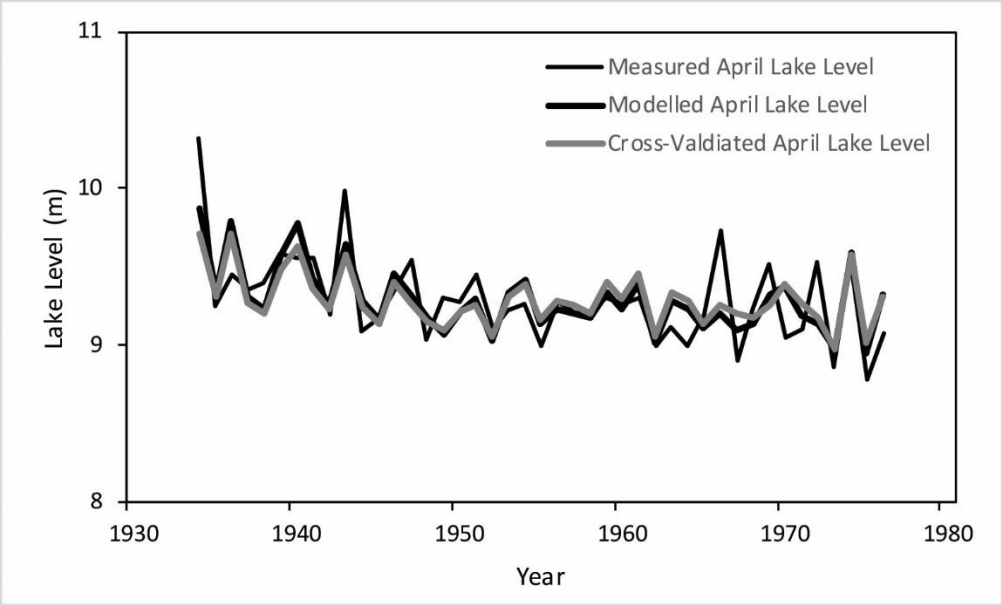

Figure 4.3: Time plot of measured, modelled, and cross-validated records from the model calibration.

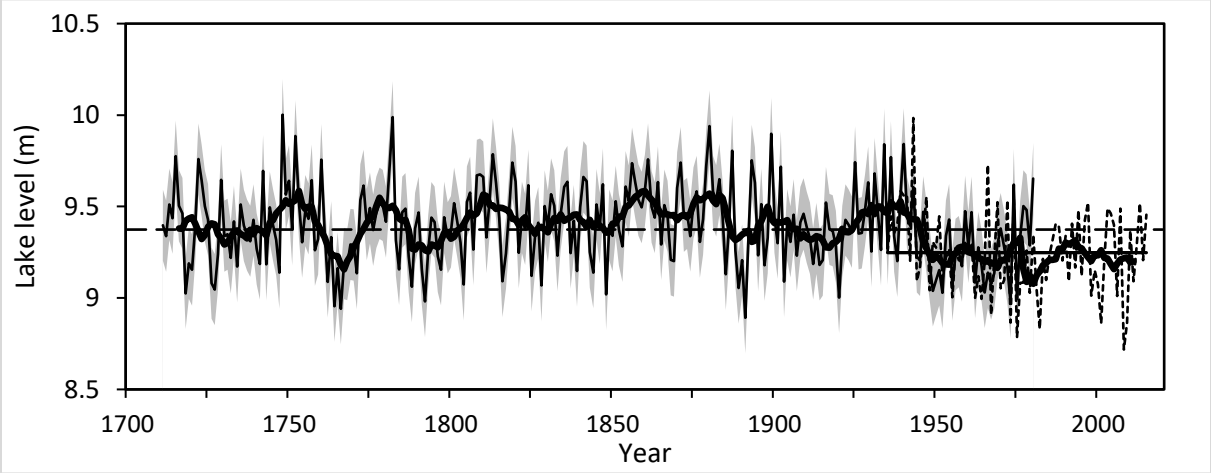

Figure 4.4: Time plot of reconstructed April Harrison Lake water level (thin black line) with a 10-year running mean (thick black line) and gauged data (dashed line). Straight dashed line indicates the modelled mean lake level; solid black line indicates the measured mean value of April lake level. Error associated with the reconstruction is represented as the grey area surrounding the model. The thin horizontal dashed line represents the 300-year reconstructed mean April lake level while the thicker solid horizontal line from 1933-2018 represents the gauged record mean.

Table 4.5: Difference-of-correlations tests for measured ENSO, PDO, PNA values against modelled and measured April Harrison Lake Level. **Bold** indicates *p<0.05*. Where only one of the two teleconnection phases is significant, it illustrates a possible non-stationary response.

Climate Oscillation	Modelled Lake Level	Measured Lake Level
Positive PDO (39)	0.21	**0.33**
Negative PDO (41)	0.23	-0.02
Negative PNA (19)	-0.08	0.03
Positive PNA (13)	0.48	0.34
Positive ENSO (15)	**-0.55**	0.06
Negative ENSO (16)	**-0.52**	-0.35

ENSO phases were negatively correlated with HLL_A (Table 4.5). No significant relationship was documented between PNA and HLL_A. These findings indicate that HLL_A has a definitive relationship to positive PDO (Table 4.5) when winter temperatures are above average and precipitation is below normal. Similarly, the reconstruction was shown to be significantly associated to both positive and negative phases of ENSO (Table 4.5).

While HLL_A was successfully reconstructed, we attempted to model other lake level properties that may have been of more significance to water resource managers. We unsuccessfully tried to model annual, maximum, minimum, and seasonal lake level values. This is likely a result of the strong relationships that April lake levels have with winter precipitation and March temperatures that are strongly associated with the tree-ring chronologies we use in this study (Marcinkowski et al., 2013).

4.7.2 Implications

Although the volumetric changes highlighted in this research equate to <1% of the total lake's volume, the research findings emphasize that even small water level variations may be significant. In smaller lakes, a similar loss in water levels may have a more substantial impact in overall water volume. The reconstruction demonstrates that April lake levels at Harrison Lake were on average 12 cm lower (equivalent to nearly 300-million litres of water) over the instrumental period when compared to levels typical of the past 300 years. While Harrison Lake is not presently used as a source for drinking water or for large-scale industrial purposes, the results should be of interest to Metro Vancouver resource managers responsible for long-term water storage planning within Capilano, Seymour, and Coquitlam lakes (Metro Vancouver, 2011).

4.8 Conclusions

The findings of this study indicate that the April water level of Harrison Lake was generally much lower over the instrumental period when compared to the proxy record from 1711-1980. These findings have implications for future water management strategies in adjacent regions and provide useful insights into the natural range of variability for other natural or manmade reservoirs in the region. The reconstruction indicates that there were several intervals where the 10-year average was below the full reconstructed mean from 1722-1743, 1760-1772, 1787-1802, 1887-1894, 1908-1924, and 1946-present. An important finding of the research was that lake levels since 1946 have remained below the 300-year average, and that the only comparable decrease in average lake levels took place from 1760-1772 over a much shorter interval. Both measured and reconstructed HLL_A are associated with climate oscillations generated from the Pacific Ocean. PDO and ENSO appear to have a significant influence on lake level variability resultant from changes in moisture delivery and temperature during the winter months.

Chapter 5: Cyclic Chinook and Coho salmon abundance over the last 300 years, southwestern British Columbia, Canada

5.1 Article information

Chapter 5 consists of a manuscript prepared for journal submission. The text and figures have been renumbered and reformatted for consistency with the dissertation.

5.1.1 Author names and affiliations

Bryan J Mood*, Cedar Welsh, and Dan J Smith

University of Victoria Tree-Ring Laboratory, Department of Geography, University of Victoria, British Columbia V8W 3R4, Canada

*Corresponding Author Email: bjmood@uvic.ca

5.1.2 Author contributions

Mood developed the study, presented the hypothesis, conducted and led the field and laboratory work, the statistical testing, wrote the manuscript, and produced the tables and figures. Welsh conducted and provided a description for the MTM and wavelet spectral analysis, and produced the related figures presented in the manuscript. Smith provided funding for the research, guidance in formatting the study design, and reviewed and edited the manuscript.

5.2 Abstract

Salmon play a vital economic, cultural, and social role in many southwestern British Columbia (BC) communities. There is mounting concern regarding their future in the region, especially as the negative impact of ongoing climate change on salmon populations is increasingly apparent. These concerns underscore the need to develop

longer-term perspectives of salmon-climate relationships. This research capitalizes on hydroclimate relationships shared between the radial growth of high-elevation trees and salmon populations in southwestern BC to extend proxy abundance records to the early 1700s. Two models of regional Coho and Chinook salmon escapement were developed from tree-ring records that explain 48.9% and 48.2%, respectively, of historical abundance variability. The records illustrate repeated salmon escapement collapses over the last three centuries in streams draining to the Pacific Ocean in southwestern BC, and ascribe these collapses to large-scale ocean-atmosphere climate oscillations. The records account for salmon life history as documented by wavelet and multi-taper spectral analysis, and illustrate unstable, inter-decadal, 25-year variability. Persistent below-average intervals of reduced abundance were documented at 1782-1837 and 1952-1992 in the Chinook records, and between 1757-1859 and 1958-1987 in Coho escapement. Both records reveal significant, relatively synchronous, relationships to climate oscillations generated from the Pacific Ocean. While Coho escapement was negatively associated with winter and spring cool phases of the El Niño-Southern Oscillation, Chinook abundance was positively correlated to cool phases of the Pacific Decadal Oscillation. The identified relationships to teleconnections generated in the Pacific Ocean to our record indicates that both species are sensitive to oceanic interactions prior to entering natal habitats. The Pacific North American pattern was negatively linked to Coho escapement. Both reconstructions provide for a better understanding of the long-term role of climate variability on salmon abundance, and offer insights essential for developing salmon management strategies.

5.3 Introduction

Pacific salmon (*Oncorhynchus spp.*) play a key economic, cultural, and social role in many southwestern British Columba (BC) communities (Lichatowich and Lichatowich, 2001; Walters et al., 2018). There is mounting concern regarding the future of salmon in this region, especially as the negative impacts of ongoing climate changes on salmon populations are increasingly apparent (Munoz et al., 2014, 2015, Mantua et al., 2015). Recent concerns about declining salmon populations underscore the necessity for developing longer-term perspectives of salmon-climate relationships in order to develop comprehensive management strategies.

Observation and historical monitoring of salmon stocks in Pacific North America over the last century reveals repeated shifts in abundance (Mantua et al., 1997; Rogers et al., 2013; Mantua et al., 2015; Litzow et al., 2018). Prior to the introduction of large-scale commercial fishing in southwestern BC, salmon populations in the region characteristically fluctuated in abundance on a 30- to 80-year cycle (Rogers et al., 2013). While overfishing and natal habitat degradation contribute significantly to recent changes in abundance dynamics (Walters et al., 2018), research shows that underlying salmon population fluctuations in 1947, 1977, and 1989 were linked to low-frequency climate variability in the North Pacific Ocean (Mantua et al., 1997, 2015; Irvine and Fukuwaka, 2011; Litzow et al., 2018). Specifically, the research attributes variations in salmon abundance to the strength and position of the Aleutian Low and sea surface temperatures (Mantua et al., 1997, 2015; Hare et al., 1999; Litzow et al., 2018). Temperature increases over the last century have added significant physiological and genetic stress to salmon returning to altered natal habitats, and hindered our understanding of long-term salmon

populations (Munoz et al., 2014, 2015; Mantua et al., 2015). The complex impact of these climate and teleconnection dynamics has encouraged research intended to develop a better understanding of salmon-climate relationships in the Pacific Northwest (e.g., Mantua et al., 2015; Litzow et al., 2018).

Dendrochronology provides an opportunity to extend and enhance relatively short records of salmon abundance. Retaining annually-resolved records of local tree ring radial growth-climate interactions (Fritts, 1976; Speer, 2010) with well-defined relationships to broad-scale atmospheric teleconnections (e.g., Gedalof and Smith, 2001; Palmer et al., 2016; Anchukatis et al., 2017), tree-ring records have previously been used to reconstruct long-term salmon population dynamics in Pacific North America. Drake et al. (2002) and Drake and Naiman (2007) established ecosystem-based relationships between migrating salmon and riparian trees in Alaska, BC, and Oregon, that helped to identify nutrient-related drivers of salmon escapement success. Starheim et al. (2013b) documented a hydrological association between annual tree ring growth in several high-elevation conifer tree species and salmon escapement success for three watersheds in north and central coastal BC. Despite the potential insights offered by these contributions, the reconstruction of long-term salmon population dynamics remains largely restricted to site-specific investigations where descriptive ecosystem variables are required for testing (Drake et al., 2002). As a result, long-term trends in salmon abundance remain poorly understood in many regions of Pacific North America.

In this chapter, two annually-resolved salmon proxy abundance models are presented that offer long-term insights of climate-related salmon population trends in southwestern BC. While most prior research focused on nutrient-limited riparian trees, I

employ the approach taken by Starheim et al. (2013b) to target relationships between tree rings, salmon abundance, and large-scale climate oscillations generated from the Pacific Ocean. The reconstructions developed in the research provide for a better understanding of the long-term role of climate variability on salmon abundance, and offer insights essential for developing sound salmon management strategies.

5.4 Research background

Pacific salmon are anadromous, with variable life histories (Pearcy, 1992). Upon birth, they spend varying time in freshwater before entering marine ecosystems. While Pink salmon (*Oncorhynchus gorbuscha*) spend less than a month in freshwater before swimming to the ocean, Sockeye salmon (*Oncorhynchus nerka*) may dwell in freshwater nurseries for up to three years (Pearcy, 1992). Chum (*Oncorhynchus kisutch*), Coho (*Oncorhynchus kisutch*), Chinook (*Oncorhynchus tshawytscha*) and Sockeye salmon spend between two and six years in the ocean, whereas pink salmon typically spend less than 18 months at sea (Pearcy, 1992). During their time in marine environments, all five species migrate hundreds to thousands of kilometres from their spawning grounds to feed (Pearcy, 1992). When approaching the end of their lives, they return to their natal habitat to spawn and die.

Ocean and atmospheric conditions affect the ability of salmon to grow and survive while residing in marine environments (Ruff et al., 2017; Cunningham et al., 2018). Research shows that salmon abundance in the northeast Pacific Ocean and western North America demonstrate low-frequency relationships to climate oscillations generated by the Pacific Decadal Oscillation (PDO), El Niño-Southern Oscillation (ENSO), and

Pacific North American pattern (PNA) shifts (Mantua et al., 1997; Hare et al., 2002; Rodenhuis et al., 2009; Mantua et al., 2015; Cunningham et al., 2018; Litzow et al., 2018). Collectively these oscillations influence hydroclimate and moisture delivery over the North Pacific and western North America (Mote et al., 2018), with increased precipitation and temperatures identified as influencing salmon productivity and survival in marine environments by triggering widespread shifts in sea surface temperatures, water column stability, nutrients, and zooplankton and phytoplankton production (Burke et al., 2016; Cunningham et al., 2018).

High-elevation trees also respond to changes in regional hydroclimate and are associated with low-frequency climate oscillations in Pacific North America (e.g., Gedalof and Smith, 2001; Starheim et al., 2013a; Couthard et al., 2016; Harvey and Smith, 2017; Welsh et al., 2019). Deep winter snowpacks in the area truncates the duration of the growing season and reduces the annual radial growth increments (Peterson and Peterson, 2001). Conversely, reduced snowpack totals can result in larger-than-average annual rings due to a prolonged growth season (Peterson and Peterson, 2001).

5.5 Study area

This research focuses on the lower Fraser River valley region of BC, including its tributaries up to the Fraser Canyon, as well as the Harrison and Lillooet river watersheds (Figure 5.1). The climate of coastal settings in this region is moderated by proximity to the Pacific Ocean, leading to short, cool summers and long, wet winters. Average air temperatures above 1000 m above sea level (asl) remain below 0°C for 0 to 5 months of

the year, and above 10°C for 1 to 3 months of the year (Pojar et al., 1991; Kottek et al., 1996) (Figure 5.2A).

The study area includes BC's wettest ecological zone, where precipitation totals range between 1700 to 5000 mm/yr, with 70% falling as snow and/or rain during the winter months (Pojar et al., 1991; Spry et al., 2014) (Figure 5.2B). Most precipitation falls as a result of orographic interactions on the windward slopes of the Pacific Ranges. Precipitation totals decrease substantially on the eastern slopes, where persistent rainshadow conditions prevail (Pojar et al., 1991; Kottek et al., 2006; Church and Ryder, 2010; Moore et al., 2010) (Figures 5.2A and 5.2B).

Prior research shows that climate variability generated from the Pacific Ocean plays a critical hydroclimate role in southwestern BC. Interactions include those characterized by the PDO, ENSO, and the PNA pattern (Rodenhuis et al., 2009; Abatzoglou, 2011; Mote et al., 2018). Warm/cool phase relationships between the regional hydroclimate and ENSO show a variability of greater than 30% of precipitation totals when characterized by the interval between 1951 and 2007 (Rodenhuis et al., 2009).

The PDO is a large-scale climate system that influences the surface climate and hydrology of Pacific North America (Whitfield et al., 2010). It is also recognized as influencing overall salmon abundance throughout the region (Mantua et al., 1997; Hare et al., 2002; Rogers et al., 2013). The PDO and its fluctuations are typically described as a long-lived ENSO event when describing variability in temperature and precipitation changes (Whitfield et al., 2010). Characteristic temperature fluctuations are apparent

Figure 5.1: Map of study area showing watershed boundaries. White circles with crosses represent points of interest (e.g., towns or mountains), triangles are tree-ring chronologies used in this study, and the outlined/faded regions are the three primary watersheds with salmon escapement information. Please note that the Lower Fraser Watershed was cut off at Hope, BC.

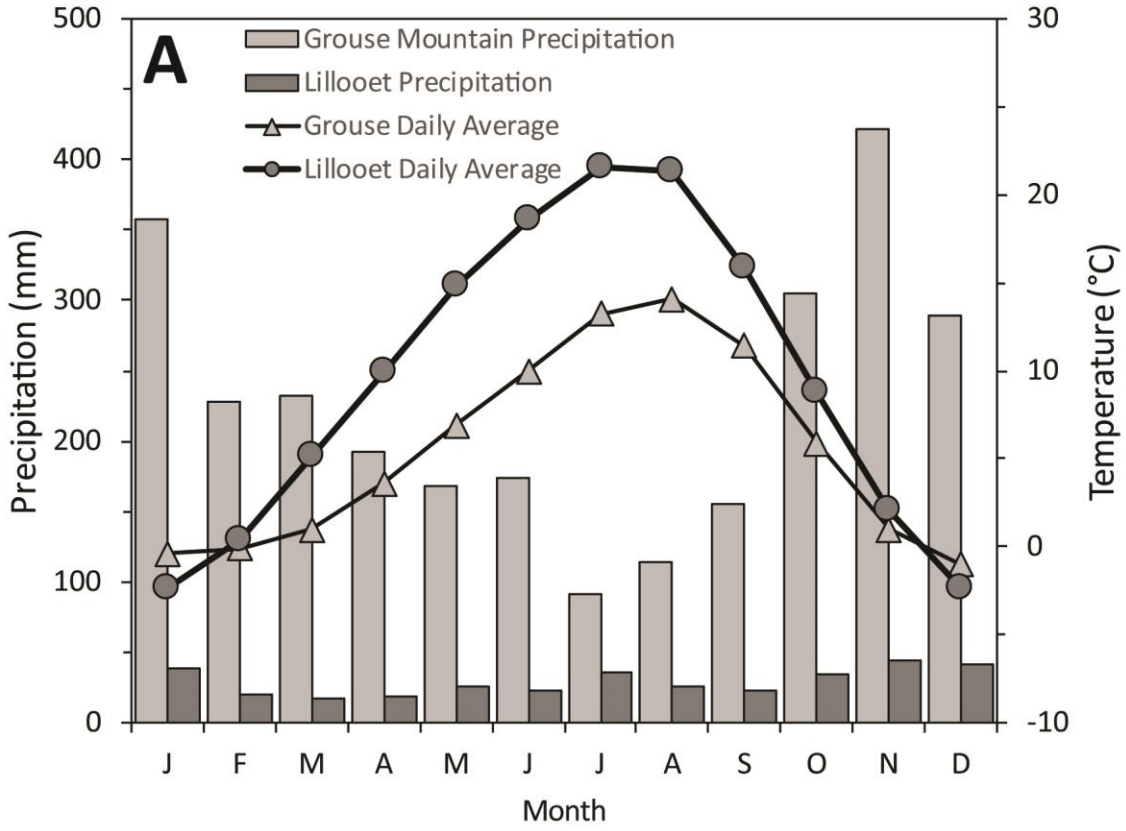

Figure 5.2: Climate normals (1981-2010) information for southwestern British Columbia for coastal (Grouse Mountain; Station ID: 1105658) and continental (Lillooet; Station ID: 1114619) regions. (Source: ECCC, 2017)

between warm and cool PDO phases (Kiffney et al., 2002; Whitfield et al., 2010), as exemplified by the abrupt 1976-77 shift change in average winter temperatures in BC (Hartman and Wendler, 2005; Stahl et al., 2006; Fleming and Whitefield, 2010). Phase changes in the PDO are known to influence the hydroclimate of southwestern British Columbia (Moore and McKendry, 1996; Rodenhuis et al., 2009). In the study area, precipitation totals tend to be higher during cool PDO phases and are lower during warm PDO phases (Kiffney et al., 2002; Stahl et al., 2006). In contrast, shifts in winter snowpack accumulation are less pronounced between warm- and cool-phases (~15% change) (Rodenhuis et al., 2009).

The PNA pattern is a quasi-polar climate relationship of semi-persistent pressure systems over the Pacific Ocean and North America that is influenced by PDO and ENSO (Latif and Barnett, 1994, 1996). The PNA influences the hydroclimatology of western North America and impacts salmon abundance in marine environments (Rogers et al., 2013; Litzow et al., 2018). The Aleutian Low is one of four primary centres of action for the PNA and is an important factor in climate-salmon relationships (Hare et al., 1999; Finney et al., 2000; Litzow et al., 2018). In southwestern BC and the Pacific Northwest, the PNA pattern is associated with freezing level elevations (Abatzoglou, 2011) that control snowpack distribution and, ultimately, the overall water equivalent storage for freshet runoff in the spring and summer months.

5.6 Methods

5.6.1 Tree-ring data

Tree ring samples were collected from mountain hemlock (*Tsuga mertensiana* (Bong.) Carr.) (MH), Pacific silver fir (*Abies amabilis* Douglas ex J. Forbes) (PSF) and Douglas-fir (*Pseudotsuga menziesii* (Mirb.) Franco) (DF) at high-elevation sites in southwestern BC in the summer of 2016. Sites were selected based on their proximity and ease-of-access to old growth subalpine forest stands. Only MH and PSF trees located above 1200 m asl were sampled, and only stands of DF trees located above 800 m asl were chosen for study. Previous research shows that the radial growth patterns of trees located above these elevations in this region is characteristically associated with hydroclimate variability (Peterson and Peterson, 2001; Ettinger et al., 2011).

Standard dendrochronological techniques were employed to collect increment cores with 5.1-mm increment borers (Fritts, 1976; Speer, 2010). After air drying and processing, the annual ring widths were measured at the University of Victoria Tree-Ring Laboratory (UVTRL) using a WinDendro™ digital measurement system (v. 2016a; Guay et al., 1992). Site-specific tree-ring chronologies were constructed by converting the ring width measurements to standardised indices using the R-package dplR to remove growth related trends (Bunn, 2008) with a 50-year cubic smoothing spline. To enhance the strength and regional signal of the reconstructions (Cook and Kairiukstis, 1990), archived tree-ring chronologies were downloaded from the International Tree-Ring Data Bank (ITRDB; NOAA, 2017). The site-specific chronologies were subsequently combined with the supplementary chronologies using a bi-weight robust mean method to create regional radial growth indices for each species (Briffa and Melvin, 2011). The site-level

series were employed in a principal component analysis (PCA) to develop records describing the underlying growth trends and to limit the influence of site-specific environmental controls (Brubaker, 1980). Only components explaining >10% of overall variability were kept and used in further statistical analysis.

Pacific Ocean climate oscillation records were retrieved from the National Ocean and Atmosphere Administration (NOAA) website (NOAA, 2017) for use as potential model inputs. Paleorecords related to hydroclimate of southwestern BC were targeted (Bonsal and Shabbar, 2002; Rodenhuis et al., 2009), including those describing PDO, ENSO and PNA (D'Arrigo and Wilson, 2006; Li et al., 2009; Trouet and Taylor, 2009).

5.6.2 Salmon escapement records

Salmon escapement records were retrieved from the New Salmon Escapement Database System (NuSEDS) (NuSEDS, 1999; Fisheries and Oceans Canada, 2018). Escapement records represent the number of returning salmon not intercepted by commercial or recreational fishing activities, and that are able to spawn. The NuSEDS database contains escapement estimates for over 9800 populations across BC and the Yukon (NuSEDS, 1999). Species-specific records were extracted where ≥ 35 years of escapement data was available in the geographic region of southwestern BC. The records were quality checked for missing information and, where the missing data was >10% in individual records, series were removed from further analysis. Records were grouped by species and input into a PCA to normalize the data and create timeseries representative of salmon escapement variability across the region. Only components explaining ≥10% of overall variability were retained and used in further statistical analysis. The PCA extracted variables of salmon proxy abundance independent of fisheries influences.

5.6.3 Weather and climate data

Climate oscillation indices were downloaded from NOAA (2017) and the University of Washington PDO data portal (2017). The Multivariate ENSO index (MEI) was retrieved for testing with the salmon and tree-ring records. MEI is the first principal component of six different parameters (sea level pressure, zonal and meridional surface wind, sea surface temperature, surface air temperature, and cloudiness) compiled using a bi-monthly sliding method (Wolter and Timlin, 1993, 1998). The PDO index is the leading principal component of North Pacific monthly sea surface temperatures (poleward of 20° N; Mantua et al., 1997) and was accessed through the University of Washington data portal (2017). The PNA oscillation index is determined by anomalies in geopotential height fields (at 700 and 500 millibars) over the western and eastern United States (Leathers et al., 1991, 1992) and was downloaded from NOAA (2017). All climate indices were seasonalized into winter (December-February; DJF), spring (March-May; MAM), and summer (June-August; JJA) values as well as annual water year (October of the previous year to September of the current year; and by averaging the targeted months for each category.

5.6.4 Reconstruction model

The salmon, tree-ring, and climate records were statistically examined to identify significant relationships between groups using Pearson's correlations. Salmon escapement reconstructions were developed using a multiple-linear regression of selected salmon species records in year *t* on candidate predictors in year *t* to *t+5*. Lagged predictors were entered to allow for tree-ring information from previous years to inform climate conditions in a given year. As different salmon species spend varying time in the

Pacific Ocean before returning to spawning grounds, I account for this by including up to 5 years of lagged predictors (Starheim et al., 2013b).

Salmon escapement models were developed from the assembled predictors. Each model was evaluated based on its explanatory power (adjusted R^2), autocorrelation (Durbin-Watson; DW), multicollinearity (variance inflation factor; VIF), uncertainty (standard error of the estimate; SE), the significance of the regression equation (*F*-ratio), and cross-validation success using the leave-one-out (LOO) method (reduction of error; RE).

5.6.5 Analysis of model

Statistical properties of shared intervals in the instrumental and reconstructed records were compared, as were salmon escapement records. This appoach allowed for an assessment of each model's skill to approximate the recorded salmon escapement value. Extreme high- and low escapement years were derived from the 5^{th}- and 95^{th}-percentile thresholds, as calculated from the full reconstruction period.

Associations between the proxy reconstructions and ENSO, PDO, and PNA were investigated. A difference-of-correlations test was used to understand whether negative or positive teleconnection phases were strongly linked with the measured or reconstructed salmon escapement values. An intervention analysis conducted over the full reconstruction period was used to detect long-term changes in salmon escapement. Intervention years were selected by employing a 30-year moving window to identify periods when there were significant differences between the first and last 15 years using a two-sample t-test. Periods of step change were calculated as a significant departure from the reconstructed mean.

Multitaper method (MTM) spectral analysis (Mann and Lees, 1996) was used to identify dominant frequencies of variability over the length of the reconstructed records. The MTM spectral analysis was conducted using the MTM-SSA Toolkit with robust background estimation (Ghil et al., 2002), and yields a more stable spectral estimate compared with other single-taper methods when examining short, noisy time series. To complement the MTM, a Morlet wavelet analysis was completed to illustrate the evolution of signal frequencies over time (Grinsted et al., 2004; Torrence and Compo, 1998). The test was conducted using a Morlet wavelet with a confidence level of 90% with the R package biwavelet (Gouhier et al., 2016).

5.7 Results

5.7.1 Tree-ring data

Five MH, three PSF, and three DF chronologies were selected for use (Table 5.1). While relatively few chronologies were constructed from trees located within the study area, all three tree species are known to be sensitive to regional-scale climate (Gedalof and Smith, 2001; Speer, 2010). The MH chronologies were all significantly correlated and were combined using a PCA representative of the underlying radial growth variability. Only the two components were used from the PCA (PC_{MH1} and PC_{MH2}), as all other components explained <10% of the total variance. Consolidating the five chronologies enhanced the explanatory power of the model but restricted the reconstruction period to 1711-1980 (Table 5.1).

Table 5.1: Times series information. Species/type are italicized and bold represents time series used as predictors in the reconstruction. Mountain hemlock PC1 and PC2 were developed by conducting a principal component analysis (PCA) on the five site-level chronologies listed. Other species did not have a sufficient number of sites to conduct PCA (<5) and were combined into regional chronologies using a bi-weight robust mean method. Climate oscillation indices were collected from NOAA (2017) for teleconnections that are known to influence the overall hydroclimate of western North America. [a] = correlations among tree-ring series collected from each site; [b] = only the length of the tree-ring index where the expressed population signal (EPS) was ≥0.85 is documented; [c] = RBAR is the average value across whole index where EPS was ≥0.85 and PC loading is the variance explained by PCA.

Time Series Name (Code)	Inter-series correlations[a]	Coordinates (Decimal Degrees)	Elevation (m asl)	Length[b]	RBAR/PC Loading[c]
Mountain hemlock					
Oakes Peak (WA051MH)[1]	0.520	48.63, -121.37	1140	1610 - 1992	0.313
Thornton Lakes (WA093MH)[2]	0.602	48.67, -121.33	1370	1706 - 1992	0.379
Heather Meadows (WA134MH)[3]	0.492	48.87, -121.68	1310	1685 – 2006	0.313
Joffre Lake (JLMH)[4]	0.607	50.34, -122.48	1550	1711 - 2012	0.428
Mount Cheam (MCMH)[5]	0.593	49.17, -121.69	1390	1637 - 2000	0.384
Mountain Hemlock PC1 (MH PC1)				**1711 - 1992**	**69.3%**
Mountain Hemlock PC2 (MH PC2)				**1711 - 1992**	**12.1%**
Pacific silver fir					
Mt. St. Helens (WA081AF)[6]	0.645	46.16, -122.15	1200	1648 – 1980	0.437
Seymour Watershed (CANA107)[7]	0.662	49.52, -123.04	1000	1686 – 1992	0.491
Hurricane Ridge (WA082)[6]	0.618	47.93, -123.41	1560	1698 – 1983	0.372
Regional Pacific Silver Fir (PSF*)*	**0.651**			**1648 – 1992**	**0.402**
Douglas fir					
Nooksak Falls (WA019)[2]	0.541	48.90, -121.80	550	1600 – 1975	0.288
Ross Lake (WA025)[2]	0.609	48.73, -121.05	612	1640 - 1975	0.451
Nahalatch Lake (DFN6)[8]	0.608	49.99, -121.71	950	1910 – 2015	0.530
Regional Douglas Fir (DF)	**0.477**			**1600 – 2015**	**0.289**
Climate Reconstructions					
Pacific Decadal Oscillation (PDO_{DW})[9]				1700 – 1980	
Pacific North American Pattern (PNA_{TT})[10]				1725 - 1999	

[1] Graumlich and Brubaker (1986); [2] Peterson and Peterson (2001); [3] Bunn (2012); [4] Wood et al. (2011); [5] Johnson and Smith (2010); [6] Schweingruber et al. (1991); [7] Dobry et al. (1996); [8] This Study; [9] D'Arrigo and Wilson (2006); [10] Trouet and Taylor (2006).

The three PSF chronologies were significantly correlated and were combined using a bi-weight robust mean into a single regional series extending from 1648 – 1992 (Table 5.1). These chronologies were not used in a PCA due to their limited number.

Three DF chronologies were significantly correlated and were combined using a bi-weight robust mean to develop a regional series extending from 1675 – 2015 (Table 5.1). The DF chronologies were not incorporated into a PCA due to their limited number.

Five MH chronologies used for the PCA had RBARs ranging from 0.313 to 0.428. The three PSF series RBARs range from 0.372 to 0.491, and the three DF series RBARs range from 0.205 to 0.530 (Table 5.1).

5.7.2 Salmon escapement data

While all five salmon species were targeted for reconstruction, the length, quantity, and quality of the relationships to Sockeye, Pink, and Chum salmon were inadequate for further investigation. In total, 55 Chinook and 13 Coho salmon records from the NuSEDS database came from monitoring sites located in the study area. Of the 55 Chinook records, 42 were suitable for further analysis (Table 5.2). The excluded records were removed because of numerous missing values (>10%). Of the 13 Coho records available, five were suitable for further analysis and the rest were removed due to high frequency of missing values (Table 5.2).

The record names and coordinates are shown in Table 5.2. Both arrays of data were input into a PCA to reduce noise associated with site-specific environmental conditions and fisheries influences, as well as to develop a regional record of escapement dynamics. For both records, only the first principal component was retained for analysis. The first principal component of Chinook salmon escapement records (Chinook PC1)

explains 37.2% of total variance; whereas the first principal component of Coho salmon escapement (Coho PC1) explains 49.6% of total variance.

5.7.3 Tree-ring and salmon escapement relationships to climate

Collected and processed salmon and tree-ring records were compared to seasonalized (DJF, MAM, JJA, and annual [A]) PDO, ENSO, and PNA climate oscillation indices (Table 5.3). Regional tree-ring indices were compared to PDO, ENSO, and PNA while Chinook PC1 and Coho PC1 were compared up to a five-year lag (Table 5.3). All tree species demonstrate strong, persistent relationships to winter, spring, and annual PDO values (Table 5.3). Only MH showed persistent associations to winter, spring, and annual PNA (Table 5.3). DF displayed a strong connection to wintertime PNA (Table 5.3). Both MH and DF were significantly correlated to winter and annual ENSO values (Table 5.3). PSF demonstrated a significant relationship to PDO (Table 5.3).

The regionalized salmon abundance records developed in this study show a very strong relationship to PDO (Table 5.3). Chinook PC1 was strongly correlated to springtime and annual PDO at all examined lag intervals (Table 5.3). Coho PC1 was less comprehensive in its association with PDO, demonstrated by significant relationships to wintertime and annual PDO from lag-1 to lag-3. ENSO-related association were not as strong but persistent for winter- and spring-time values to Chinook PC1 at lag-2 to lag-4 (Table 5.3). Coho PC1 exhibit similar association at lag-1, lag-3, and lag-4 (Table 5.3). PNA was only associated to Coho PC1 (Table 5.3). Where annual teleconnection values are expressed as providing the highest significance, 2 or more seasonal variables are highly correlated to a salmon record in Table 5.3.

Table 5.2: Watersheds (bold) and stream location names of Coho and Chinook salmon escapement records collected from NuSEDS database suitable for use. Coordinates are not provided for each stream as they were not documented in the NuSEDS database. x = record used for Coho and/or Chinook principal component analysis.

Waterbody Name	Coho	Chinook	Waterbody Name	Coho	Chinook
Chilliwack River			**Lower Fraser River**		
Borden Creek	x		Alouette River	x	
Chilliwack River	x	x	Blaney Creek	x	
Dunville Creek	x		Bouchier Creek	x	
Elk Creek	x		Clayburn Creek	x	
Luckakuck Creek	x		Coho Creek	x	
Salwein Creek	x		Coquitlam River	x	
Sumas River	x		Kanaka Creek	x	
			Macintyre Creek	x	
Harrison River			North Alouette River	x	
Chelhalis Creek	x	x	Nathan Creek	x	
Harrison Creek		x	Silverdale Creek	x	
Hicks Creek	x		Stave River	x	
Inch Creek	x		Sweltzer Creek	x	
Lorenzetta Creek	x		Upper Pitt River	x	x
Norrish Ceek	x		West Creek	x	
Pye Creek	x		Whonnock Creek	x	
Siddall Creek	x		Widgeon Creek	x	
Squakum Creek	x		Yorkson Creek	x	
Weaver Creek	x				
Worth Creek	x				
Lillooet River					
Birkenhead River	x	x	Ryan River	x	
Green River	x		Salmon River	x	
Pemberton Creek	x		Salmon Creek	x	
Poole Creek	x				

5.7.4 Reconstruction model

Two models were identified for reconstruction:

$$Coho\ PC1 = -2.92 + (-0.55*MHPC2_{t-1}) + (2.86*DF_{t-4}) + (-0.29*PNA_{t-2}) \pm 0.71$$

$$Chinook\ PC1 = -1.24 + (0.22*MHPC1_{t-1}) + (0.92*PSF) + (0.86PDO_{t-5}) \pm 0.54$$

where: Coho PC1 is the first principal component of collected salmon escapement records in southwestern British Columbia; $MHPC2_{t-1}$ is the previous year's second principle component of the regional mountain hemlock tree-ring index; DF_{t-4} is the regional Douglas first tree-ring record value from four years prior; PNA_{t-2} is the Pacific-North American pattern tree-ring reconstruction value from two years prior (Trouet and Taylor, 2009); Chinook PC1 is the first principal component of collected salmon escapement records in southwestern BC; $MHPC1_{t-1}$ is the previous year's first principle component of the regional mountain hemlock tree-ring index; PSF is the regional Pacific silver fir tree-ring index of the current year; and PDO_{t-5} is a Pacific Decadal Oscillation reconstruction (D'Arrigo and Wilson, 2006) from five years prior.

Time plots of the Coho and Chinook reconstructions are shown in Figures 5.3A and 5.3B, respectively. The Coho reconstruction spans the period the 1727-1987 interval and uses the first principal component of 42 independent abundance records spanning the interval from 1951-1987 (Coho PC1). The model selected for use explains 48.9% of variance in Coho PC1, accounting for lost degrees of freedom (Table 5.4). The model has a DW statistic of 1.60, VIF of 1.08, and F-ratio of 10.25 (Table 5.4). The model was

Table 5.3: Correlation values for salmon escapement and tree-ring records to seasonalized climate oscillation indices. For salmon escapement records, only the most significant correlation was documented and others may exist (see Appendix A for full list of salmon correlations). DJF = December (of the previous year), January, and February; MAM = March, April, and May; JJA = June, July, and August; A = Annual. September, October, November was excluded from the Table 5.3 as no significant correlations were documented.

	Salmon Escapement Records					*Tree-Ring Records*				
	Chinook PC1		*Coho PC1*							
ENSO	Value	Season	Value	Season	Interval	*MH PC1*	*MH PC2*	*MH*	*DF*	*PSF*
lag-0					DJF		**0.52**	0.38	**0.39**	
lag-1			-0.30	DJF	MAM					
lag-2	0.30	DJF			JJA					
lag-3	0.33	MAM	**-0.39**	**A**	A		**0.42**	0.33	**0.45**	
lag-4	0.33	MAM	0.33	MAM						
lag-5										
PNA										
lag-0					DJF		0.32	0.35	**0.40**	
lag-1					MAM			0.31		
lag-2					JJA					
lag-3			-0.31	A	A			0.33		
lag-4										
lag-5										
PDO										
lag-0	**0.48**	**A**			DJF		**0.66**	**0.44**	**0.47**	**0.40**
lag-1	**0.42**	**A**	**-0.36**	**DJF**	MAM		**0.51**	**0.41**	0.33	**0.43**
lag-2	**0.48**	**A**	**-0.44**	**A**	JJA					
lag-3	**0.50**	**MAM**	**-0.43**	**A**	A		**0.54**	**0.39**	0.36	**0.43**
lag-4	**0.47**	**MAM**								
lag-5	**0.47**	**MAM**								

successfully cross-validated using the LOO method (RE = 0.16) and a time plot of calculated, modelled, and cross-validate Coho PC1 are shown in Figure 5.4A. The Chinook reconstruction uses the first principal component of five independent abundance records from 1951 to 2017 (Chinook PC1) and spans the interval from 1712 to 1980. The model selected for use explains 48.2% of variance in Coho PC1, accounting for lost degrees of freedom (Table 5.4). The model has a DW statistic of 1.60, VIF of 1.08, and an F-ratio of 10.51 (Table 5.4). The model was successfully cross-validated using the LOO method (RE = 0.26) and a time plot of calculated, modelled, and cross-validate Chinook PC1 are shown in Figure 5.4B.

5.7.5 Analysis of reconstructions

The reconstructed and observed Chinook PC1 and Coho PC1 records were compared to the PNA, PDO, and ENSO teleconnection indices. Difference-of-correlations tests revealed strong relationships between reconstructed Chinook PC1 and negative PDO, with the strongest relationships observed during the spring time and over the length of the water year (March – May and November-October; $p< 0.01$) (Table 5.5). Negative spring ENSO and reconstructed Chinook PC1 were also significantly linked ($p<0.05$) (Table 5.5). No significant relationships were revealed between the calculated Chinook PC1 and climate indices. Reconstructed Coho PC1 was significantly related to negative winter and spring ENSO ($p<0.01$) (Table 5.5). Calculated Coho PC1 was significantly related to negative winter ENSO and positive summer PNA (Table 5.5).

Intervention analysis was used over the full reconstruction period for both models to detect long-term changes or shifts in abundance. A two-sample test identified 17

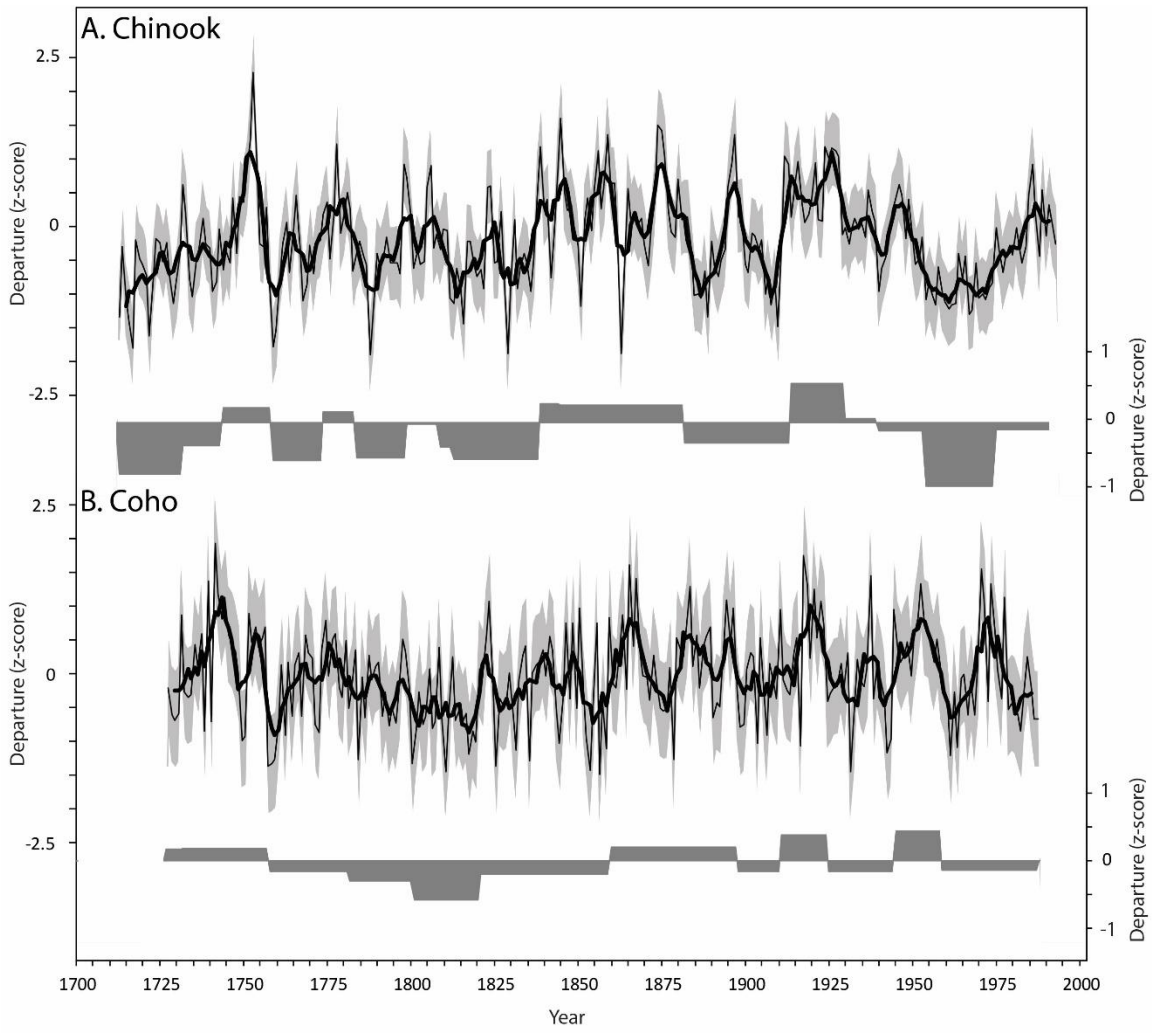

Figure 5.3: Full reconstructed record of (A) Chinook PC1 and (B) Coho PC1.The thin-black line represents actual modeled values, thick-black lines are a 5-year running mean, and grey areas are error calculated by the cross-validation RMSE. The grey-filled areas below each reconstruction show changes in the long-term mean. Grey-filled areas above 0 indicate long-term above average conditions while below indicate below average conditions. Step changes from one long-term mean to another are where significant intervention years were detected using a two-sample t-test on the previous and future 15 years for year *t*. long-term averages were calculated as the mean value between intervention years.

Table 5.4: Reconstruction, cross-validation, and descriptive statistics. D-W = Durbin-Watson Statistic; VIF = variance inflation factor; SE = standard error; RE = reduction of error; RMSE = root mean squared error; CV = coefficient of variance.

Reconstruction	R^2	Adj. R^2	D-W	VIF	SE	F-ratio
Chinook PC1	0.48	0.43	1.60	1.08	0.55	10.25
Coho PC1	0.48	0.44	1.60	1.08	0.75	10.51

Cross-Validation	RE	RMSE
Chinook PC1	0.16	0.54
Coho PC1	0.27	0.71

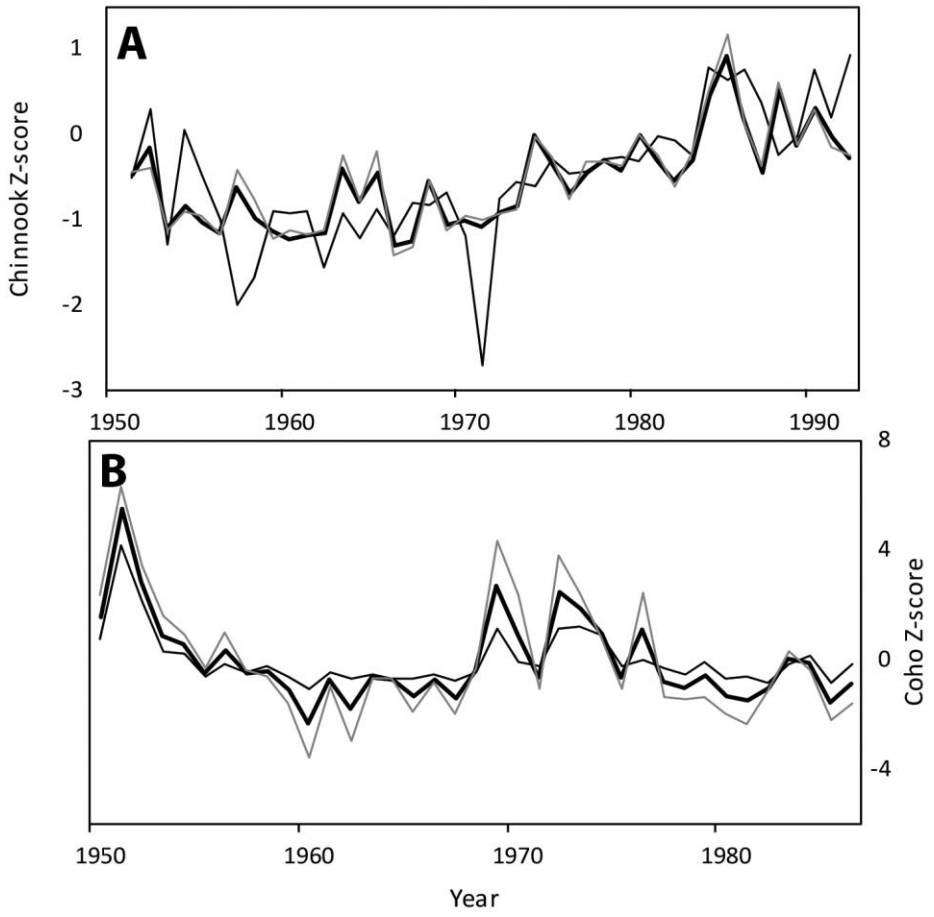

Figure 5.4: Time plot of (A) Coho PC1 and (B) Chinook PC1 calculated (thin black), reconstructed (thick black), and cross-validated (grey) for the calibration period (1951-1992).

Table 5.5: Difference-of-correlations test results for Chinook PC1 and Coho PC1. Climate oscillation indices were grouped into negative and positive values then correlated to both the calculated and reconstructed Chinook and Coho PC1 values. Values shown are *p<0.05* while **bold** values indicate *p<0.01*. Where only one of two teleconnection phases is significantly correlated, it illustrates the possibility of a non-stationary response.

	Chinook PC1				Coho PC1			
	Reconstructed		Calculated		Reconstructed		Calculated	
	Negative	Positive	Negative	Positive	Negative	Positive	Negative	Positive
PNA								
DJF								
MAM								
JJA								-0.47
A								
ENSO								
DJF					**-0.39**		**-0.57**	
MAM	0.38				**-0.42**			
JJA								
A								
PDO								
DJF	0.36							
MAM	**0.41**							
JJA	0.29							
A	**0.41**							

significant changes in the Chinook PC1 record and 12 shifts in Coho PC1 over the reconstruction period (Figure 5.3). Chinook PC1 demonstrates a significant shift every 16 years on average, while Coho PC1 showed significant changes approximately every 21 years. The interval between Chinook PC1 interventions ranged from 37 (1843-1880) and 4 (1807-1811) years, while Coho PC1 ranged from 39 (1820-1859) and 5 (1924-1929) years (Figure 5.3). The most significant departures in the long-term mean occurred from 1973-1952 (-0.95) and 1928-1912 (+0.57) for Chinook PC1 and 1800-1820 (-0.59) and 1958-1944 (+0.43) for Coho PC1 (Figure 5.3).

The MTM and Morelet wavelet spectral analyses revealed several dominant frequencies in both the Coho and Chinook reconstructions over time. Analysis of the Coho PC1 reconstruction revealed significant frequencies of inter-annual variability at intervals of between 2 and 4 years, as well as inter-decadal fluctuations at 25-year intervals (Figure 5.5A). Complementary Morelet wavelet analyses corroborated the presence of these variabilities, but also demonstrated that fluctuations over a 25-year interval were unstable over time. Specifically, the wavelet analysis illustrates that the 25-year dominant frequency becomes less pronounced after 1850 within the Coho PC1 reconstruction (Figure 5.5B).

Spectral analysis of Chinook PC1 using the MTM method shows that the inter-annual variability at between 3 and 6 years was stable over the length of the reconstruction (Figure 5.5C). While inter-decadal variability was not recognized as significant over the full length of the Chinook PC1 reconstruction, unstable variability was detected in the Morelet wavelet spectral analysis from the 1750s to the late 1700s, as well as from the 1850s to the early 20th century (Figure 5.5D).

5.8 Discussion

5.8.1 Model summary

The proxy Chinook and Coho abundance models estimate salmon variability in southwestern BC over the past 300 years. The lowest single-year abundance was identified in 1787 (z-score = -1.90) for Chinook and in 1856 (-1.51) for Coho. The highest magnitude, multi-year interval of below-average abundance occurred from 1869-1872 (average of -1.33) in the Chinook population and from 1931-1932 (average -1.13) in Coho. Intervention analysis revealed long-term changes in mean abundance characterized by prolonged below-average periods for both species. Of particular note are persistent low abundance values from 1782-1837 (55 years) and 1952-1992 (40 years) in Chinook, and in the Coho escapement reconstruction over the interval 1757-1859 (98 years) and 1958-1987 (29 years).

Both reconstructions indicate that Chinook and Coho experienced significant, repeated, and quasi-periodic changes in abundance at intervals averaging 16 and 21 years, respectively. In contrast to a single ≥10-year interval of proxy abundance in the Coho reconstruction when the annual values fell below the long-term average, there are six ≥10-year periods in the Chinook reconstruction when the annual abundance fell below the long-term average. The longest interval of consecutive below-average proxy abundance was 33 years (1949-1983) for Chinook and 10 years (1959-1968) for Coho.

The first principal component of both species that was used for reconstruction successfully removed fisheries-related influences. This is highlighted by the strong statistical relationships between Coho PC1 and Chinook PC1 to low frequency climate variability generated from the Pacific Ocean.

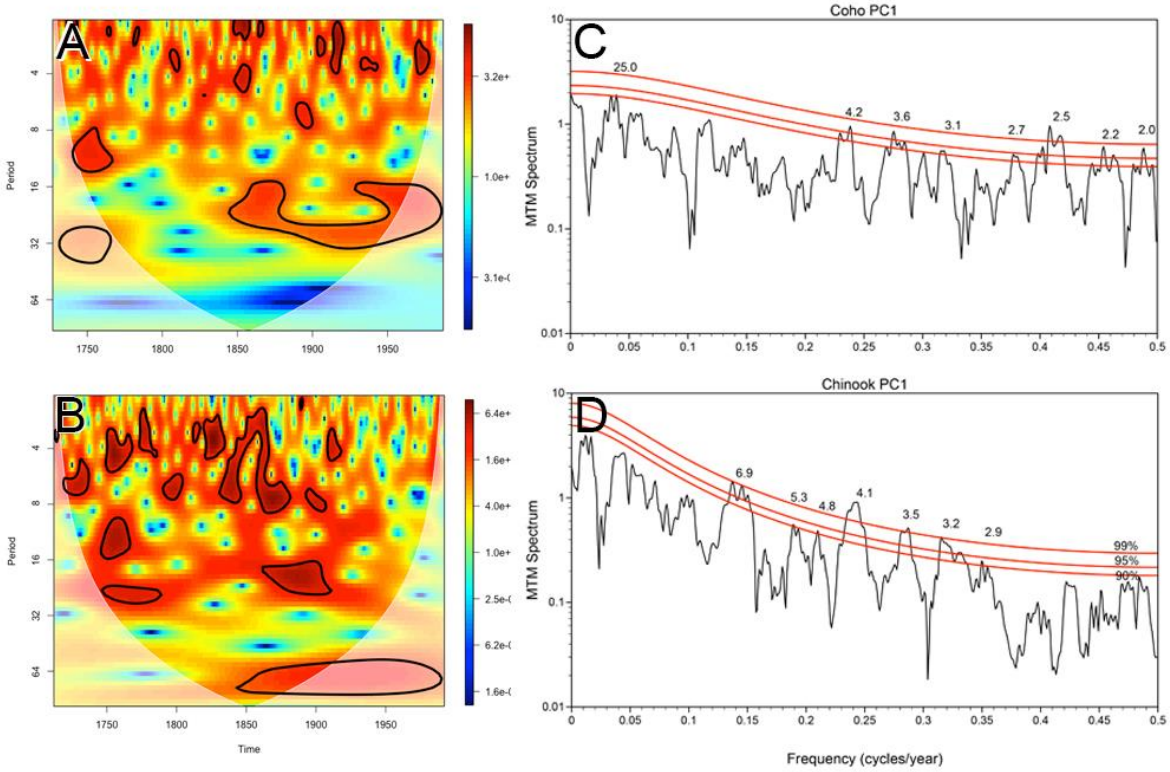

Figure 5.5: Spectral analysis of Coho (A, C) and Chinook (B, D) PC1 reconstructions: Morlet wavelet power spectrum of the proxy Coho (A) and Chinook (B) records. Black enclosed areas represent a 95% confidence interval based using a white-noise background spectrum. The faded areas represent periods and frequencies of the analysis that is susceptible to zero padding effects due to sample depth. Multitaper method (MTM) spectral analysis of Coho (C) and Chinook (D) proxy records. Red curves represent 90%, 95%, and 99% (bottom-top) significance. Significant ($p \leq 0.10$) power exists at labelled frequencies.

5.8.2 Relationship to teleconnections

It is generally accepted that large-scale salmon population fluctuations in the eastern Pacific Ocean region are related to the impact of climate oscillations on marine environments (e.g., Pearcy, 1992; Mantua et al., 1997, 2015; Litzow et al., 2018). In the case of marine Coho and Chinook populations, prior research indicates that both ENSO and PDO are strongly linked to escapement success (e.g., Wells et al., 2006). The results of this study corroborate this relationship in southwestern BC by finding that the return success of both species shows strong relationships to ENSO and PDO (Table 5.5). While Chinook PC1 exhibited positive relationships to ENSO and PDO, Coho PC1 demonstrated a negative association to both. Similar relationships have been identified for salmon across large geographic regions, but not between species returning to the same natal habitat (Wells et al., 2006). In this instance, the different associations are presumed related to the north and south ocean gyre transition zones (Hare et al., 1999) that may correspond with the different migratory pathways used by Coho and Chinook in the eastern Pacific Ocean (e.g., Quinn and Dittman, 1990; Wells et al., 2006; Litzow et al., 2018).

Chinook abundance was shown to be significantly associated with PDO at seasonal and annual scales across multiple years. Similarly, long-term Coho abundance is correlated with PDO at seasonal and annual scales across multiple years. The association of Chinook abundance to PDO was strongest during the spring, at a time in the year that has previously been associated with the species' overall health in marine environments (Daly et al., 2017). The long-term reconstructions for both species also demonstrate an association to spring and winter ENSO conditions. While Chinook demonstrate up to five

years of lagged relationship to PDO, Coho exhibited associations for only up to four years with ENSO. Similar relationships are documented elsewhere in Pacific North America and are presumed related to the shorter life history of Coho when compared to Chinook (e.g., Wells et al., 2006; Drake et al., 2007; Starheim et al., 2013b).

Phase dependent relationships between salmon abundance and climate oscillations were examined to reveal whether any non-stationary associations exist as previously postulated (Litzow et al., 2018). Despite prior findings pointing to salmon population variability as related to the relative strength of an oscillation rather than its phase, this analysis revealed the presence of a significant correlation between proxy abundance trends and negative phases of both ENSO and PDO (Table 5.5). Chinook proxy abundance was specifically shown to be linked to negative PDO and spring ENSO, while Coho PC1 was associated to spring and winter negative ENSO.

A significant 25-year abundance cycle was documented in the MTM analysis for Coho (Figure 5.5). This cycle was interpreted as associated with climate oscillation-related fluctuations linked to PDO similar to results from Welsh et al. (2019). Mortlet wavelet analysis also described a dominant 25-year frequency, but suggests this association was not time-stable before the 1850s, where it was not statistically significant (Figure 5.5). Similar instabilities reside in the long-term reconstruction of Chinook abundance, where a dominant 25-year frequency was documented from the 1750s to the late 1700s, and again from the 1850s to the early 20th century (Figure 5.5). This relationship was attributed to relative strength of both PDO and ENSO (Mantua et al., 1997; Hare et al., 2002; Litzow et al., 2018). In both instances, the inter-decadal variability exists only during certain periods and is not significant across the entire time

series (Figure 5.5). This finding likely reflects a non-stationary response to the relative strength of the Aleutian Low over long intervals (Litzow et al., 2018).

5.8.3 Chinook and Coho cohort resonance

Cohort resonance is the sensitivity shown by fish populations to environmental variability on timescales approximating one generation (Bjornstad et al., 2004; Worden et al., 2010; Botsford et al., 2014). Spectral analysis of proxy Coho and Chinook abundance revealed 3-7- and 2-4-year dominant frequencies over the length of the records that was presumed associated with generational cohort resonance. Identification of cohort resonance at these frequencies provides evidence of stochastic interactions that may be shaping the dynamics of both Coho and Chinook populations, respectively (Bjornstad et al., 2004). Resonance also substantiates climatic variability as a strong component of population change, rather than behavioral shifts driving population (Bjornstad et al., 2004; Botsford et al., 2014). Further, it corroborates the findings of recent studies that show that environmental controls may be a more critical factor of overall abundance than other known controlling factors (Mantua et al., 2015; Munez et al., 2015, 2016), discoveries of particular interest to fisheries managers charged with establishing annual catch quotas (Hilborn and Walkters, 1992).

5.8.4 Comparison to other records

The proxy Chinook and Coho abundance records developed in this research differ from prior tree ring-based reconstructions of long-term salmon populations in western North America (Drake et al., 2007; Starheim et al., 2013b). These differences are attributed to several factors. First, the records developed in this study target climate-related influences on escapement. This approach differs from that of Drake et al. (2007)

and Starheim et al. (2013b) who employed ecological and hydrological associations in the development of their reconstruction models, respectively. My reconstructions cannot be directly compared to either of these studies as they sought to understand different components of long-term salmon abundance variability (e.g., Drake et al. (2007) sought to determine nutrient related variability). Second, my reconstructions focused on achieving a regional-scale understanding of Chinook and Coho salmon variability, while Drake et al. (2007) and Starheim et al. (2013b) sought to develop local and basin level approximations. Third, neither Drake et al. (2007) or Starheim et al. (2013b) were able to reconstruct proxy escapement records for Coho, and thus their findings are not directly comparable to this reconstruction because of the varying life histories of it to other species (Pearcy, 1992). Finally, while Drake et al. (2007) and Starheim et al. (2013b) do present proxy Chinook escapement records, prior research shows that salmon populations across large geographical regions are distinct and respond differently to Pacific Ocean climate oscillations (Hare et al., 1999). For example, population trends in California and Gulf of Alaska show that salmon respond differently to climate oscillations generated from the Pacific Ocean (Hare et al., 1999; Wells et al., 2006). When PDO or ENSO are positive, coastal California experiences decreased surface upwelling, higher sea surface temperatures, less nutrients and overall reduced primary and salmon production while the opposite is true in the Gulf of Alaska (Wells et al., 2006). Previous research shows that this differential response to PDO and ENSO are associated with the residence of salmon within both the North Pacific and California currents (Kilduff et al., 2015). Both currents diverge at the approximate latitude of my study area and the contrasting relationships between proxy records and climate oscillations suggests salmon in southwestern British

Columbia may migrate with either ocean current once they reach marine environments (Kilduff et al., 2015). I hypothesize that Chinook populations from southwestern British Columbia subsist in the Gulf of Alaska region current while Coho thrive in the more southerly regions associated with the California Current.

5.9 Conclusions

The proxy reconstructions developed in this study suggest that the full range of escapement variability for Chinook and Coho is underestimated if solely based on observed population dynamics since 1951. The intervention analysis revealed that Chinook PC1 has been at below or at normal abundance since 1951 when compared to the full reconstruction period. In contrast, proxy Coho abundance has been either above or close to normal levels since 1951, when compared to the full reconstructions. The Chinook PC1 reconstruction indicates that the longest uninterrupted period of below average proxy abundance values occurred during the observed period from 1949-1983, but three other timespans were characterized by larger magnitude escapement numbers. Similarly, the proxy Coho PC1 record indicates the longest continuous span of below-average abundance occurred during the observed period from 1959-1968 but, again, other intervals experienced greater multi-year collapses. Based upon these discoveries, fisheries management strategies should be revised to accommodate the discovery of long-term abundance variability not recorded over the historical observation period.

The findings of the research illustrate the important role of both high- and low-frequency climate oscillations on salmon populations returning to their natal habitat in southwestern British Columbia watersheds. The PDO is identified as particularly

important driver of Chinook abundance, with ENSO appearing as a more dominant influence on Coho abundance. Interestingly, the abundance of the two species shows opposing relationships with PDO and ENSO. While Chinook salmon illustrate a positive relationship to negative PDO, Coho salmon exhibits negative associations to ENSO. I hypothesize that the contrasting relationships are associated with salmon migration patterns following entry to marine environments. Coho may migrate southward towards the California Current while Chinook likely migrate to more northerly areas associated with the Gulf of Alaska and North Pacific. Increasing intensity of ocean-atmosphere interactions linked to anthropogenic climate change may cause more extreme fluctuations in salmon populations in the immediate future. The discovery of phase-specific relationships suggests further study is necessary to understand the interactions between non-stationary climate oscillations and species abundance.

An important finding of the research was documentation of the cyclical nature of salmon population abundance within the Chinook PC1 reconstruction. Coho PC1 also exhibited marked periodic decreases and long-term changes in mean abundance but Chinook PC1 changed with a regular frequency over the last 300 years. Both records are an excellent resource for fisheries managers charged with planning and implementing safety measures for salmon populations throughout southwestern British Columbia. The records also provide valuable insights into regional-scale climate-salmon relationships across the study region rather than providing site-specific information.

Chapter 6: Conclusion

6.1 Introduction

This dissertation describes the hydroclimate history of southwestern British Columbia (BC) over the last three centuries and identifies the climate-related factors that play a role in its variability over time. Specifically, I provide a long-term assessment of three critical water supply components in southwestern BC: (1) snowpack; (2) lake levels, and; (3) streamflow. The records of streamflow (Chapter 3) and salmon (Chapter 5) are of immediate use to resource managers because of their direct application to present and future management strategies and policies. The proxy records of snowpack (Chapter 2) and lake levels (Chapter 4) serve to advance and augment our understanding of hydrology and water supply as it relates to historical storage capacity and variability.

While each of the proxy records developed in the dissertation uses different variables to reconstruct hydroclimate fluctuations beyond the instrumental period, a common theme arises from each – the historical records of snowpack, streamflow, lake level and salmon escapement all fail to capture their full range of natural variability. Further, the mean values associated with the instrumental records all tend to be less than those reported by the reconstructions. For the Metro Vancouver area, this finding indicates that present-day streamflow totals in July-August are typically only 77% of the 300-year average. For Harrison Lake, the research shows that the average volume of water stored in the lake in April has decreased by approximately 283-million litres between 1933 and present when compared to the past 300 years. Both summer streamflow and spring lake levels in the region are influenced by snowpack delivered

during the winter months and the changes documented in the dissertation are a consequence of both climate change and long-term teleconnection variability.

6.2 Primary research results

The following identifies key findings of this dissertation:

1. Coastal April 1 Snow water equivalent (SWE) was more sensitive to annual changes when compared to continental zones. While trends between the two geographic regions demonstrate similar long-term fluctuations over time, the amplitude of SWE variability in coastal regions was much greater than in continental areas. In comparison to continental sites in southwestern BC that experienced eight significant changes in average April 1st SWE values, the reconstruction suggests coastal settings experience greater SWE variability with at least 11 distinct step-changes recorded in the long-term average April 1st record.
2. The seasonal snowpack, streamflow, and lake level reconstructions indicate that, in recent years, annual water supply quantities in southwestern BC are below their 300-year average, and that the instrumental record does not account for the full range of variability. For instance, since 1977 average July-August streamflow in the Capilano and Seymour watersheds has been well-below the average value characterizing the past three centuries. Since 1900, the reconstruction also indicates an increased frequency of consecutive below-average July-August streamflow intervals. Similarly, since 1933 the amount of water stored in Harrison Lake on April 1st represents an average annual volumetric loss of 283-million

litres. The trend of below-average summer runoff and reduced water storage should be expected to continue under present and future climate change.

3. Salmon abundance in the streams and rivers of southwestern BC has undergone cyclical changes over the past 300 years, and the instrumental record does not account for the full range of variability in either Chinook or Coho populations. Both reconstructions were able to account for life histories and illustrated that Chinook and Coho salmon reside in distinct marine settings following their freshwater natal stage.
4. Snowpack was shown to be a primary control of both streamflow and natural lake level variability over the last 300 years in southwestern BC. Further, April 1 SWE was shown to be strongly linked to PDO variability. Negative phases of the PDO were shown to be significantly associated with SWE trends, summer streamflow characteristics, and salmon abundance. Intervals of positive PDO were correlated to long-term April lake levels at Harrison Lake.

Previous research demonstrated that the PDO significantly influences regional hydroclimatic variability (e.g., Belmechari et al., 2015; Coulthard et al., 2016; Mote et al., 2018; Welsh et al., 2019). This dissertation confirms those findings and documents phase-dependent associations between negative phases of PDO and ENSO to snowpack, streamflow, lake level, and proxy salmon abundance.

6.3 Application for water resource management

The hydroclimate variables reconstructed in this dissertation will be useful to natural resource managers charged with developing management plans and policy in southwestern BC:

1. Both coastal and continental April 1 SWE reconstructions illustrate contrasting variability and sensitivity to teleconnections and reinforce our current understanding of regional interactions. They demonstrate that long-term changes in average snowpack should be considered in management plans and decisions in southwestern BC.
2. The long-term record of dry-season streamflow of Metro Vancouver's water supply confirms that the full range of July-August runoff is likely measured in the instrumental record. The long-term reconstruction does, however, indicate that the frequency of low-flow events may be misinterpreted if based on solely on the instrumental records. The combined Capilano and Seymour watershed July-August streamflow records, when combined with climate change projections, will augment new water policy and management strategies by providing a better overall understanding of variability, trends, and relationships to teleconnections.
3. The Harrison Lake April 1st water level reconstruction identifies a decrease in lake storage over the past 300 years. While the lake is not a reservoir for Metro Vancouver, it is the largest lake in southwestern BC and provides water supply for other areas of the Lower Mainland The information developed in this study may help local water resource managers understand how the storage of natural, mountainous lakes in southwestern BC varied over the past three centuries.

4. Reconstruction of proxy Chinook and Coho abundance returning to streams in southwestern BC suggests that they have contrasting relationships to long-term regional climate oscillations. While similar associations have been documented previously, they were typically observed across broad geographic regions and were not focused on species-specific relationships. The reconstructions will be of interest to fisheries managers, as they provide a long-term understanding of climate-related salmon abundance variability essential for developing sound policy and management strategies under present and future climate change.

6.4 Research limitations

"All models are wrong but some are useful" - Box (1976)

6.4.1 Model accuracy and strength

The goal of this dissertation was to describe hydroclimate variability prior to the instrumental record using tree radial growth and teleconnection relationships to develop linear models of important hydrological variables. While all the developed models pass statistical cross-validation (e.g., RE > 0) and are considered accurate, the outcomes of my findings should be tempered. Excluding Chapter 4, all the developed models are either normalized or based on principal component analysis (PCA) and are unable to describe the full range of variability. This is especially demonstrated in my July-August streamflow reconstruction of the Capilano and Seymour watersheds (Chapter 3). It is evident that the instrumental record is much more variable than the reconstructed record.

This could be accurate but it may also indicate that the model is unable to describe the full range of variability. The normalization of the records, although necessary, may have also caused both the instrumental and reconstructed record to underestimate variability as well.

In both April 1 SWE and salmon escapement population reconstructions (Chapter 2 and 5, respectively) were developed using the first principal component of regional instrumental records. No component explains 100% of variability that is reconstructed and explained variance ranges from 37% (Chinook PC1) to 89% (coastal SWE_{PC}). Regardless of linear model strength, they were unable to account for total variability although accurately describe general long-term trends in all reconstructed records.

6.4.2 Teleconnection inferences

All the models developed in this dissertation used teleconnection reconstructions to supplement tree-ring data. As a result, difference-of-correlations analysis outputs for reconstruction models should be taken with some caution. For example, the July-August streamflow reconstruction (Chapter 3) has incredibly high correlation values to PDO (e.g., >0.80 at an annual timestep) that can be attributed to the use of it as a model predictor. Difference-of-correlation outputs for instrumental records should be given more weight although sample size is typically much lower. Where similar relationships are observed between it and the reconstructed records, it serves to illustrate the accuracy of the model.

Where both the instrumental and reconstructed records illustrate significant relationships to only positive or negative phases of a given teleconnection, it indicates a non-stationary response to ENSO, PDO, or PNA. A non-stationary response

demonstrates that the model may not account for the full range of fluctuations in power over time. Where significant relationships are identified in both phase of a teleconnection, it may suggest more the reconstructed record is able to account for a wider range of possible variability.

6.5 Future research

Following the completion of the dissertation research, I identified several areas for future research.

1. Prior research focusing on snowpack and other hydroclimate reconstructions primarily used tree-ring width chronologies as was done in this dissertation. Moving forward, other underutilized annually-resolved measurements from tree-rings could be used to enhance and expand on past hydroclimate variability. In particular, tree-ring isotopes and density properties could prove useful for future research. Other variables, such as cell-properties could be applied as well. All these variables are linked to temperature fluctuations and could be used to augment interpretations of hydroclimate-related variability associated with fluctuations in temperature.
2. The approach taken to develop a long-term lake level history offers a new water resource-based focus for future dendrohydrological studies. Where lake level records are sufficient, they should be reconstructed to develop a better understanding of water storage in critical basins. Methods could be augmented by using other complementary proxy measurements including lake sediment records or tree-ring isotopes. Lake sediment cores may provide a better overall

understanding of lake level changes over the full season rather than at monthly scales conducted in this study. Tree-ring isotopes may offer a better understanding of evaporative rates of large lake bodies through temperature relationships.

3. The research presented in Chapter 4 illustrates the potential to reconstruct long-term salmon abundance using their common climate relationship to high-elevation trees. The reconstructions could be enhanced by combining my methods with those of Drake et al. (2002). This would require the collection of climate-sensitive tree-ring records in high elevation regions and riparian tree-rings sensitive to nutrient availability.

6.6 Summary

This dissertation presents six tree-ring based reconstructions of April 1 SWE, streamflow, lake levels, and salmon abundance. Chapter 2 provides a long-term understanding of April 1 SWE trends over the last 300 years in southwestern BC. Chapter 3 presents a regionalized July-August streamflow reconstruction of the Capilano and Seymour watersheds. The record will provide local water supply managers with a greater understanding of dry-season streamflow variability and long-term trends illustrating that recent discharge has been well-below the reconstructed average. Chapter 4 presents a reconstruction of waters levels in Harrison Lake and provides a long-term understanding of water storage trends in southwestern BC in hybrid-regime systems. Chapter 5 presents two records of proxy salmon abundance in southwestern BC. The Chinook and Coho proxy abundance records highlight cyclical fluctuations in population levels which are linked to negative PDO and ENSO. The records have contrasting relationships to climate

oscillations. Coho was negatively linked to PDO and ENSO while Chinook was positively linked to both. Each record independently highlights the importance of teleconnections generated from the Pacific Ocean especially negative phases of PDO and ENSO.

References

Abatzoglou JT (2011) Influence of the PNA on declining mountain snowpack in the western United States. *International Journal of Climatology*, 31: 1135-1142.

Anchukatis KJ, Wilson R, Briffa KR, Buntgen U, Cook ER, D'Arrigo R, Davi N, Esper J,Frank D, Gunnarson BE, Hegerl G, Helama S, Klesse S, Kursic PJ, Linderholm HW, Myglan V, Osborn TJ, Zhang P, Rydval M, Schneider L, Schurer A, Wiles G, and Zorita E (2017) Last millennium Northern Hemisphere summer temperatures from tree rings: Part II, spatially resolved reconstructions. *Quaternary Science Review*, 163: 1-22.

Asong ZE, Wheater Hs, Bonsal, B, Razavi S, and Kurkute S (2018) Historical drought patterns over Canada and their teleconnections with large-scale climate signals. *Hydrology and Earth System Sciences*, 22: 3105-3124.

Ballinger TJ, Rohli RV, Allen MJ, Robinson DA, and Estilow TW (2018) Half-century perspectives on North American spring snowline and snow cover associations with the Pacific-North America teleconnection pattern. *Climate Research*, 74: 201-216.

Beaulieu M, Schrier H, and Jost G (2012) A shifting hydrological regime: a field investigation of snowmelt runoff processes and their connection to summer base flow, Sunshine Coast, British Columbia. *Hydrological Processes*, 26: 2672-2682.

Belcmecheri S, Babst F, Wahl ER, Stahle DW, and Trouet V (2015) Multi-century evaluation of Sierra Nevada snowpack. *Nature Climate Change*, 6: 2-3.

Berkelhammer M and Stott L (2008) Recent and dramatic changes in Pacific storm track trajectories recorded in ^{18}O from bristlecone pine tree ring cellulose. *Geochemistry, Geophysics, and Geosystems*, 9: Q04008.

Bevington, AR, Gleason HE, Foord VN, Floyd WC, and Griesbauer HP (2019) Regional influence of ocean-atmosphere on the timing and duration of MODIS-derived snow cover in British Columbia, Canada. *The Cryophere*, 13: 2693-2712.

Bhave AG, Conway D, Dessai S, and Stanforth DA (2018) Water resources planning under future climate and socioeconomic uncertainty in the Cauvery River Basin in Karnataka, India. *Water Resources Research*, 54: 708-728.

Bjornstad ON, Nidbet RM, and Fromentin J-M (2004) Trends and cohort resonant effects in age-structured populations. *Journal of Animal Ecology*, 73: 1157-1167.

Bohr GS and Aguado E (2001) Use of April 1 SWE measurements as estimates of peak seasonal snowpack and total cold-season precipitation. *Surface Water and Climate*, 37: 51-60.

Bonsal B and Shabbar A (2008) Impacts of large-scale circulation variability on low streamflows over Canada: A review. *Canadian Water Resources Journal*, 33: 137-158.

Botsford LW, Holland MD, Field JC, and Hastings A (2014) Cohort resonance: a significant component of fluctuations in recruitment, egg production, and catch of fished populations. *ICES Journal of Marine Science*, 71: 2158-2170.

Box, G (1976) Science and statistics. *Journal of the American Statistical Association*, 71: 791-799.

Bridgman H and Oliver JE (2006) The Global Climate System: Patterns, Processes, and Teleconnections. University of Cambridge Press, Cambridge, UK, 358 pp.

Briffa KR and Melvin TM (2011) A closer look at regional curve standardization of tree-ring records: justifications of the need, a warning of some pitfalls, and suggested improvements in its application. In *Developments in Paleoenvironmental Research – Dendroclimatology: Progress and Prospects* (eds.: Hughes MK, Swetnam TW, and Diaz HF) Springer Publishing, Dordrecht, 113-145.

Brukbaker LB (1980) Spatial patterns of tree growth anomalies in the Pacific Northwest. *Ecology*, 61: 798-807.

Bunn AG (2008) A dendrochronology program library in R (dplR). *Dendrochronolgia*, 25: 115-124.

Bunn AG (2012) ITRDB Heather Meadows, Mt Baker – TSME – ITRDB WA134. < https://www.ncdc.noaa.gov/paleo-search > Accessed July 2017.

Burke BJ, Anderson JJ, Miller JA, Tomaro L, Teel DJ, Banas NS, and Bapista AM (2016) Estimating behavior in a black box: how coastal oceanographic dynamics influence yearling Chinook salmon marine growth and migration behaviors. *Environmental Biology of Fishes*, 99: 671-686.

Castle SL, Thomas BF, Reager JT, Rodell M, Swenson SC, and Famiglietti JS (2014) Groundwater depletion during drought threatens future water security of the Colorado River Basin. *Geophysical Research Letter*, 41: 5904-5911.

Cayan DR, Kammerdiener SA, Dettinger MD, Caprio JM, and Peterson DM (2001) Changes in the onset of spring in the western United States. *Bulletin of the American Meteorological Society*, 82: 399-416.

Chang DKM, Lee S, and Swanson KL (2002) Storm track dynamics. *Journal of Climate*, 15: 2163-2183.

Christensen N and Lettenmaier DP (2006) A multimodel ensemble approach to assessment of climate change impacts on the hydrology and water resources of the Colorado River Basin. *Hydrology and Earth System Sciences Discussions*, 3: 3727-3770.

Church M and Ryder JM (2010) Physiography of British Columbia. *In*: Compendium of Forest Hydrology and Geomorphology in British Columbia (eds: Pike RG, Redding TE, Moore RD, Winkler RD, and Bladon KD). Land Management Handbook 66, Victoria, BC, Canada. 17-46.

Cochrane H (2004) Economic loss: myth and measurement. *Disaster Prevention and Management*, 13: 290-296.

Cohen SJ, Sheppard S, Shaw A, Flanders D, Burch S, Taylor B, Hutchinson D, Cannon A, Hamilton S, Burton B, and Carmichael J (2011) Downscaling and visioning of mountain snowpacks and other climate change implications in North Vancouver, British Columbia. *Mitigation and Adaptation Strategies for Global Change*, 17: 25-49.

Cook BI (2019) Drought: An Interdisciplinary Perspective. University of Columbia Press, New York, 215 pp.

Cook ER and Kairiukstis LA (1990) Methods of Dendrochronology: Applications in the Environmental Sciences, 394 pp.

Cook BI, Williams AP, Mankin JS, Seager R, Smerdon J, and Singh D (2018) Revisiting the leading drivers of Pacific coastal drought variability in the contiguous United States. *Journal of Climate*, 31: 25-43.

Cook BI, Seager R, Williams P, Puma MJ, McDermid S, Kelley M, and Nazarenko L (2019) Climate change amplification of natural drought variability: The historic mid-twentieth century North American drought in a warmer world. *Journal of Climate*, JCLI-D-18-0832.1

Coulthard B and Smith DJ (2015) A 477-year dendrohydrological assessment of drought severity for Tsable River, Vancouver Island, British Columbia, Canada. *Hydrological Processes*, 30: 1676-1690.

Coulthard B, Smith DJ, and Meko DM (2016) Is worst-case scenario streamflow drought underestimated in British Columbia? A multi-century perspective for the south coast, derived from tree-rings. *Journal of Hydrology*, 534: 205-218.

Crawford PD and Oliver CD (1990) Pacific Silver *Fir*. In *Silvics of North America* (Eds.: Burns RM and Honkala), Forest Service, United States Department of Agriculture, 6-25.

Cunningham CJ, Westley PAH, and Adkison MD (2018) Signals of large-scale climate drivers, hatchery enhancement, and marine factors in Yukon River Chinook salmon

survival revealed with a Bayesian life history model. *Global Change Biology*, 24: 4399-4416.

D'Arrigo R and Wilson R (2006) On the Asian expression of the PDO. *International Journal of Climatology*, 26: 1607-1617.

Daly C, Halbleib M, Smith JI, Gibson WP, Doggett MK, Taylor GH, Curtis J, and Pasteris PP (2008) Physiologically sensitive mapping of climatological temperature and precipitation across the conterminous United States. *International Journal of Climatology*, 28: 2031-2064.

Delucia EH (1986) Effect of low root temperature on net photosynthesis, stomatal conductance and carbohydrtate concentration in Engelmann spruce seedlings. *Tree Physiology*, 2: 143-154.

Dery SJ, Hernandez-Henriques MA, Burford JE, and Wood EF (2009) Observational evidence of an intensifying hydrological cycle in northern Canada. *Geophysical Research Letters*, 26: L13402.

Dery SJ, Hernandez-Henriques MA, Owens PN, Parkes MW, and Petticrew EL (2012) A century of hydrological variability and trends in the Fraser River Basin. *Environmental Research Letters*¸ 7: 024019.

Dobry J, Kyncl J, Klinka K, and Blackwell BA (1996) Climate signals in coastal old-growth forest trees near Vancouver, British Columbia. *In*: Trees, Environmental, and Humanity (eds.: Dean JS and Swetnam TW). Radiocarbon, 733-741 pp.

Desloges JR and Gilbert R (1991) Sedimentary record of Harrison Lake: implications for deglaciation in southwestern British Columbia. *Canadian Journal of Earth Sciences*, 28: 800-815.

Dettinger M, Udall B, and Georgeakakos A (2015) Western water and climate change. *Ecological Applications*, Centennial Paper 25: 2069-2093

DeRose RJ, Wang S, Buckley BM, and Bekker MF (2014) Tree-ring reconstruction of the level of Great Salt Lake, USA. *The Holocene*, 24: 805-813.

Ding Y, Hayes MJ, and Widhalm M (2011) Measuring economic impacts of drought: a review and discussion. *Disaster Prevention and Management: An International Journal*, 20: 434-446.

Dobry J, Kyncl J, Klinka K, and Blackwell BA (1996) Climate signals in coastal old-growth forest trees near Vancouver, British Columbia. In: Trees, Environmental, and Humanity (eds.: Dean JS, Meko DM and Swetnam TW). 733-741.

Doll P, Jimenez-Cisneros B, Oki T, Arnell NW, Benito G, Cogley JG, Jiang T, Kundzewicz ZW, Mwakalila S, and Nishijima A (2015) Integrating risks of climate change into water management. *Hydrological Sciences Journal*, 1: 4-13.

Drake DC and Naiman RJ (2007) Reconstruction of Pacific salmon abundance from riparian tree-ring growth. *Ecological Applications*, 17: 1523-1542.

Drake DC, Naiman RJ, and Helfield JM (2002) Reconstructing salmon abundance in rivers: an initial dendrochronological evaluation. *Ecology*, 83: 2971-2977.

Eaton B and Moore R (2010) Regional hydrology *In*: Compendium of Forest Hydrology and Geomorphology in British Columbia (eds: Pike RG, Redding TE, Moore RD, Winkler RD, and Bladon KD). Land Management Handbook 66, Victoria, BC, Canada, 85-110.

[ECCC] Environment and Climate Change Canada (2017) Historical Data. < http://climate.weather.gc.ca/historical_data/search_historic_data_e.html > Accessed July 2017.

Ettinger AK, Ford KR, and HilleRisLambers J (2011) Climate determines upper, but not lower, altitudinal range limits of Pacific Northwest conifers. *Ecology*, 92: 1323-1331.

Finney BP, Greory-Eaves I, Sweetman J, Douglas MS, and Smol JP (2000) Impacts of climatic change and fishing on Pacific salmon abundance over the past 300 years. *Science*, 290: 795-799.

Fisheries and Oceans Canada (2018) < https://www.dfo-mpo.gc.ca/index-eng.htm > Accessed December 2018.

Fleming SW and Quilty EJ (2006) Aquifer responses to El Nino-Southern Oscillation, southwest British Columbia. *Groundwater*, 44: 595-599.

Fleming Sw, Hood E, Dahlke HE, and O'Neel S (2016) Season flows of internation British Columbia-Alaska rivers: The nonlinear influence of ocean-atmosphere circulation patterns. *Advances in Water Resources*, 87: 42-55.

Fleming SW and Whitfield PH (2010) Spatiotemporal mapping of ENSO and PDO surface meteorological signals in British Columbia, Yukon, and southeast Asia. *Atmosphere-Ocean*, 48: 122-131.

Fleming SW, Whitfield PH, Moore RD, and Quilty EJ (2007) Regime-dependent streamflow sensitivities to Pacific climate modes cross the Georgia-Puget transboundary ecoregion. *Hydrological Processes*, 21: 3264-3287.

Fritts HC (1976) Tree-Rings and Climate. Academic Press, London, UK, 582 pp.

Gedalof Z and Smith DJ (2001) Interdecadal climate variability and regime-scale shifts in Pacific North America. *Geophysical Research Letters*, 28: 1515-1518.

Ghil, M, Allen MR, Dettinger MD, Ide K, Kondrashov D, Mann ME, Robertson AW, Saungers A, Tian Y, Varadi F, and Yiou P (2002) Advanced spectral methods for climatic time series. *Reviews of Geophysics*, 40: 1-3.

Gillies RR, Chung OY, Wang SYS, DeRose RJ, and Sun Y (2015) Added value from 576 years of tree-ring records in the prediction of the Great Salt Lake level. *Journal of Hydrology*, 529: 962-968.

Gouhier TC, Grinsted A, and Simko V (2016) R package 'biwavelet': Conduct univariate and bivariate wavelet analysis.
Graumlich LJ and Brubaker LB (1986) Reconstruction of annual temperature (1590-1979) for Longmire, Washington, derived from tree rings. *Quaternary Research*, 25: 223-234.

Grindsted A, Moore JC, and Jevrejeva S (2004) Application of the cross wavelet transform and wavelet coherence to geophysical time series. *Nonlinear Processes in Geophysics*, 11: 561-566.

Guay R, Gagnon R, and Morin H (1992) A new automatic tree-ring measurement system based on a line scan camera. *Forestry Chronicle*, 68: 138-141.

Hamlet AF, Mote PW, Clark MP, and Lettenmaier DP (2005) Effects of temperature and precipitation variability on snowpack trends in the western United States. *Journal of Climate*, 18: 4545-4561.

Hansen-Bristow K (1986) Influence of increasing elevation on growth characteristics at timberline. *Canadian Journal of Botany*, 64: 2517-2523.

Hare SR, Mantua NJ, and Francis RC (1999) Inverse production regimes: Alaska and west coast Pacific salmon. *Fisheries*, 24: 6-14.

Hart SJ, Smith DJ, and Clague JJ (2010) A multi-species dendroclimatic reconstruction of Chilko River streamflow, British Columbia, Canada. *Hydrological Processes*, 24: 2752-2761.

Hartmann B and Wendler G (2005) The significance of the 1976 Pacific climate shift in the climatology of Alaska. *Journal of Climate*, 18: 4824-4839.

Harvey JE and Smith DJ (2017) Interannual climate variability drives regional fires in west central British Columbia, Canada. *Journal of Geophysical Research: Biogeosciences*, 122: 1758-1774.

Heideman M, Menounos B, and Clague JJ (2017) A multi-century estimate of suspended sediment yield from Lillooet Lake, southern Coast Mountains, Canada. *Canadian Journal of Earth Sciences*, 55: 18-32.

Hilborn R and Walters CJ (1992) Quantitative fisheries stock assessment: choice, dynamics and uncertainty. *Reviews in Fish Biology and Fisheries*, 2: 177-178.

Holzhauser H, Magny M, and Zumbuuhl HJ (2005) Glacier and lake-level variations in west-central Europe over the last 3500 years. *The Holocene*, 15: 789-801.

Howitt R, Medellin-Azuara J, MacEwan D, Lund JR, and Summer D (2015) Economic analysis of the 2015 drought for California agriculture. Davis: University of California-Davis, Center for Watershed Sciences, 31 pp.

Irvine JR and Fukuwaka MA (2011) Pacific salmon abundance trends and climate change. *ICES Journal of Marine Science*, 68: 1122-1130.

Jacob M and Weatherly H (2003) A hydroclimatic threshold for landslide initiation on the North Shore Mountains of Vancouver, British Columbia. *Geomorphology*, 54: 137-156.

Johnson AL and Smith DJ (2010) Geomorphology of snow avalanche impact landforms in the southern Canadian Cordillera. *The Canadian Geographer*, 54: 87-103.

Kiffney PM, Bull JP, and Feller MC (2002) Climatic and hydrologic variability in a coastal watershed of southwestern British Columbia. *Journal of the American Water Resources Association*, 38: 1437-1451.

Kilduff DP, Di Lorenzo E, Botsford LW, and Teo SL (2015) Changing central Pacific El Ninos reduce stability of North American salmon survival rates. *Proceedings of the National Academy of Sciences*, 112: 10962-10966.

Kjellstrom T, Briggs D, Freyberg C, Lemke B, Otto M, and Hyatt O (2016) Heat, human performance, and occupational health: a key issue for the assessment of global climate change impacts. *Annual Review of Public Health*, 37: 97-112.

Koop SHA, Koetsier L, Doornhof A, Reinstra O, Van Leeuwen CJ, Brouwer S, Dieperink C, and Driessen PPJ (2017) Assessing the governance capacity of cities to address challenges of water, waste, and climate change. *Water Resources Management*, 31: 3427-3443.

Kottek M, Friser J, Beck C, Rudolf B, and Rubel F (2006) World map of the Koppen-Geiger climate classification. *Meteorologische Zeitschrift*, 15: 259-263.

Kulshreshtha SN, Grant CW, Marleau R, and Guenther E (2003) Technical report: Canadian droughts of 2001 and 2002. Saskatchewan Research Council, Saskatchewan.

Latif M and Barnett TP (1994) Causes of decadal climate variability over the North Pacific and North America. *Science*, 266: 634-637.

Latif M and Barnett TP (1996) Decadal climate variability over the North Pacific and Pacific North America: Dynamics and predictability. *Journal of Climate*, 9: 2407-2423.

Leathers DJ, Yarnal B, and Palecki MA (1991) The Pacific/North American teleconnection pattern and United States climate: Part I: Regional temperatures and precipitation associations. *Journal of Climate*, 4: 517-528.

Leathers DJ, Yarnel B, and Paleck MA (1992) The Pacific/North American teleconnection pattern and United States climate: Part II: temporal characteristics and index specification. *Journal of Climate*, 5: 707-716.

Li J, Xie P, Cook ER, Haung G, D'Arrigo R, Liu F, Ma J, and Zheng X (2011) Interdecadal modulation of El Nino amplitude during the past millennium. *Nature Climate Change*, 1: 114-118.

Lichatowich J and Lichatowich JA (2001) Salmon Without Rivers: A History of the Pacific Salmon Crisis. Island Press, Washington, USA, 253 pp.

Litzow Ma, Ciannelli L, Puerta P, Wettstein JJ, Rykaczewski RR, and Opiekun M (2018) Non-stationary climate-salmon relationships in the Gulf of Alaska. *Proceedings of the Royal Society B*, 285: 20181855.

Lledo L, Bellprat O, Doblas-Reyes FJ, and Soret A (2018) Investigating the effects of Pacific sea surface temperatures on the wind drought of 2015 over the United States. *Journal of Geophysical Research: Atmospheres*, 123: 4837-4849.

Loukas A Vasililiades L, and Dalezios N (2002) Climatic impacts on the runoff generation processes in British Columbia, Canada. *Hydrology and Earth Systems Science Discussions*, 6: 211-228.

Mann ME and Lees JM (1996) Robust estimation of background noise and signal detection in climatic time series. *Climatic Change*, 33: 409-445.

Mantua NJ and Hare SR (2002) The Pacific Decadal Oscillation. *Journal of Oceanography*, 58: 35-44.

Mantua BJ, Hare SR, Zhang Y, Wallace JM, and Francis RC (1997) A Pacific interdecadal climate oscillation with impacts on salmon production. *Bulletin of the American Meteorological Society*, 78: 1069-1079.

Mantua NJ, Crozier LG, Reed TE, Schindler DE, and Waples RS (2015) Response of chinook salmon to climate change. *Nature Climate Change*, 5: 613-615.

Marcinkowski K, Perterson DL, and Ettl GJ (2015) Nonstationary temporal response of mountain hemlock growth to climatic variability in the North Cascade Range, Washington, USA. *Canadian Journal of Forest Research*, 45: 676-688.

Margolis E, Meko D, and Touchan R (2011) A tree-ring reconstruction of streamflow in the Santa Fe River, New Mexico. *Journal of Hydrology*, 397: 118-127.

McCabe GJ and Dettinger MD (1999) Decadal variations in the strength of ENSO teleconnections with precipitation in the western United States. *International Journal of Climatology*, 19: 1399-1410.

McCabe GJ and Dettinger MD (2002) Primary modes and predictability of year-to-year snowpack variations in the western United Stations from teleconnections with Pacific Ocean climate. *Journal of Hydrometeorology*, 3: 13-25.

McCabe GJ, Palecki MA, and Betancourt JL (2004) Pacific and Atlantic influences on multidecadal drought frequency in the United States. *Proceedings of the National Academy of Sciences*, 101: 4136-4141.

Medellin-Azuara J, Harou JJ, Olivares, MA, Madani K, Lund JR, Howitt RE, Tanaka SK, Jenkins MW, and Zhu T (2009) Adaptability and adaptations of California's water supply system to dry climate warming. *Climatic Change*, 87: 75-90.

Meko D (2006) Tree-ring inferences on water-level fluctuations of Lake Athabasca. *Canadian Water Resources Journal*, 31: 229-248.

Meko D and Woodhouse C (2011) Application of streamflow reconstruction to water resources management. *In*: Dendroclimatology (eds: Hughes MK, Swetnam TW and Diaz HF) Springer, Netherlands, 231-261.

Meko DM, Therrell MD, Baisan CH, and Hughes MK (2001) Sacramento River flow reconstruction to A.D. 869 from tree rings. *JAWRA Journal of the American Water Resources Association*, 37: 1029-1039.

Meko D, Touchan R, and Anchukaitis K (2011) Seascorr: a MATLAB program for identifying the seasonal climate signal in an annual tree-ring time series. *Computers and Geoscience*, 37: 1234-1241.

Metro Vancouver (2011) Drinking Water Management Plan. June 2011. < http://www.metrovancouver.org/services/water/WaterPublications/DWMP-2011.pdf > Accessed November 2017.

Metro Vancouver (2017) Water Services. < http://www.metrovancouver.org/services/water/Pages/default.aspx) Accessed November 2017.

Milly PCD, Betancourt J, Falkenmark M, Hirsch RM, Kundzewicz ZW, Lettenmaier DP, and Stouffer RJ (2008) Stationarity is dead: Whither water management? *Science*, 319: 573-574.

Minobe S (1997) A 50-70 year climatic oscillation over the North Pacific and North America. *Geophysical Research Letters*, 24: 683-686.

Monger JWH (1989) Overview of Cordilleran geology. *In:* Western Canada Sedimentary Basin: A Case History, Alberta Geological Survey, 9-32.

Moore RD and McKendry (1996) Spring snowpack anomaly patterns and winter climatic variability, British Columbia, Canada. *Water Resources Research*, 32: 623-632.

Moore RD, Fleming SW, Menounos B, Wheate R, Fountain A, Stahl K, Holm K, and Jakob M (2009) Glacier change in western North America: Influences on hydrology, geomorphic hazards and water quality. *Hydrological Processes*, 23: 42-61.

Moore RD, Spittlehouse DL, Whitfield PH, and Stahl K (2010) Weather and Climate. *In*: Compendium of Forest Hydrology and Geomorphology in British Columbia (eds: Pike RG, Redding TE, Moore RD, Winkler RD, and Bladon KD). Land Management Handbook 66, Victoria, BC, Canada. 47-83.

Mote PW (2003) Trends in snow water equivalent in the Pacific Northwest and their climatic causes. *Geophysical Research Letters*, 30: 1601.

Mote PW, Li S, Lettenmaier DP, Xiao M, and Engel R (2018) Dramatic declines in snowpack in the western US. *Npj Climate and Atmospheric Science*, 1: 1-6.

Mote PW, Hamlet AF, Clark MP, and Lettenmaier D (2005) Declining mountain snowpack in western North America. *Bulletin of the American Meteorological Society*, 86: 39-49.

Munoz NJ, Farrell AP, Health JW, and Neff BD (2014) Adaptive potential of a Pacific salmon challenged by climate change. *Nature Climate Change*, 5: 163-166.

Munoz NJ, Farrell AP, Health JW, and Neff BD (2015) Reply to 'Response of chinook salmon to climate change'. *Nature Climate Change*, 5: 615.

Murphy SF, Writer JJ, McCleskey RB, and Martin DA (2015) The role of precipitation type, intensity, and spatial distribution in source water quality after wildfire. *Environmental Research Letters*, 11: 079501.

Mote PW, Li S, Lettenmaier DP, Xiao M, and Engel R (2018) Dramatic declines in snowpack in the western US. *npj Climate and Atmospheric Science*, 1: 2.

Musselman KN, Clark MP, Liu C, Ikeda K, and Rasmussen R (2017) Slower snowmelt in a warmer world. *Nature Climate Change*, 7: 214-219.

Newman M, Compo GP, and Alexander MA (2003) ENSO-forced variability of the Pacific Decadal Oscillation. *Journal of Climate*, 16: 3853-3857.

NOAA (National Oceanic and Atmospheric Administration) (2017) Paleoclimatology Datasets. <Accessed February 2017>

NuSEDS (1999) NuSEDS: New Salmon Escapement Database System. https://open.canada.ca/data/en/dataset/c48669a3-045b-400d-b730-48aafe8c5ee6 < Accessed November 2018 >

Olmstead SM (2014) Climate change adaptation and water resource management: A review of the literature. *Energy Economics*, 46: 500-509.

Padhy SK, Sarkar S, Panigrahi M, and Paul S (2015) Mental health effects of climate change. *Indian Journal of Occupational and Environmental Medicine.* 19: 3-7.

Palmer JG, Turney CS, Cook ER, Fenwick P, Thomas Z, Helle G, Jonse R, Clement A, Hogg A, Southon J, and Ramsey CB (2016) Changes in El Nino-Southern Oscillation (ENSO) conditions during the Greenland Stadial 1 (GS-1) chronozone revealed by New Zealand tree-rings. *Quaternary Science Reviews*, 153: 139-155.

Pathak P, Kalra A, Lamb KW, Miller WP, Ahmad S, Amerineni R, and Ponugoti DP (2018) Climate variability of the Pacific and Atlantic Oceans and western US snowpack. *International Journal of Climatology*, 38: 1257-1269.

Pearcy WG (1992) Ocean ecology of North Pacific salmonids. *Books in Recruitment Fishery Oceanography (USA)*. University of Washington Press, Seattle, USA, 179 pp.

Pederson GT, Gray ST, Woodhouse CA, Betancourt JL, Fagre DB, Littell JS, Watson E, Luckman BH, and Graumlich LJ (2011) The unusual nature of recent snowpack declines in the North American Cordillera. *Science*, 333: 332-335.

Peterson DW and Perterson DL (2001) Mountain hemlock growth responds to climatic variability at annual and decadal time scales. *Ecology*, 82: 3330-3345.

Poff NL, Brown CM, Grantham TE, Matthews JH, Palmer MA, Spence CM, Wilby RL, Haasnoot M, Mendoza GF, Cominique KC, and Baeza A (2016) Sustainable water management under future uncertainty with eco-engineering decision scaling. *Nature Climate Change*, 6: 25-34.

Pojar J, Klinka K, and Meidinger DV (1991) Ecosystems of British Columbia. Special Report Series 6, February 1991, BC Ministry of Forests.

Quinn TP and Dittman AH (1990) Pacific salmon migrations and homing: mechanisms and adaptive significance. *Trends in Ecology and Evolution*, 5: 174-177.

River Forecast Centre (2017) Snow Conditions and Water Supply Bulletin. <Accessed February 2017>

Rodenhuis D, Bennett KE, Werner AT, Murdock TQ, and Bronaugh D (2009) Climate Overview 2007: Hydro-climatology and Future Climate Impacts in British Columbia. *Pacific Climate Impacts Consortium*, University of Victoria, British Columbia, 152 pp.

Roesch A and Schmidbauer H (2015) R package 'WaveletComp': computation wavelet analysis.

Rogers LA, Schindler DE, Lisi PJ, Holtgrieve GW, Leavitt PR, Bunting L, Finney BP, Selbie DT, Chen G, Gregory-Eaves I, and Lisac MJ (2013) Centennial-scale fluctuations and regional complexity characterize Pacific salmon population dynamics over the past five centuries. *Proceedings of the National Academy of Sciences*, 110: 1750-1755.

Ruff CP, Anderson JH, Kemp IM, Kendall NW, Mchugh PA, Velez-Espino A, Greene CM, Trudel M, Molt CA, and Dyding KE (2017) Salish Sea chinook salmon exhibit weaker coherence in early marine survival trends than coastal populations. *Fisheries Oceanography*, 26: 625-637.

Sauchyn D and Ilich N (2017) Nine hundred years of weekly streamflows: Stochastic downscaling of ensemble tree-ring reconstructions. *Water Resources Research*, 53: 9266-9283.

Sauchyn DJ, Vanstone J, St. Jacques JM, and Sauchyn R (2015) Dendrohydrology in Canada's western interior and applications to water resource management. *Journal of Hydrology*, 529: 548-558.

Schweingruber FH, Briffa KR, and Jones PD (1991) Yearly maps of summer temperatures in Western Europe from AD 1750 to 1975 and Western North America from 1600 to 1982: results of a radiodensitometrical study on tree rings. *Vegetatio*¸92: 5-71.

Seager R and Ting M (2017) Decadal drought variability over North America: mechanisms and predictability. *Current Climate Change Reports*, 3: 141-149.

Sellars CD, Garret M, and Woods S (2008) Influence of the Pacific Decadal Oscillation and El Nino Southern Oscillation on the operation of the Capilano Water Supply Reservoir, Vancouver, British Columbia. *Canadian Journal of Water Resources*, 33: 155-164.

Shabbar A, Bonsla B, and Khandekar M (1997) Canadian precipitation patterns associated with the Southern Oscillation. *Journal of Climate*, 10: 3016-3027.

Slaymaker O, Clague JJ, Gilbert R, Friele P, Jordan P, Menounos B, and Shiefer E (2017) Lillooet-Harrison Drainage Basin: variable landscapes within the Coast Mountains. *Landscapes and Landforms of Western Canada* (eds.: Slaymaker O), World Geomorphological Landscapes, Springer Press, 303-320.

Smith DJ and Laroque CP (1998) Mountain hemlock growth dynamics on Vancouver Island. *Northwest Science*, 72: 67-70.

Smith P, House JI, Bustamante M, Sobocka J, Harper R, Pan G, West PC, Clark JM, ADhya T, Rumpel C, Paustian K, Cotrufo MF, Elliot JA, MCDowell R, Griffiths RI, Asakawa S, Bondeeau A, Jain AK, Meersmans J, and Pugh TAM (2015) Global change pressures on soils from land use and management. *Global Change Biology*, 22: 1008-1028.

Speer JH (2010) Fundamentals of Tree Ring Research. University of Arizona Press Tucson, USA, 368 pp.

Spry CM, Kohfeld KE, Allen DM, Dunkley D, and Lertzman K (2014) Characterizing Pineapple Express storms in the Lower Mainland of British Columbia, Canada. *Canadian Water Resources Journal*, 39: 302-323.

Stahl K, Moore RD, and Mckendry IG (2006) The role of synoptic-scale circulation in the linkage between large-scale ocean-atmosphere indices and winter surface climate in British Columbia, Canada. *International Journal of Climatology*, 26: 541-560.

Stagge JH, Rosenberg DE, DeRose RJ, and Rittenour TM (2018) Monthly paleostreamflow reconstruction from annual tree-ring chronologies. *Journal of Hydrology*, 557: 791-804.

Starheim CCA, Smith DJ, and Prowse TD (2013a) Dendrohydroclimate reconstructions of July-August runoff for two nival-regime rivers in western central British Columbia. *Hydrological Processes*, 27: 405-420.

Starheim CCA, Smith DJ, and Prowse TD (2013b) Multi-century reconstructions of Pacific salmon abundance from climate-sensitive tree rings in west central British Columbia, Canada. *Ecohydrology*, 6: 228-240.

Stewart IT, Cayan DR, and Dettinger MD (2005) Changes toward earlier streamflow timing across western North America. *Journal of Climate,* 18: 1136-1155.

Stockton CW and Fritts HC (1976) Long-term reconstruction of water level changes for Lake Athabasca by analysis of tree rings. *Journal of the American Water Resources Association*, 9: 73074.

Torrence C and Compo GP (1998) A practical guide to wavelet analysis. *Bulletin of the American Meteorological Society*, 79: 61-78.

Trouet V and Taylor AH (2009) Multi-century variability in the Pacific North American circulation pattern reconstructed from tree rings. *Climate Dynamics*, 35: 953-963.

Turner SWD and Galelli S (2016) Regime-shifting streamflow processes: implications for water supply reservoir operations. *Water Resources Research*, 52: 3984-4002.

Van der Maaten E, van der Maaten-Theunissen M, Buras A, Scharnweber T, Simard S, Kaiser K, Lorenz S, and Wilking M (2015) Can we use tree rings of Black Alder to reconstruct lake levels? A case study for the Mechlenburg Lake District, Northeastern Germany. *PloS One*, 10: e0137054.

Wallace JM and Gutzler DS (1981) Teleconnections in the geopotential height field during the Northern Hemisphere winter. *Monthly Weather Review*, 109: 784-812.

Walters C, English K, Korman J, and Hilborn R (2019) The managed decline of British Columbia's commercial salmon fishery. *Marine Policy*, 101: 25-32.

Wang T, Hamann A, Spittlehouse D, and Murdock TN (2012) ClimateWNA – High-resolution spatial climate data for western North America. *Journal of Applied Meteorology and Climatology*, 61: 16-29.

Wells BK, Grimes CB, Field JC, and Reiss CS (2006) Covariation between the average lengths of mature coho (*Oncorhynchus kisutch*) and Chinook (*O. tshawytscha*) and the ocean environment. *Fisheries Oceanography*, 15: 67-79.

Welsh C, Smith DJ, and Coulthard B (2019) Tree-ring records unveil long-term influence of the Pacific Decadal Oscillation on snowpack dynamics in the Stikine River basin, northern British Columbia. *Hydrological Processes*, 33: 720-736.

Whitfield PH, Moore RD, Fleming SW, and Zawadzki A (2010) Pacific Decadal Oscillation and the hydroclimatology of western Canada – review and prospects. *Canadian Water Resources Journal*, 35: 1-28.

Winkler RD, Moore RD, Redding TE, Spittlehouse DL, Carlyle-Moses DE, and Smerdon BD (2010) Hydrological Processes and Watershed Response. *In*: Compendium of Forest Hydrology and Geomorphology in British Columbia (eds: Pike RG, Redding TE, Moore RD, Winkler RD, and Bladon KD). Land Management Handbook 66, Victoria, BC, Canada. 133-177.

Wise EK, Wrzesian ML, Dannenberg MP, and McGinnis DL (2015) Cool-season precipitation patterns associated with teleconnection interactions in the United States. *Journal of Applied Meteorology and Climatology*, 54: 494-505.

Wolter K and Timlin MS (1998) Measuring the strength of ENSO events: How does the 1997/1998 rank? *Weather* 53: 315-324.

Wood LJ, Smith DJ, and Demuth MN (2011) Extending the Place Glacier mass-balance record to AD 1585, using tree rings and wood density. *Quaternary Research*, 76: 305-313.

Woodhouse CA and Lukas JJ (2006) Multi-century tree-ring reconstructions of Colorado streamflow for water resource planning. *Climatic Change*, 78: 293-315.

Worden L, Botsford LW, Hastings A, and Holland MD (2010) Frequency responses of age-structured populations: Pacific salmon as an example. *Theoretical Population Biology*, 78: 239-249.

[WSC] Water Survey of Canada (2017) Historical Hydrometric Data Search. < https://wateroffice.ec.gc.ca/search/historical_e.html > Accessed July 2017.

Yu B and Zwiers FW (2007) The impact of combined ENSO and PDO on the PNA climate: a 1000-year climate modelling study. *Climate Dynamics*, 29: 837-851.

Appendix A: Lagged salmon correlations

		Chinook PC1	*Coho PC1*		*Chinook PC1*	*Coho PC1*
		Lag-0			**Lag-3**	
PNA	**DJF**	0.2063	-0.09651		0.193261	-0.17802
	MAM	0.066483	0.07824		0.333931	-0.14594
	JJA	-0.0865	-0.20779		-0.08335	-0.23639
	a (water year)	0.078006	-0.08906		0.160885	-0.39013
ENSO	**DJF**	0.189349	-0.02058		0.191514	-0.22438
	MAM	0.260421	-0.07044		0.276218	-0.30235
	JJA	0.143962	-0.24228		0.28186	-0.29639
	a (water year)	0.22657	-0.10966		0.285981	-0.31233
PDO	**DJF**	0.387913	-0.16762		0.296372	-0.37313
	MAM	0.453489	-0.2059		0.500494	-0.38045
	JJA	0.354408	-0.2172		0.426604	-0.40296
	a (water year)	0.478407	-0.19645		0.471177	-0.42654
		Lag-1			**Lag-4**	
PNA	**DJF**	0.215655	-0.30459		0.222929	-0.06744
	MAM	0.174867	0.269159		0.331807	0.33316
	JJA	-0.14826	-0.11788		-0.04275	-0.11208
	a (water year)	0.06512	-0.13375		0.249583	0.059826
ENSO	**DJF**	0.094644	-0.10775		0.125237	0.044042
	MAM	0.139024	-0.06549		0.150289	0.026421
	JJA	0.166995	0.052799		0.154205	-0.12007
	a (water year)	0.15572	-0.04432		0.171425	-0.03161
PDO	**DJF**	0.264191	-0.35931		0.386665	-0.03967
	MAM	0.36971	-0.24153		0.472518	-0.08127
	JJA	0.451631	-0.14799		0.299673	-0.13672
	a (water year)	0.415109	-0.29258		0.4652	-0.09065
		Lag-2			**Lag-5**	
PNA	**DJF**	0.300565	-0.28999		0.275146	-0.22607
	MAM	0.178552	0.12764		0.104591	0.077588
	JJA	-0.10177	-0.151		-0.12684	0.158101
	a (water year)	0.128823	-0.28108		0.094996	-0.01044
ENSO	**DJF**	0.212671	-0.23178		0.014244	0.117384
	MAM	0.204913	-0.29137		0.003452	0.089037
	JJA	0.098951	-0.18316		0.0662	0.020007

	a (water year)	0.203826	-0.27199		0.043241	0.083057
PDO	**DJF**	0.381085	-0.43293		0.312158	-0.01901
	MAM	0.452386	-0.40632		0.465589	0.143233
	JJA	0.374577	-0.33314		0.337696	0.098693
	a (water year)	0.475924	-0.44059		0.452172	0.088878